DIGITAL SIGNAL PROCESSING ANALYSIS OF SWITCHED CAPACITOR FILTERS

by

Jose Velazquez Ramos

Thesis submitted to the Faculty of the

Virginia Polytechnic Institute and State University

in partial fulfillment of the requirements for the degree of

MASTER OF SCIENCE

in

ELECTRICAL ENGINEERING

APPROVED:

Dr. F. W. Stephenson

Dr. A. A. Riad

Dr. S. M. Riad

October, 1982
Blacksburg, Virginia

DIGITAL SIGNAL PROCESSING ANALYSIS

OF SWITCHED CAPACITOR FILTERS

by

Jose Velazquez Ramos

(ABSTRACT)

A deterministic and stochastic signal analysis is presented on switched capacitor filters. This relatively new discrete-time circuit design technology provides a wide field of applications in the areas of filters, circuitry, and communications. It also raises numerous problems and challenges in both discrete-time design implementation and noise analysis. Basic principles of switched capacitor integration/summation networks and their interfacing is first presented. A review of fundamental discrete-time system design techniques which are, and can be, adopted in the design of switched capacitor filters is then provided along with a discussion of frequency design criteria to deal with frequency warping and aliasing effects. An analysis of computer and test results of a 7th-order bilinear and a 8th-order LDI leapfrog switched capacitor lowpass filter is then presented. Finally, with the intent of presenting an

alternative approach to current analytical procedures in switched capacitor noise spectrum analysis, various spectrum estimation techniques are presented along with test results of noise spectrum estimation of a typical switched capacitor integration circuit.

ACKNOWLEDGEMENTS

I like to express my deep appreciation to Dr. Frederick W. Stephenson for the opportunity and assistance he has provided me in the pursuit and realization of this thesis. His boundless friendship and professional support, without which this thesis would not have been possible, has been priceless. It has been a true honor to have worked with him. I would like to express my gratitude to Bill McCall, who has honored me with his friendship and moral support. I would also like to thank Dr. Aicha A. Riad and Dr. Sedki M. Riad for serving on my advisory committee, for their friendship, and for providing me with many helpful suggestions. Special thanks must also be accorded to Dr. A.A. Beex for his valuable professional assitance. To my friends Mohammad and Barbara Feshami I am truly indebted for their friendship and support. I would also like to express my love and gratitude to my mother, my sisters Carmen and Marisela, and my brother Miguel for their precious and unending love, understanding, and moral support. To them I say: Gracias, los quiero mucho. Finally, to my father, of whom a memory of courage, sacrifice, and love for me, my brother, and sisters I will always cherish, I say: Gracias, siempre te recordare.

CONTENTS

LIST OF FIGURES

* Chapter 3 *

* Chapter 4 *

* LIST OF TABLES *

Chapter I

INTRODUCTION

Switched capacitor (SC) technology is a relatively new field in electrical engineering, with promising applications in the areas of digital filters, digital controllers, and integrated circuit implementations. In conventional RC circuits, frequency and time response characteristics are closely related to RC time constants. In most situations, these RC time constants fix capacitor and resistor values. Thus, at low frequencies, there is the risk of circuit implementations using large capacitors and resistors. In contrast, frequency and time response characteristics of switched capacitor circuits are closely dependent on capacitor ratios. Therefore, there is more freedom in selecting low capacitor values to implement smaller circuits. An additional advantage of switched capacitor systems lie in the tighter tolerances which are incurred in IC fabrication while working with capacitor ratios instead of RC time constants. Another advantage of switched capacitor systems is the capability of implementing both analog and digital signal processing in the same ciruit (where switched capacitors act as data-storage time-delay registers). Hence, there is

no need for A/D converters in implementing SC systems which, among other things, can be an advantage in the design of telephone switching systems. However, SC circuits, being discrete-time systems, usually have problems in frequency warping and aliasing which do not occur in conventional RC circuits. These problems, when acute, may require designing for higher filter and system orders and clock frequencies.

There are currently two main areas of research in switched capacitor technology. The first of these, which has attracted most of the research and widespread interest, is the area of analog-to-digital (S/Z) transformation using SC integrated circuits and SC filter designs. The two S/Z-Transformations of most use in SC filter and circuit designs are the bilinear and the LDI. Contributions to the development of bilinear SC integration circuits and filters have principally been made by Temes [38], Temes and Young [38], Lee and Chang [21], Knob [19], and Laker [20]. Principal contributions to the development and analysis of the LDI SC integration circuit have been made by Laker [20], Brodersen, Gray, and Hodges [7], Allstot, Brodersen, and Gray [2], Choi and Brodersen [8], Lee and Chang [21],[22], and Jacobs, Allstot, Brodersen, and Gray [16]. Significant research in leapfrog SC filter designs have been made by Laker [20], Ja-

cobs,et al. [16], Choi, et al. [8], Allstot et al. [2], and Brodersen et al. [7]. In the area of non-leapfrog SC filter designs, such as biquads, important contributions have been made by Szentermai and Temes [37], Lee, Temes, Chang, and Ghaderi [23], Gregorian [14], and Martin and Sedra [26]. To this date no significant inroads have been made in designing and realizing impulse invariant switched capacitor filters and systems.

The second most important, and most recent, area of research in switched capacitor technology is noise power spectrum analysis. This area has proven to be the most difficult field in SC research. It has demanded more complicated analyses than the first research area. When pursuing noise power spectrum investigations, SC systems, can be analyzed in both the analog and the discrete-time domain. For both cases severe complications arise in analyzing signal sampling SC circuit topologies with noise source models. Various techniques and approaches have been proposed for noise power spectrum analysis of SC circuits. In the area of analog domain noise power spectrum analysis of SC systems principal contributions have been made by Gobet and Knob [13], and Maloberti, Montecchi, and Suelto [25]. Research contributions in discrete-time noise power spectrum analysis

of SC systems have been made by Orchard and Temes [29], Weinrichter [41], and Furrer and Guggenbuhl [10], [11]. An alternative noise spectrum analysis of SC systems, and one which lends itself appropriately to computer implementation, is the adjoint network analysis concept, discussed by both Vandewalle and Rabey [40] and Rohrer, Nagel, Meyer, and Weber [35]. An alternative approach for noise analysis of SC circuits by means of power spectrum estimation will be proposed and presented in chapter 5 of this thesis.

One main objective of this thesis is to provide basic and useful deterministic and stochastic digital signal processing concepts which are applied, and can be applied, in switched capacitor systems design and analysis. Another principal objective is to summarize research work I contributed in the development and test of bilinear and LDI filters. Chapter 2 reviews fundamental principles of pole/zero S/Z-domain mapping, S/Z-transformations, and frequency warping. In this chapter two bilinear and one LDI SC integration/summation parasitic capacitance-free circuits will be presented and analyzed. In chapter three a summary of fundamental discrete-time system design strategies which are applied, and can be applied, to SC system designs is presented. Included in this chapter is an analysis of aliasing and

frequency warping effects incurred in SC filters, and a discussion on how these effects influence design objectives and criteria. A presentation is also provided on the leapfrog filter design as a way of realizing S/Z-transformations and obtaining the desired digital SC filter. Chapter 4 summarizes system analyses, computer simulations, and test results of the 7th-order bilinear and 8th-order LDI lowpass SC filters. Chapter 5 presents an alternative approach, namely noise power spectrum estimation, to current analytical power spectrum analysis of SC systems. Various power spectrum estimation techniques are presented and a comparison in terms of computational efficiency is made between these techniques and common analytical spectral analysis methods. Finally, Chapter 6 summarizes conclusions and recomendations on SC bilinear and LDI filter designs, drawn from the results in chapter 4, and recommendations on SC circuit noise spectral estimation analysis.

Chapter II

PRINCIPLES OF SWITCHED CAPACITOR NETWORKS

Different analog (s-domain) to discrete-time (Z-domain) transformations have been developed for use in digital filter and controls system design. In the design of switched-capacitor (SC) filters the two transformations of most use are the trapezoidal (bilinear) and the midpoint rectangular (LDI) transformations. Three types of SC integrator will be developed which realize either the bilinear or the LDI transformations on typical analog integrators. Pole-zero mapping and frequency prewarping characteristics of the LDI and the bilinear S/Z-domain transformations will first be discussed.

2.1 Theoretical S/Z-Transformation

The discrete-time complex variable Z is related to the analog complex variable s by the theoretical S/Z-transformation:

$$Z = e^{s\tau} \qquad 2.1.1$$

Where τ is the sampling period of the digital system. Equation 2.1.1 is the S/Z-transformation used in impulse invari-

ant discrete-time filter designs (see section 3.2). S-domain poles and zeroes are mapped into the Z-plane in the manner depicted in figure 2.1. Note in figure 2.1(a) that s-plane strips of frequency width $2\pi/\tau$ are mapped onto the entire Z-plane. The left half of each strip, which contains stable poles and zeroes, maps inside the unit circle of the Z-plane. Marginally stable (high Q) poles and zeroes on the immaginary axis of each strip are mapped onto the unit circle, while unstable s-domain singularities are mapped outside the unit circle. Figure 2.1(b) illustrates how the stable, marginally stable, and unstable poles and zeroes of a particular analog transfer function are mapped to corresponding poles and zeroes in the Z-plane by expressing equation 2.1.1 in the following manner:

$$\text{Let:} \quad s_i = \sigma_i + jw_i$$

$$Z_i = \gamma_i + j\Omega_i$$

$$\text{Then:} \quad Z_i = e^{si\tau} = e^{(\sigma i\tau + jwi\tau)}$$

$$Z_i = (R_i)\cos(w_i\tau) + j(R_i)\sin(w_i\tau)$$

$$\text{where:} \quad R_i = e^{\sigma i\tau}$$

$$\text{Thus:} \quad \gamma_i = (R_i)\cos(w_i\tau)$$

$$\Omega_i = (R_i)\sin(w_i\tau)$$

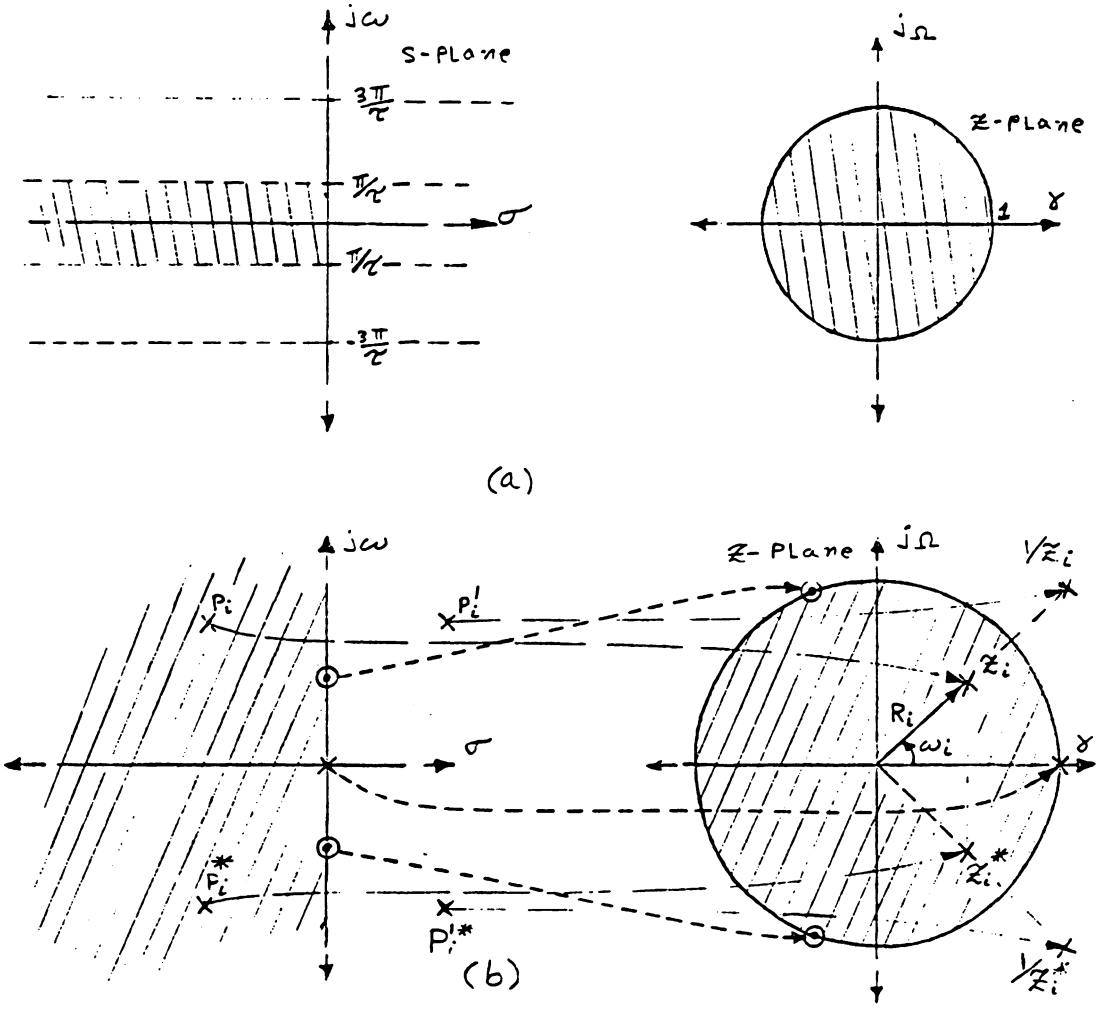

Figure 2.1. Pole/Zero mapping by the theoretical S/Z-transformation.

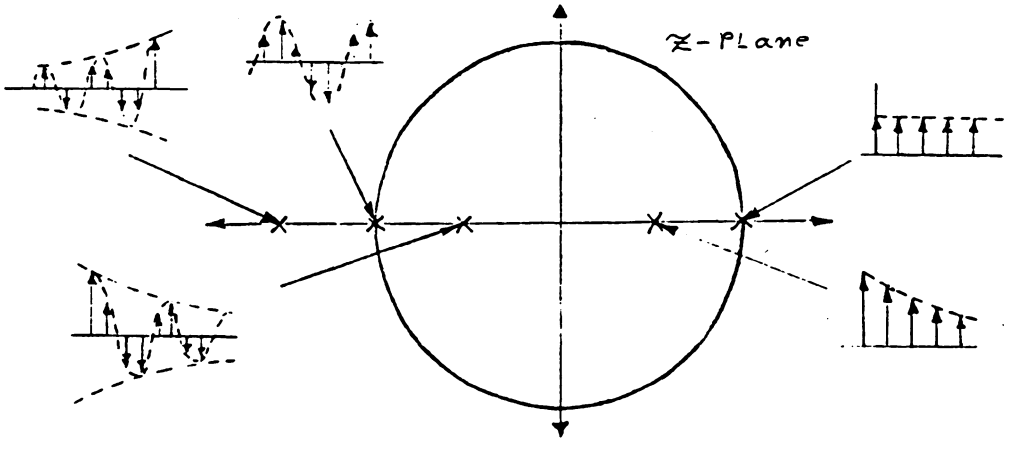

Figure 2.2. Z-domain dominant poles impulse response representations.

Note: The only use of the theoretical S/Z-transformation is in impulse invariant system designs (section 3.2) where poles and zeroes are not necessarily guaranteed to be mapped according to equation 2.1.1.

Figure 2.2 illustrates the impulse response of discrete-time systems with dominant root locations shown. A similar performance of mapping stable, marginally stable, and unstable s-domain singularities inside, onto, and outside of the Z-domain unit circle respectively must be met by any approximate S/Z-domain transformation.

Analog and discrete-time D.C. gains must satisfy the following equivalence relationship:

$$H_A(s)\Big|_{s=0} = H_D(Z)\Big|_{Z=1} \qquad 2.1.2$$

Equation 2.1.2 is usually satisfied not only by a proper S/Z transformation but by an extra adjustment of gain in the digital filter. A generalization of 2.1.2 for highpass, bandpass, and bandstop filter designs is that analog and digital passband gains should be made equivalent; if necessary, by a proper adjustment of gain in the digital filter.

2.2 S/Z-Transformation by Numerical Integration

The development of bilinear and LDI transformations may be illustrated by considering an analog integration characterized by the following transfer function:

$$H(s)= \frac{Y(s)}{X(s)} = \frac{1}{Ks} \qquad 2.2.1$$

Where K= integration constant

This is equivalent to the differential equation:

$$\dot{Y}(t) = (1/K)X(t) \qquad 2.2.2$$

$$Y(t) = (1/K)\int_0^t X(\beta)d\beta$$

In the analog integration above the width $d\beta$ of each successive integrating area $X(\beta)d\beta$ can of course be made infinitesimally small, thereby assuring high accuracy in the computation of the overall area of the integral. In discrete-time domain simulations of analog systems a numerical analysis approach may be adopted for approximating successive integrating areas with time-widths limited by the size of the sampling period τ of the digital system. This is illustrated in figure 2.3. Equation 2.2.2 can be rewritten into the following form:

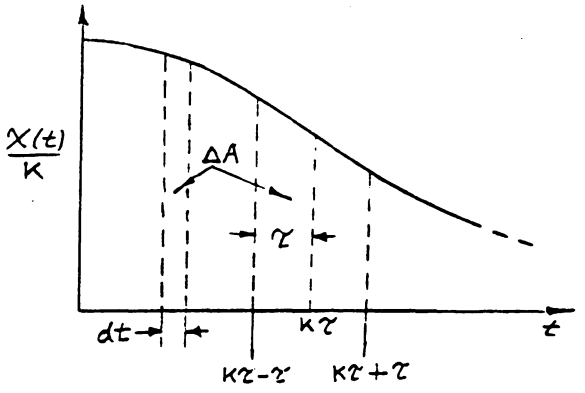

Figure 2.3. Analog and numerical discrete-time integration.

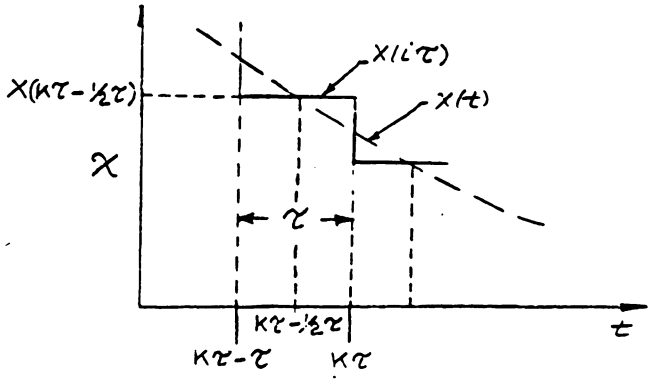

Figure 2.4. Midpoint-rectangular rule discrete-time integration

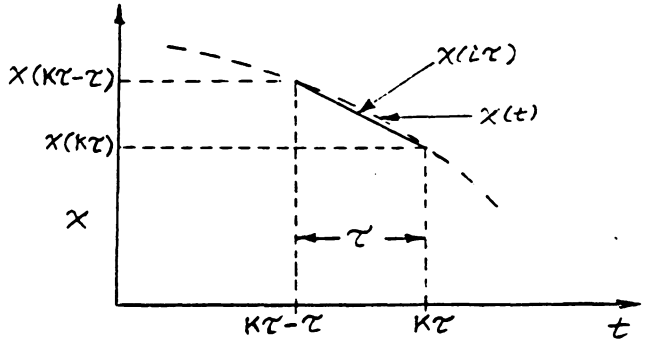

Figure 2.5. Trapezoidal rule discrete-time integration.

$$Y(K\tau) = (1/K)\int_0^{K\tau-\tau} X(\beta)d\beta + (1/K)\int_{K\tau-\tau}^{K\tau} X(\beta)d\beta \quad 2.2.3$$

By adopting a numerical analysis approach the above equation can be rewritten as:

$$Y(K\tau) \cong Y(K\tau-\tau) + \quad 2.2.4$$

$$(1/K)\left[\begin{array}{l}\text{approximate area of } X(t) \\ \text{over the interval: } (K\tau-\tau) \leq \beta \leq K\tau\end{array}\right]$$

Both the midpoint rectangular and the trapezoidal rules to be discussed differ in the manner and the accuracy with which they approximate the incremental area of equation 2.2.4. In each method, the accuracy of integration diminishes with larger sampling periods.

2.2.2 Midpoint Rectangular Rule (LDI Transformation)

The incremental area term is approximated by a rectangle as illustrated in figure 2.4, such that:

$$Y(K\tau) \cong Y(K\tau-\tau) + (\tau/K)[X(K\tau-\tau/2)] \quad 2.2.5$$

taking the Z-transformation yields:

$$Y(Z) = Y(Z)Z^{-1} + (\tau/K)X(Z)Z^{-1/2}$$

$$Y(Z)(1 - Z^{-1}) = X(Z)(\tau/K)Z^{-1/2}$$

$$H_D(Z) = \frac{Y(Z)}{X(Z)} = \left[\frac{\tau}{K}\right]\cdot\left[\frac{Z^{-1/2}}{1 - Z^{-1}}\right] \quad 2.2.6$$

comparison with equation 2.2.1 yields the LDI S/Z-domain transformation:

$$s = \left[\frac{1}{\tau}\right] \cdot \left[\frac{1 - Z^{-1}}{Z^{-1/2}}\right] \qquad 2.2.7$$

2.2.3 Trapezoid Rule (Bilinear Transformation)

The incremental area term is approximated by a trapezoid as shown in figure 2.5 such that:

$$Y(K\tau) \cong Y(K\tau-\tau) + (\tau/2k)[X(K\tau-\tau) + X(K\tau)] \qquad 2.2.8$$

Taking the Z-transform yields:

$$Y(Z) = Y(Z)Z^{-1} + [\tau/(2K)][X(Z)Z^{-1} + X(Z)]$$

$$Y(Z)(1-Z^{-1}) = X(Z)[\tau/(2K)][Z^{-1} + 1]$$

$$H_D(Z) = \frac{Y(Z)}{X(Z)} = \left[\frac{\tau}{2K}\right] \cdot \left[\frac{1 + Z^{-1}}{1 - Z^{-1}}\right] \qquad 2.2.9$$

Comparing to equation 2.2.1 yields the bilinear S/Z-transformation:

$$s = \left[\frac{2}{\tau}\right] \cdot \left[\frac{1 - Z^{-1}}{1 + Z^{-1}}\right] \qquad 2.2.10$$

2.3 Pole/Zero S/Z-Domain LDI and Bilinear Mapping

2.3.1 Bilinear Transformation

Equation 2.2.10 can be written in the form:

$$z = \frac{(2/\tau)+s}{(2/\tau)-s} \qquad 2.3.1$$

Letting $s = \sigma+jw$ and $z = Re^{j\phi}$ we obtain [3]:

$$R = \left[\frac{(2/\tau+\sigma)^2 + w^2}{(2/\tau-\sigma)^2 + w^2}\right]^{\frac{1}{2}} \qquad 2.3.2$$

$$\phi = \mathrm{Tan}^{-1}\left[\frac{w}{2/\tau+\sigma}\right] - \mathrm{Tan}^{-1}\left[\frac{w}{2/\tau-\sigma}\right] \qquad 2.3.3$$

Note from equations 2.3.2 and 2.3.3:

$R > 1$	for	$\sigma > 0$	$\phi = 0$	for	$w = 0$
$R = 1$	"	$\sigma = 0$	$\phi \Rightarrow \pi$	"	$w \Rightarrow \infty$
$R < 1$	"	$\sigma < 0$	$\phi \Rightarrow -\pi$	"	$w \Rightarrow -\infty$

The above results are depicted in figure 2.6. Note that the entire left-half s-plane containing stable singularities is mapped inside the Z-domain unit circle, the entire jw axis is mapped onto the unit circle, and the right-half s-plane is mapped outside the unit circle.

2.3.2 LDI Transformation

Equation 2.2.7 can be reduced to the following form:

$$Z - (s\tau)Z^{1/2} - 1 = 0 \qquad 2.3.4$$

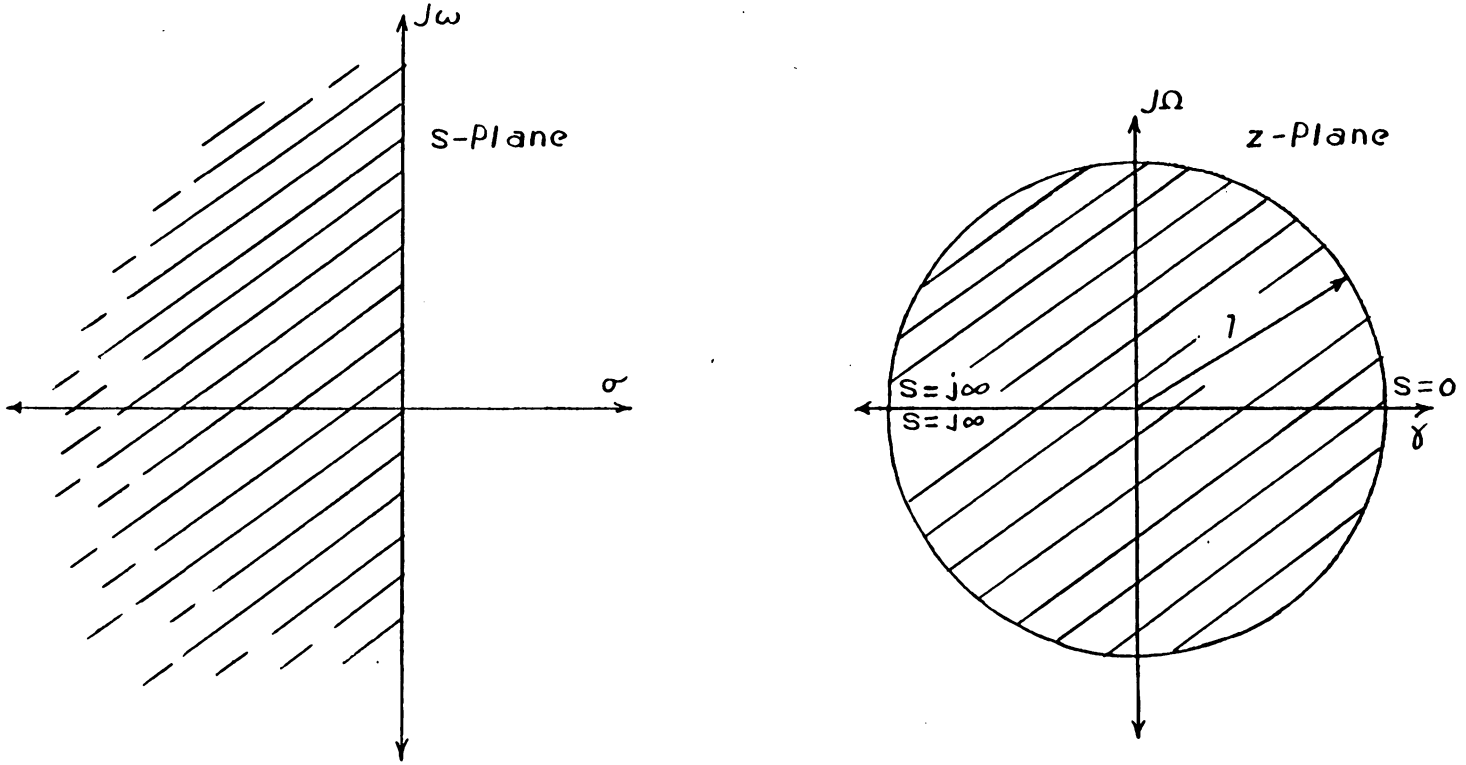

Figure 2.6. Pole/zero mapping by the bilinear S/Z-transformation.

Equation 2.3.4 expresses Z as a complex dependent variable with s as the complex independent variable. A simple closed-form expression similar to equation 2.3.1 does not exist for equation 2.2.7 since for each point in the s-plane, other than the origin, there corresponds two distinct points in the Z-plane. A simple computational procedure has nevertheless been developed which maps a desired s-domain singularity to the Z-domain, such that equation 2.2.7 is satisfied [9]. Consider a stable s-domain singularity:

$$s_i = \sigma_i + jw_i \qquad ; \qquad \sigma_i < 0$$

Let $P = Z^{1/2}$

By equation 2.3.4:

$$P^2 - (s\tau)P - 1 = 0 \qquad 2.3.5$$

Equation 2.3.5 contains a stable singularity, P_i, inside the Z-domain unit circle, hence the correct value of Z_i corresponding to S_i is:

$$Z_i = P_i^2$$

Where Z_i would be inside the Z-plane unit circle.

A similar illustrative S/Z-domain mapping to that of figures 2.1 and 2.6 has yet to be developed. Nonetheless, apart from a proper pole-zero mapping, any S/Z-transformation should map the s-plane jw-axis onto the Z-plane unit circle (see section 2.4). Equation 2.2.7 accomplishes this by map-

ping sections of length $4\pi/\tau$ along the s-plane jw axis onto the Z-plane unit circle.

2.4 Frequency Warping

Frequency warping results from the nonlinear relationship existing between the analog frequency w and the discrete-time frequency Ω which occurs with the LDI and the bilinear S/Z-transformations. The distances between discrete-time frequencies Ω_i's, are not proportionally maintained with their corresponding analog frequencies , w_i's, (see section 3.3). For the impulse invariant system design (section 3.2), which employs the theoretical transformation, there is no frequency warping effect as previously defined but a linear scaling of discrete-time frequencies to corresponding analog frequencies which maintains a propotional distance between w_i's as existed between Ω_i's. This scaling for the impulse invariant design is defined below.

$$w_i = \Omega_i/\tau \qquad 2.4.1$$

A proper S/Z-transformation should map the s-domain jw-axis onto the Z-domain unit circle so that the following relationship is satisfied [33]:

$$H_D(e^{jw\tau})\Big|_{z=1} = H_A(jw)\Big|_{\sigma=0} \qquad 2.4.2$$

With this concept in mind, frequency prewarping relations can be developed for the LDI and the Bilinear S/Z-transformation which relate discrete-time frequencies (Ω_i) with corresponding analog frequencies (w_i).

2.4.1 LDI Prewarping Relation

From equation 2.2.7 we have:

$$s = \frac{1}{\tau} \cdot \left[\frac{Z - 1}{Z^{1/2}} \right]$$

Substituting $Z=e^{j\Omega\tau}$ yields:

$$s = \left[\frac{1}{\tau}\right] \cdot \left[\frac{e^{j\Omega\tau} - 1}{e^{j\Omega\tau/2}}\right] = \left[\frac{2j}{\tau}\right] \cdot \left[\frac{e^{j\Omega\tau/2} - e^{-j\Omega\tau/2}}{2j}\right] \qquad 2.4.3$$

From which:

$$s = \sigma + jw = j(2/\tau)\sin(\Omega\tau/2) \qquad 2.4.4$$

Hence, the equivalent analog prewarped frequency, w, of a digital frequency, Ω, is:

$$w = (2/\tau)SIN(\Omega\tau/2) \qquad 2.4.5$$

2.4.2 Bilinear Prewarping Relation

From equation 2.2.10 we have:

$$s = \frac{2}{\tau} \cdot \left[\frac{Z - 1}{Z + 1} \right]$$

Substituting $Z=e^{j\Omega\tau}$ yields:

$$s = \frac{2}{\tau} \cdot \left[\frac{e^{j\Omega\tau} - 1}{e^{j\Omega\tau} + 1}\right] \qquad 2.4.6$$

$$s = \sigma + jw = j(2/\tau)\mathrm{TAN}(\Omega\tau/2) \qquad 2.4.7$$

Hence, the equivalent analog prewarped frequency w of a discrete-time frequency Ω is:

$$w = (2/\tau)\mathrm{TAN}(\Omega\tau/2) \qquad 2.4.8$$

2.5 Bilinear and LDI Switched Capacitor Integration/Summation Circuits

2.5.1 introduction

Switched-capacitor (SC) circuits can be developed to implement the LDI and the bilinear S/Z-transformation. Usually, these circuits will require clock-phased sampling schemes when they are interfaced in switched-capacitor filter (SCF) networks. Before developing switched-capacitor LDI and bilinear integrators/summers, a brief analysis of the switched-capacitor concept will be considered. Figure 2.7(a) depicts a switched-capacitor circuit element composed of a sampling capacitor Cu and an upper plate parasitic capacitance Cp. In most implementations, Cp is the most

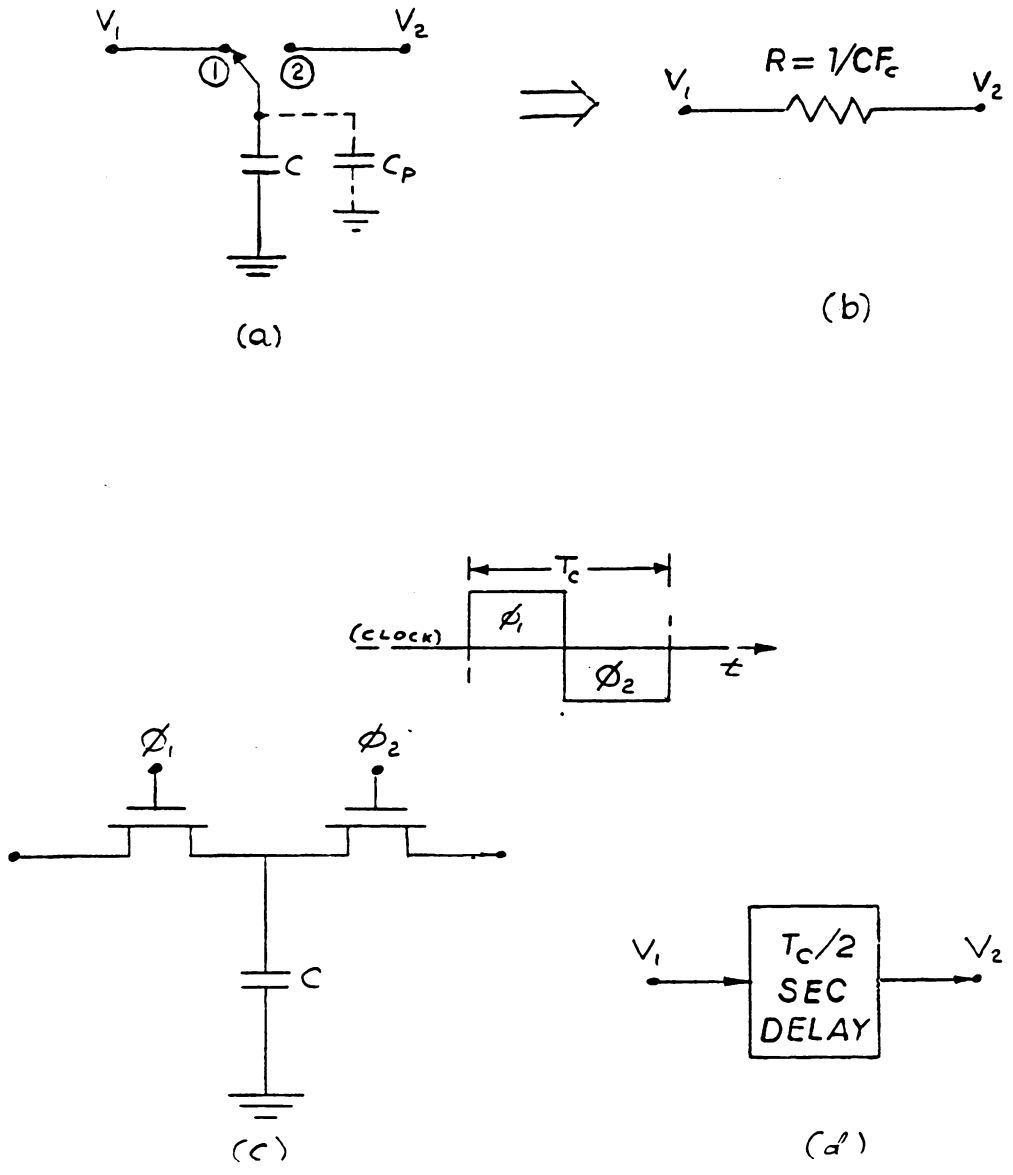

Figure 2.7. Switched-capacitor element: equivalance and implementation.

important of the parasitic capacitors to consider in circuit analysis since it will drain charge to ground that is intended for transfer to succeeding elements. If Cp is assumed to be negligible, a simple charge analysis of figure 2.7(a) yields:

In position (1): $q_1 = CV_1$

In position (2): $q_2 = CV_2$

The amount of charge transfer by switching from position (1) to (2) is:

$$q = C(V_1 - V_2)$$

For a switching rate or sampling frequency (Fs) the average current flow is:

$$I = C(V_2 - V_1)Fs$$

Comparing this current flow to that through a resistor between voltages V_1 and V_2, the following equivalent 'resistance' relationship can be obtained:

$$R = 1/CFs$$

This resistor equivalance is depicted in figure 2.7(b) while the typical MOS implementation of the SC circuit element is shown in figure 2.7(c).

If Cp is not assumed to be negligible there is a drain of charge to ground during the process in which the circuit samples and transfers charge (or signal data) from V_1 to V_2.

The total amount of charge that is actually transferred during one sampling period Ts is:

$$q = (C + Cp)(V_1 - V_2)$$

Accuracy in the processing of signals is more critically demanding in digital systems than in the equivalent analog systems they are to emulate or approximate. Thus, it is important that any SC integrator/summation circuit configure switched-capacitors in ways that best diminish drainage of current by parasitic upper-plate capacitances. The bilinear and LDI integration/summation circuits (depicted in figure 2.8) accomplish this by having their parasitic upper plate capacitances switching between ground and the virtual ground of the negative inputs to the op-amps. The SC circuit element of figure 2.7(a) can furthermore be looked upon as a momentary storage device (or register in digital electronics) configured to delay the transfer of signal charge (or data) by approximately one-half the clock period, Tc/2, as depicted in figure 2.7(d). It is important to bear this concept in mind when clock-phased sampling schemes for SCF circuits are discussed in section 2.6.

2.5.2 Bilinear Single-Sampled (BSS) design.

The basic BSS SC integrator stage with an inverting summer is shown in figure 2.8(I), from which it is seen that

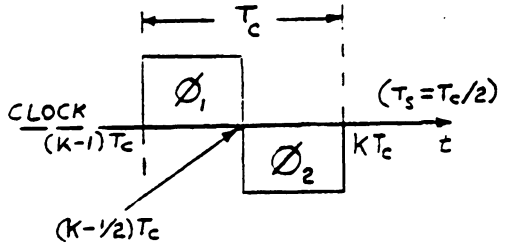

I. Bilinear Single-Sampled (BSS).

$$Vo(Z)= \frac{Cu}{2Ck}\left[\frac{Z-1}{Z+1}\right](V2(Z)-V1(Z)) - \frac{Cx}{Ck}V3(Z)$$

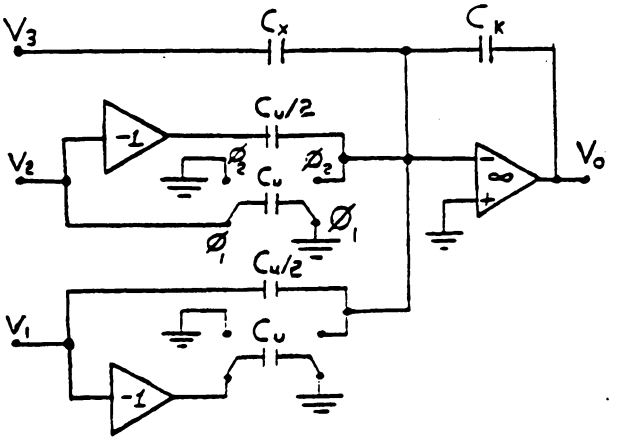

II. Bilinear Double-Sampled (BDS).

a: Positive input configuration.

b: Negative input configuration.

$$Vo(Z)= \frac{Cu}{Ck}\left[\frac{Z-1}{Z+1}\right](V2^{(a)}(Z)-V1^{(b)}(Z)) - \frac{Cx}{Ck}V3(Z)$$

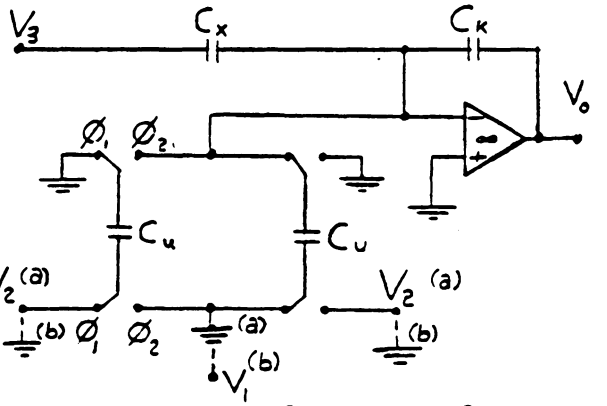

III. LDI.

$$Vo(Z)= \frac{Cu}{Ck}\left[\frac{1}{Z-1}\right](V2(Z)-V1(Z)Z^{1/2}) - \frac{Cx}{Ck}V3(Z)$$

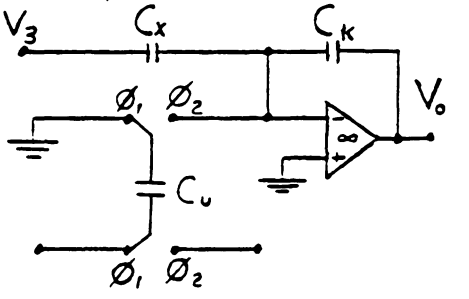

Figure 2.8. BSS, BDS, and LDI integration/summation stages and respective output relations.

the sampling period (τ) is equal to the clock period (Tc). This bilinear integrator is a refined version of the Lee and Chang integrator [21]. Assuming virtual ground at the negative input to the op-amp, a charge analysis yields:

For $(K-1)Tc \leq t \leq (K)Tc$:

$$\begin{aligned} 0 = {} & (Ck)\{Vout[(K-1)Tc] - Vout[(K)Tc]\} \\ & (Cx)\{V_3[(K-1)Tc] - V_3[(K)Tc]\} \\ & (Cu/2)\{V_1[(K-1)Tc - V_1[(K)Tc]\} \\ & (-Cu/2)\{V_2[(K-1)Tc] - V_2[(K)Tc]\} \\ & (Cu)V_2[(K-1)Tc] - (Cu)V_1[(K-1)Tc] \end{aligned}$$

Taking the Z-transform yields:

$$\begin{aligned} Vout(Z)Ck(1-Z^{-1}) = {} & V_2(Z)Cu(1/2)(1+Z^{-1}) \\ & - V_1(Z)Cu(1/2)(1+Z^{-1}) \\ & - V_3(Z)Cx(1-Z^{-1}) \end{aligned}$$

Rearranging leads to the following expression:

$$Vout(Z) = \frac{Cu}{2Ck} \cdot \left[\frac{1 + Z^{-1}}{1 - Z^{-1}}\right] \cdot (V_2(Z) - V_1(Z)) - \frac{Cx}{Ck} \cdot V_3(Z) \qquad 2.5.1$$

where: (i) $z = \exp(jw\tau)$

(ii) $\tau = Tc$

Comparing the integration part of equation (2.5.1) to that of equation (2.2.9) we can derive the following relation for the capacitor ratio Cu/Ck:

$$\frac{Cu}{Ck} = \frac{\tau}{K} = \frac{Tc}{K} \qquad 2.5.2$$

The aliasing frequency (Fa) is given as:

$$Fa = Fc \qquad 2.5.3$$

The corresponding prewarping relationship is obtained with the use of 2.5.2 and 2.2.1:

$$\frac{Cu}{2Ck} \cdot \left[\frac{1 + Z^{-1}}{1 - Z^{-1}}\right] = \frac{Tc}{2K} \cdot \left[\frac{1 + Z^{-1}}{1 - Z^{-1}}\right] = \frac{1}{Ks}$$

$$s = \frac{2}{Tc} \cdot \left[\frac{1 - Z^{-1}}{1 + Z^{-1}}\right]\Bigg|_{z=e^{jw\tau}}$$

$$w = (2Fc)\tan[\Omega/(2Fc)] \qquad 2.5.4$$

where: (i) w - analog prewarped frequency (r/s)

(ii) Ω - discrete-time frequency (r/s)

(iii) Fc - clock frequency (Hz)

2.5.3 Bilinear Double Sampled (BDS) Design

The basic BDS integrator/summation stage, first developed by Temes *et al.* [39], is depicted in figure 2.8(II). This integrator has one limitation: its SC inputs must be either all positive or all negative signals. A charge analysis of

the integrator yields the bilinear transfer function whether the input is positive or negative. Arbitrarily selecting the positive input configuration, a charge analysis yields:

For $(K-1)Tc \leq t \leq (K-1/2)Tc$:

(For $(K-1/2)Tc \leq t \leq (K)Tc$ a charge analysis yields the same results)

$$0 = Ck\{Vout[(K-1)Tc] - Vout[(K-1/2)Tc]\} \qquad 2.5.5$$
$$+ Cx\{V_3[(K-1)Tc] - V_3[(K-1/2)Tc]\}$$
$$+ Cu\{V_2[(K-1)Tc] + V_2[(K-1/2)Tc]\}$$

Taking the z-transform:

$$Vout(Z)Ck(Z^{-1/2}-Z^{-1}) = V_2(Z)Cu(Z^{-1/2}+Z^{-1}) - Cx\,V_3(Z)(Z^{-1/2}-Z^{-1})$$

$$Vout(Z) = \frac{Cu}{Ck} \cdot \left[\frac{Z^{-1/2}+Z^{-1}}{Z^{-1/2}-Z^{-1}}\right] V_2(Z) - \frac{Cx}{Ck} V_3(Z) \qquad 2.5.6$$

where: (i) $Z = \exp(jw\tau)$

(ii) $\tau = Tc$

Since $Tc=2Ts$ (see figure 2.8(II)):

$$Z = \exp(jw2Ts) = [\exp(jwTs)]^2$$
$$Z\{\tau=Tc\} = Z^2\{\tau=Ts\} \qquad 2.5.7$$

Substituting 2.5.7 into 2.5.6 yields:

$$Vout(Z) = \frac{Cu}{Ck} \cdot \left[\frac{Z^{-1} + Z^{-2}}{Z^{-1} - Z^{-2}}\right] \cdot V_2(Z) - \frac{Cx}{Ck} \cdot V_3(Z) \qquad 2.5.8$$

$$Vout(Z) = \frac{Cu}{Ck} \cdot \left[\frac{1 + Z^{-1}}{1 - Z^{-1}}\right] \cdot V_2(Z) - \frac{Cx}{Ck} \cdot V_3(Z) \qquad 2.5.9$$

where: (i) $Z = \exp(jw\tau)$

(ii) $\tau = Ts = Tc/2$

Equating the integration part of 2.5.9 to that of 2.2.9 yields the following capacitor ratio Cu/Ck relationship:

$$\frac{Cu}{Ck} = \frac{\tau}{2k} = \frac{Tc}{4K} \qquad 2.5.10$$

The aliasing frequency (Fa) is given as:

$$Fa = 2Fc \qquad 2.5.11$$

The corresponding prewarping relationship is obtained with the use of 2.5.10 and 2.2.1:

$$\frac{Cu}{Ck} \cdot \left[\frac{1 - Z^{-1}}{1 + Z^{-1}}\right] = \frac{Tc}{4K} \cdot \left[\frac{1 + Z^{-1}}{1 - Z^{-1}}\right] = \frac{1}{Ks}$$

$$s = \frac{4}{Tc} \cdot \left[\frac{1 - Z^{-1}}{1 + Z^{-1}}\right] \Bigg|_{Z=e^{jw\tau}}$$

$$w = (4Fc)\tan[\Omega/4Fc] \qquad 2.5.12$$

where: (i) w - analog prewarped frequency (r/s)

(ii) Ω - discrete-time frequency (r/s)

(iii) Fc - clock frequency (Hz)

Note: the aliasing frequency is twice that of the BSS (section 2.5.2) and the LDI (section 2.5.4) integrators.

The BDS integrator can also be configured as a differential integrator. An example of this is depicted in the termination stages of a BDS 7th-order elliptic lowpass filter shown in figure 4.9.

2.5.4 LDI SC Integration/Summation Circuit Design

The basic LDI SC integration/summation circuit design is shown in figure 2.8(III). A charge analysis yields:

For $(K-1)Tc \leq t \leq (K)Tc$:

$$0 = Ck\{Vout[(K-1)Tc] - Vout[(K)Tc]\} + Cx\{V_3[(K-1)Tc] - V_3[(K)Tc]\} + CuV_2[(K-1)Tc] - CuV_1[(K-1/2)Tc] \qquad 2.5.13$$

Taking the Z-transform yields:

$$Ck(1 - Z^{-1})Vout(Z) = Cu(V_2(Z)Z^{-1} - V_1(Z)Z^{-1/2}) - Cx(1 - Z^{-1})V_3(Z) \qquad 2.5.14$$

Equation 2.5.14 reduces to:

$$Vout(Z) = \frac{Cu}{Ck} \cdot \left[\frac{1}{1-Z^{-1}}\right] \cdot (V_2(Z)Z^{-1} - V_1(Z)Z^{-1/2}) - \frac{Cx}{Ck} \cdot V_3(Z) \qquad 2.5.15$$

where: (i) $Z = \exp(jw\tau)$

(ii) $\tau = Tc$

Note that V_2 exhibits a half cycle delay over V1 and that the function $(1/(1-Z^{-1}))$ is not equivalent to that called for by the LDI transformation of equation 2.2.6, namely $(Z^{-1/2}/(1-Z^{-1}))$. If, however, a half cycle lead is added to V_2 then the SC integrator stage becomes an LDI stage. Thus, setting $V_2 = V_2 * Z^{-1/2}$ yields:

$$Vout(Z) = \frac{Cu}{Ck} \cdot \left[\frac{Z^{-1/2}}{1-Z^{-1}}\right] \cdot (V_2(Z) - V_1(Z)) - \frac{Cx}{Ck} \cdot V_3(Z) \qquad 2.5.16$$

where: (i) $Z = \exp(jw\tau)$

(ii) $\tau = Tc$

Comparing the integration coefficient of equation 2.5.16 to that of 2.2.6 we can derive the following relation for the capacitor ratio Cu/Ck:

$$\frac{Cu}{Ck} = \frac{\tau}{K} = \frac{Tc}{K} \qquad 2.5.17$$

The aliasing frequency (Fa) is given as:

$$Fa = Fc \qquad 2.5.18$$

The corresponding prewarping relationship is obtained with the use of equations 2.5.17 and 2.2.1:

$$\frac{Cu}{Ck} \cdot \left[\frac{Z^{-1/2}}{1 - Z^{-1}}\right] = \frac{Tc}{K} \cdot \left[\frac{Z^{-1/2}}{1 - Z^{-1}}\right] = \frac{1}{Ks}$$

$$s = \frac{2j}{Tc} \cdot \left[\frac{1 - Z^{-1}}{(2j)Z^{-1/2}}\right]\Bigg|_{z=e^{jw\tau}}$$

$$w = (2Fc)\sin[\Omega/(2Fc)] \qquad 2.5.19$$

where: (i) w - analog prewarped frequency (r/s)

(ii) Ω - discrete-time frequency (r/s)

(iii) Fc - clock frequency (Hz)

2.6 Clock Phasing in SC Ladder Networks

Unlike the BDS integrator stage, where stored charge or signal data in the input switched capacitors is transferred for processing to the op-amp on both phases (ϕ_1 and ϕ_2) of the clock (see figure 2.8(II)), for the LDI and the BSS integrator stages delayed signal data is transferred on only one phase of the clock. It then becomes imperative for any BSS or LDI SC filter to adopt sampling schemes for transfer-

ring and processing sampled signal data from the input to the output of the circuit. Such schemes, which primarily apply to ladder networks of SC integration/summation stages, involves proper clock-phased signal-sampling of the stages. The clock-phased signal-sampling schemes to be discussed have not been mathematically proven to be correct. They are primarily based on observations made on switched capacitor circuit simulations.

Both the LDI and the BSS integrator stages can be treated as a signal processing unit, P, with inputs either delayed or not by a half-clock-cycle time lead of $Z^{1/2}$ as depicted in figure 2.9. For the present clock phase, ϕ_1, SC charge is delivered to P after a half clock period time delay of $Z^{1/2}$, while on a ϕ_2 clock phase setup, no time delay is added to the SC charge delivery. The overall input signal to either the LDI or the BDS integrator stages can be any combination of positive and negative input signals. There is only one restriction: sampled charge of all input signals to an integration/summation stage, whether or not delayed by a half clock period, must be transferred to the processor P simultaneously. There cannot be situations where in the same integration stage and on the same clock phase some switched capacitors are sampling unconnected to the op-amp

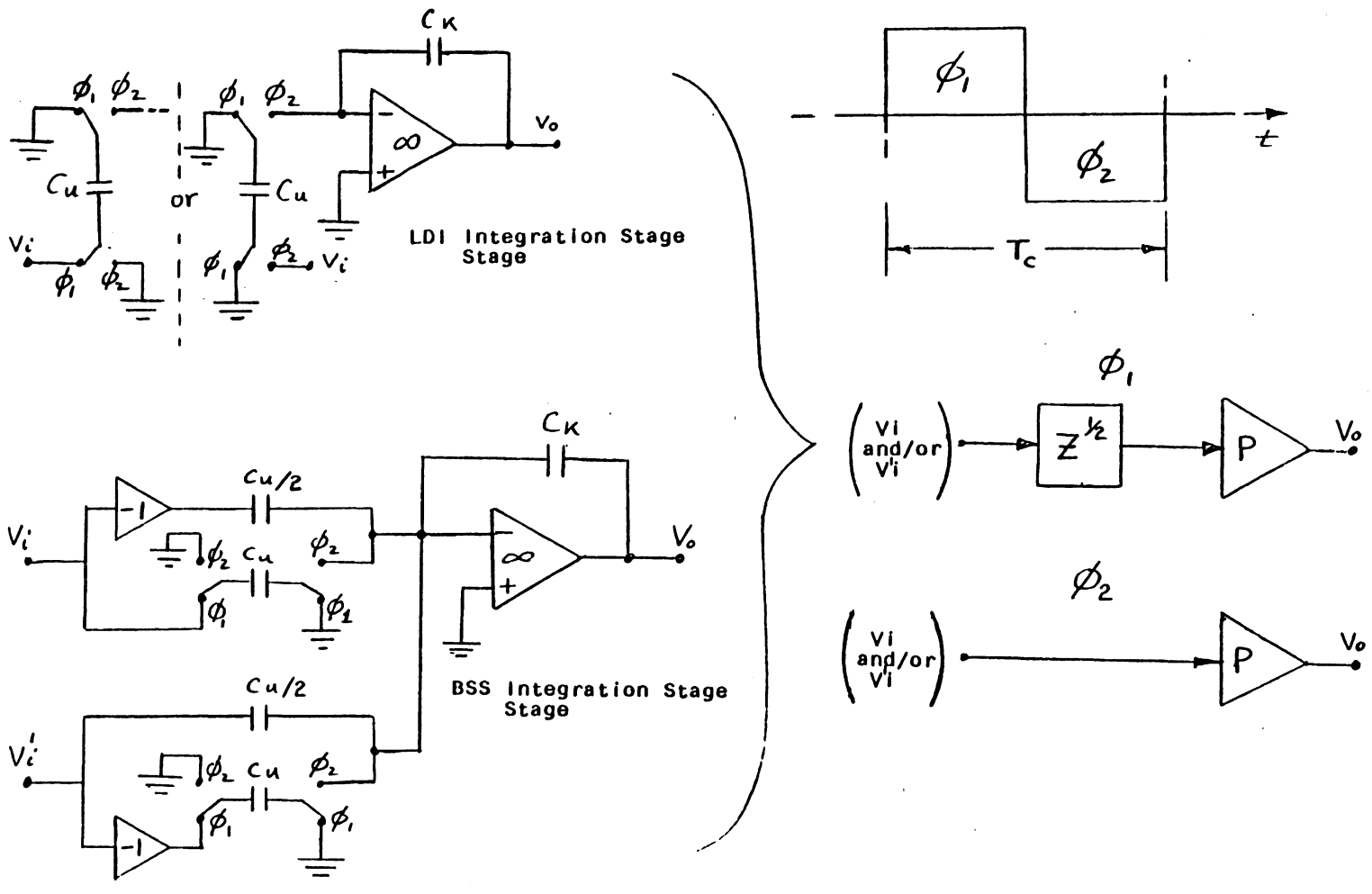

Figure 2.9. signal data processor concept of the LDI and the BSS integration stage.

while others are transferring charge to the op-amp. This situation is depicted for an example integration stage in figure 2.10. Here Cu1 is transferring charge to the op-amp while Cu2 is unconnected to the op-amp sampling V1 on the same clock phase. The op-amp (or processor P) does not receive a charge for processing on the same clock phase which is proportional to the difference between the two input signals (V1-V2) but one which is proportional to either one of the input signals, depending on the clock phase. There are two distinct clock-phased sampling schemes which apply to both BDS and LDI SC filter or discrete-time system designs. Both schemes will be analyzed by means of a example 3rd order leapfrog LDI low-pass elliptic SC filter depicted by the signal flow diagram of figure 2.11.

Clock-phased sampling Scheme I has alternate integrator stages receiving and processing input data on the same clock phase ,with (or without) leading half clock period delays. Scheme I as applied to figure 2.11 is depicted in figure 2.12(a) with the corresponding SC circuit diagram in figure 2.12(b). For the current clock phase ϕ_1, P2 receives and processes input data (figure 2.12(a)-i) while P1 and P3 wait for the next clock phase ϕ_2 to receive and process data (figure 2.12(a)-ii). Clock-phased sampling scheme II has

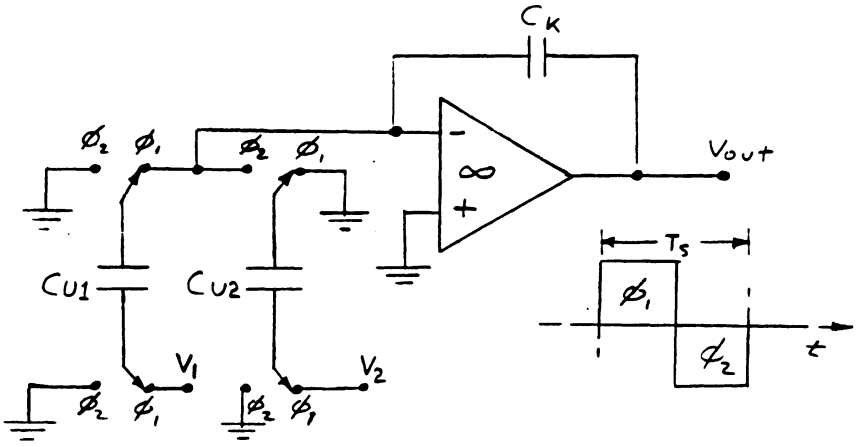

Figure 2.10. Improper clock-phased signal sampling implementation for an example LDI integrator.

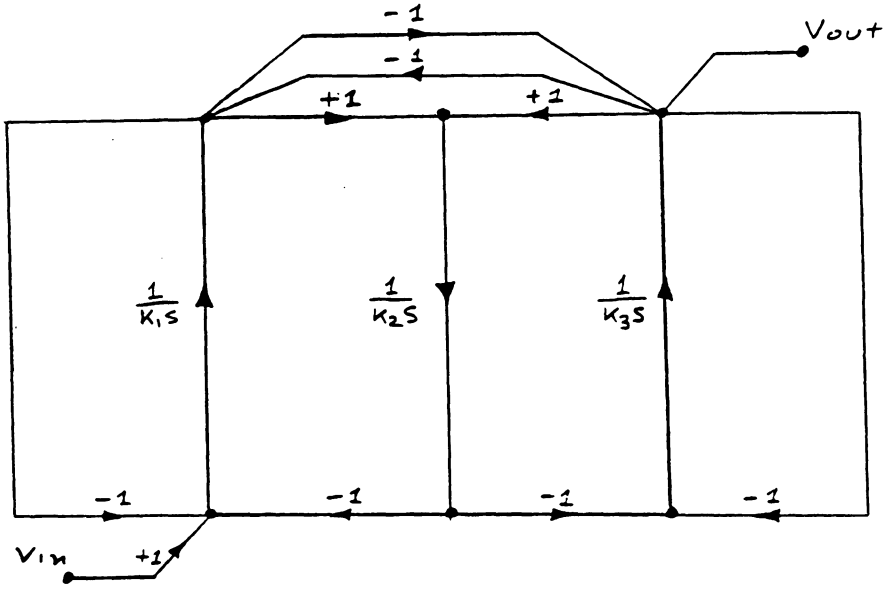

Figure 2.11. 3rd-order elliptic lowpass sc filter leapfrog signal flow diagram.

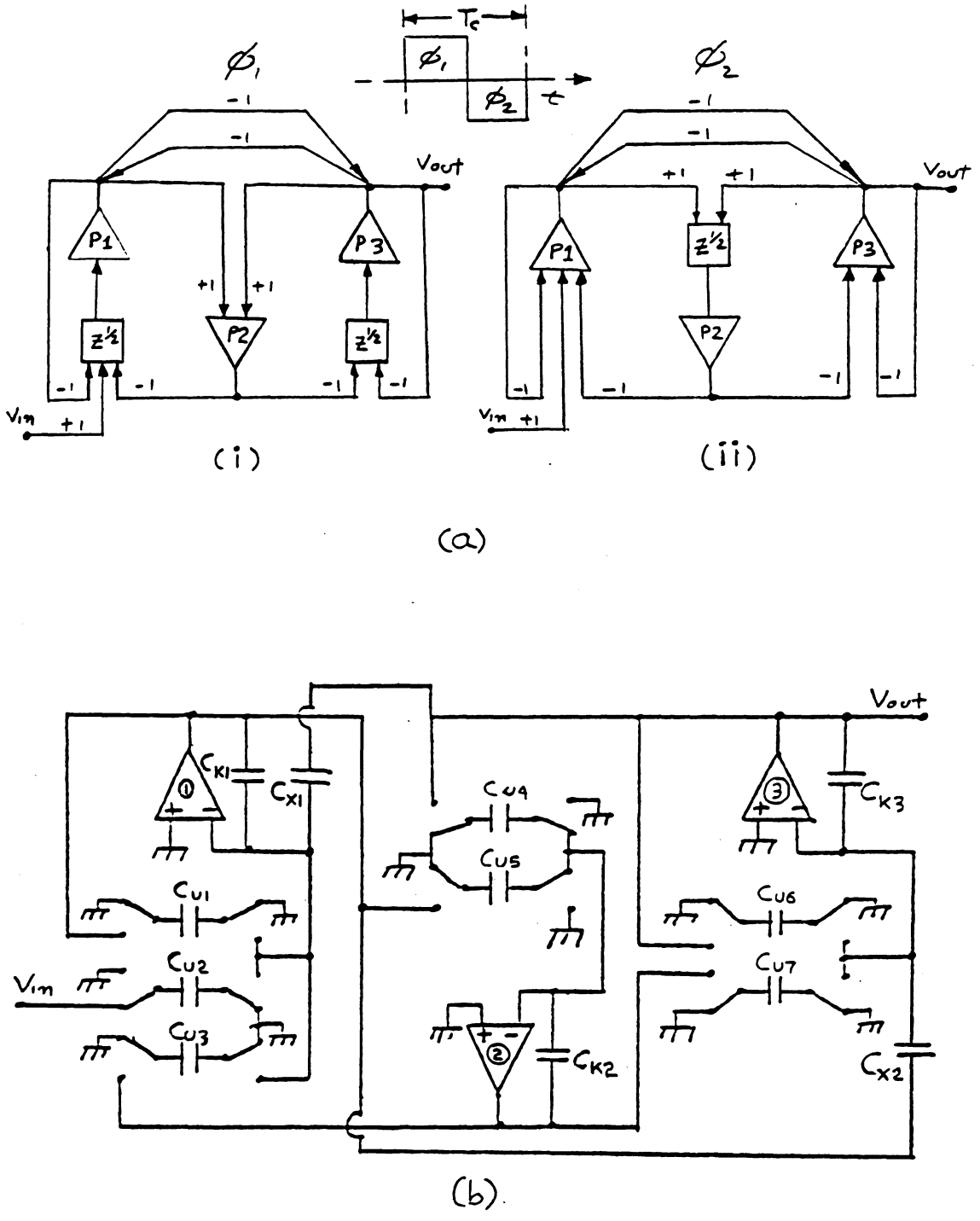

Figure 2.12. Clock-phased signal-sampling scheme I implementation for the 3rd-order elliptic lowpass sc filter of figure 2.11.

all integrator stages receiving and processing input data on the same clock phase, with (or without) leading half clock period delays, while on the next clock phase they wait while the switched capacitors sample input signals or discharge to ground. Scheme II as applied to figure 2.11 is depicted in figure 2.13(a) with the corresponding SC circuit diagram in figure 2.13(b). For a current clock phase ϕ_1, processors P1, P2, and P3 receive and process data (figure 2.13(a)-i) while on the next clock phase $,\phi_2$, they all wait while the switched capacitors sample the input signal (figure 2.13(a)-ii).

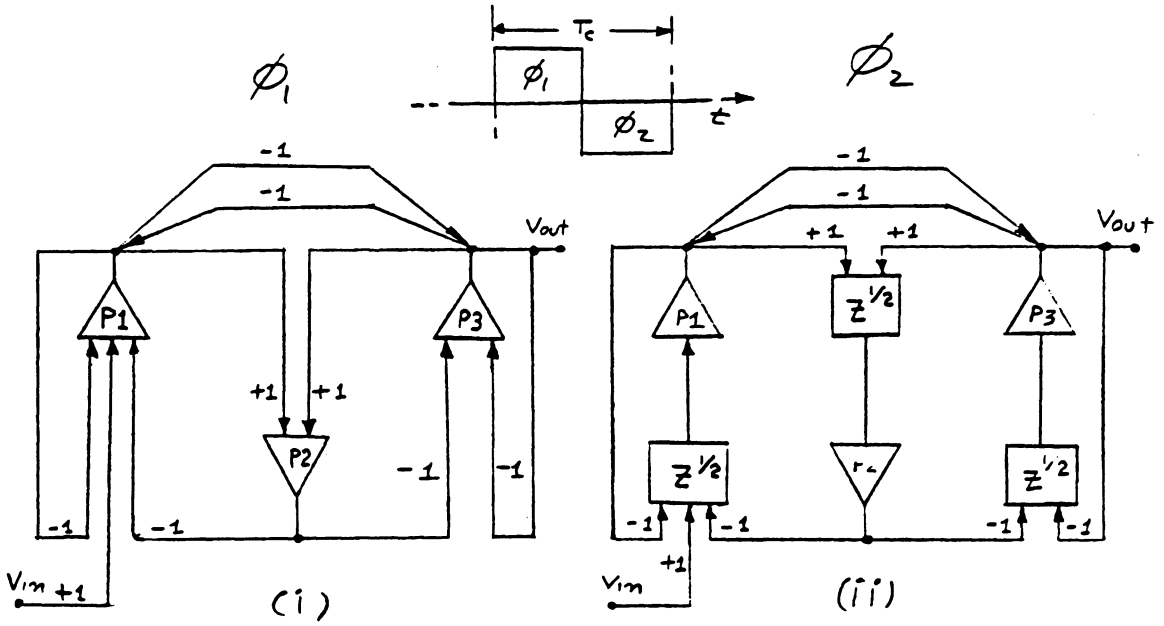

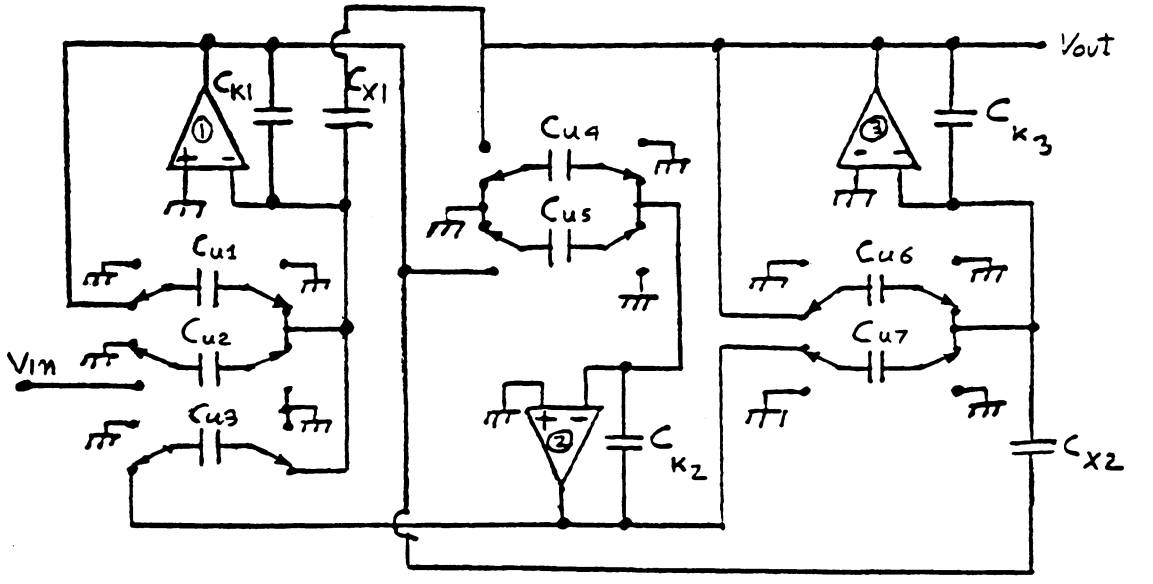

Figure 2.13. Clock-phased signal-sampling scheme II implementation for the 3rd-order elliptic lowpass sc filter of figure 2.11.

Chapter III

DISCRETE-TIME SYSTEM DESIGN STRATEGIES AS APPLIED TO SWITCHED CAPACITOR FILTERS

3.1 introduction

The purpose of this chapter is to provide and review fundamental concepts in discrete-time system analysis and design which are, or can potentially be, applied to switched capacitor system designs. There will first be a review of fundamental discrete-time filter design strategies. The impulse invariant (II) filter design technique, with its use of the ideal S/Z-transformation (equation 2.1.1), will then be discussed. This design technique represents the ideal approach in designing discrete-time filters, since it lacks frequency warping effects and it provides a preservation of both gain and phase in its S/Z-transformation, for a sufficiently bandlimited analog filter. There has yet to be developed a switched capacitor realization technique for implenting II filter designs. Nevertheless, the II filter design will here be presented as a means for evaluating the design performance of the less accurate bilinear and LDI filter design techniques. A discussion of frequency warping, classical prewarping, and aliasing effects in bilinear and LDI filter designs will then be presented, followed by de-

sign formulations by Antoniou [3] and Constantinides [6]. Finally, a switched capacitor realization approach for implementing bilinear and LDI filter designs using the leapfrog technique [12] will be presented by way of an example.

Figure 3.1 illustrates the different design strategies which can be implemented in the design of discrete-time filters. There are 4 main strategies to follow, starting with the discrete-time specifications:

1. Adopt a normalized lowpass filter which best meets the discrete-time attenuation characteristics. Classically prewarp the discrete-time attenuation characteristic at one denormalizing frequency. Obtain the denormalized analog filter. S/Z-transform to obtain the denormalized discrete-time filter.
2. Similar strategy to that of 1) except that the normalized low-pass filter is S/Z-transformed to a normalized lowpass digital filter. Using Constantinides [6] z-domain denormalizing transformations, the denormalized digital filter is then obtained.
3. Prewarp the characteristic frequencies of the passband-stopband transition: the passband edge frequency (Ω_{pe}) and the stopband edge frequency (Ω_{se}) (see figures 3.9(a)-(b)). Derive or adopt the normalized

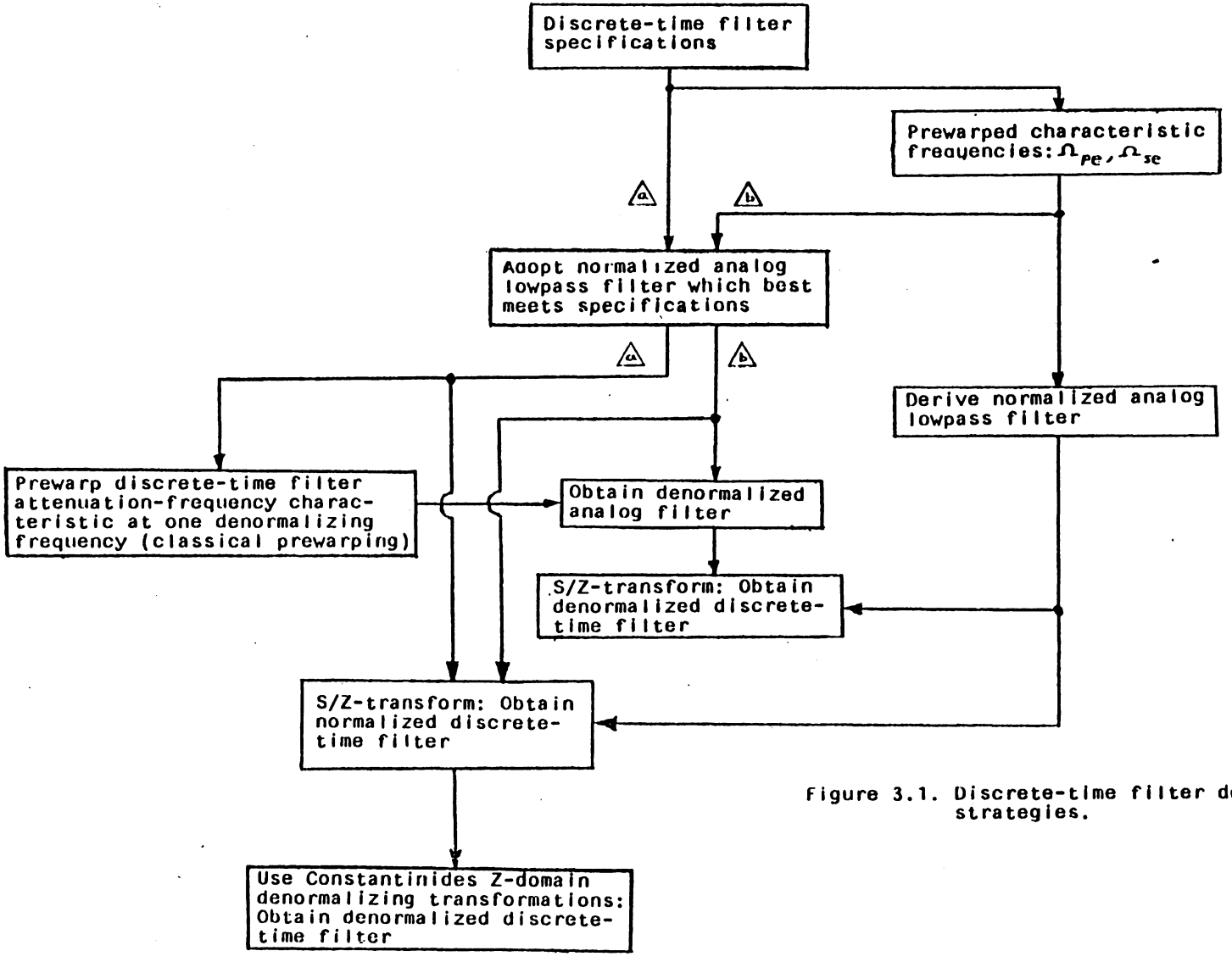

Figure 3.1. Discrete-time filter design strategies.

lowpass filter that best meets the prewarped passband-stopband transition (along with the passband loss). Obtain the denormalized analog filter and S/Z-transform to obtain the denormalized discrete-time filter.

4. Similar strategy to that of 3) except that the normalized lowpass filter is S/Z-transformed to a discrete-time normalized lowpass filter. Constantinides z-domain transformations are then employed to obtain the denormalized discrete-time filter.

As will be discussed in section 3.3, the frequency warping distortions which occur in any S/Z-domain filter transformation can adversely affect the final attenuation response to the extent that a higher order filter design may be required to compensate. Strategies 3 and 4 (with the actual derivation of the normalized analog lowpass filter) are in general the best design schemes to implement. This is because they involve the computation of the required filter order and filter approximation which best meets the prewarped passband edge and stopband edge frequencies for a fixed passband loss. Overall, the second best strategy is number 3 with the required filter approximation adopted from filter tables instead of being more accurately derived. As will be

discussed in chapter 4, an LDI 8th-order elliptic lowpass switched-capacitor (SC) filter was designed, built, and tested using this strategy. The third preferable design strategy is 1, which was adopted in the design, construction, and test of a 7th-order bilinear double-sampled elliptic lowpass SC filter as discussed in chapter 4. Adopting design strategy number 2 with which a discrete-time filter is directly computed without previously prewarping the characteristic frequencies risks too much frequency warping distortion in the final attenuation-frequency response. This is particularly true at low sampling-to-signal frequency ratios.

There are no restrictions involved in adopting bilinear or LDI S/Z- transformations with design strategies 1,3, and 4. The impulse-invariant S/Z-transformation on the other hand can create acute aliasing distortion problems in high-pass,and bandstop filter designs which are best alleviated by adopting design strategies which use the Constatinides z-domain denormalizing transformations.

3.2 Impulse Invariant (II) Design: Frequency Transformation, Aliasing Effects, and Design Technique.

The following discussion concerns the transformation of any s-domain transfer function, $H_A(s)$, to its discrete-time equivalent, $H_D(Z)$, using the theoretical S/Z-transformation[28].

$$Z = e^{s\tau} \qquad 3.2.1$$

Defining the unit-sample response of the digital filter as equally spaced samples of the impulse response of the analog filter as:

$$h_D(n) = h_A(n\tau) \qquad 3.2.2$$

the z-transformation of $h_D(n)$ is related to the Laplace transformation of the $h_A(n)$ as [28]:

$$H_D(Z)\Big|_{Z=e^{s\tau}} = (1/\tau) \sum_{K=-\infty}^{\infty} H_A(s + j((2\pi/\tau)K)) \qquad 3.2.3$$

The frequency response of the digital filter can be expressed as:

$$H_D(e^{jw\tau}) = (1/\tau) \sum_{K=-\infty}^{\infty} H_A(jw + j((2\pi/\tau)K)) \qquad 3.2.4$$

From the discussion of the theoretical S/Z-transformation in chapter 2 it can be concluded:

<u>if</u> $\quad H_A(jw) = 0 \quad , \quad \pi/\tau \leq |w| \qquad 3.2.5$

Then

$$H_D(e^{jw\tau}) = (1/\tau)H_A(jw) \quad , \quad -\pi/\tau \leq w \leq \pi/\tau \qquad 3.2.6$$

No practical analog filter is strictly bandlimited. Therefore, the interference of successive terms in 3.2.4 creates aliasing between successive reproductions of $H_A(jw)$ by $H_D(e^{jw\tau})$. This is depicted in figure 3.2.

For impulse invariant filter designs the analog frequencies (w) and the discrete-time frequencies (Ω) are related in the following manner:

$$w = \Omega/\tau \qquad 3.2.7$$

The above equation is analogous to the frequency prewarping relations of the LDI and the bilinear S/Z-tranformations with the fundamental difference that the analog and digital frequencies in 3.2.7 are in linear proportion to each other. With equation 3.2.7 there are no frequency warping effects which occur with LDI and bilinear transformations where the proportional differences between frequencies in the analog domain are not preserved in the discrete-time domain. For this reason, impulse invariant filter designs require the same order as their equivalent analog counterparts to meet given specifications. Furthermore, for a sufficiently bandlimited filter, or one with small aliasing distortions, there are no critical magnitude and phase distortions that can exist in LDI and bilinear filters (see section 3.3). The phase and attenuation loss characteristic of the analog

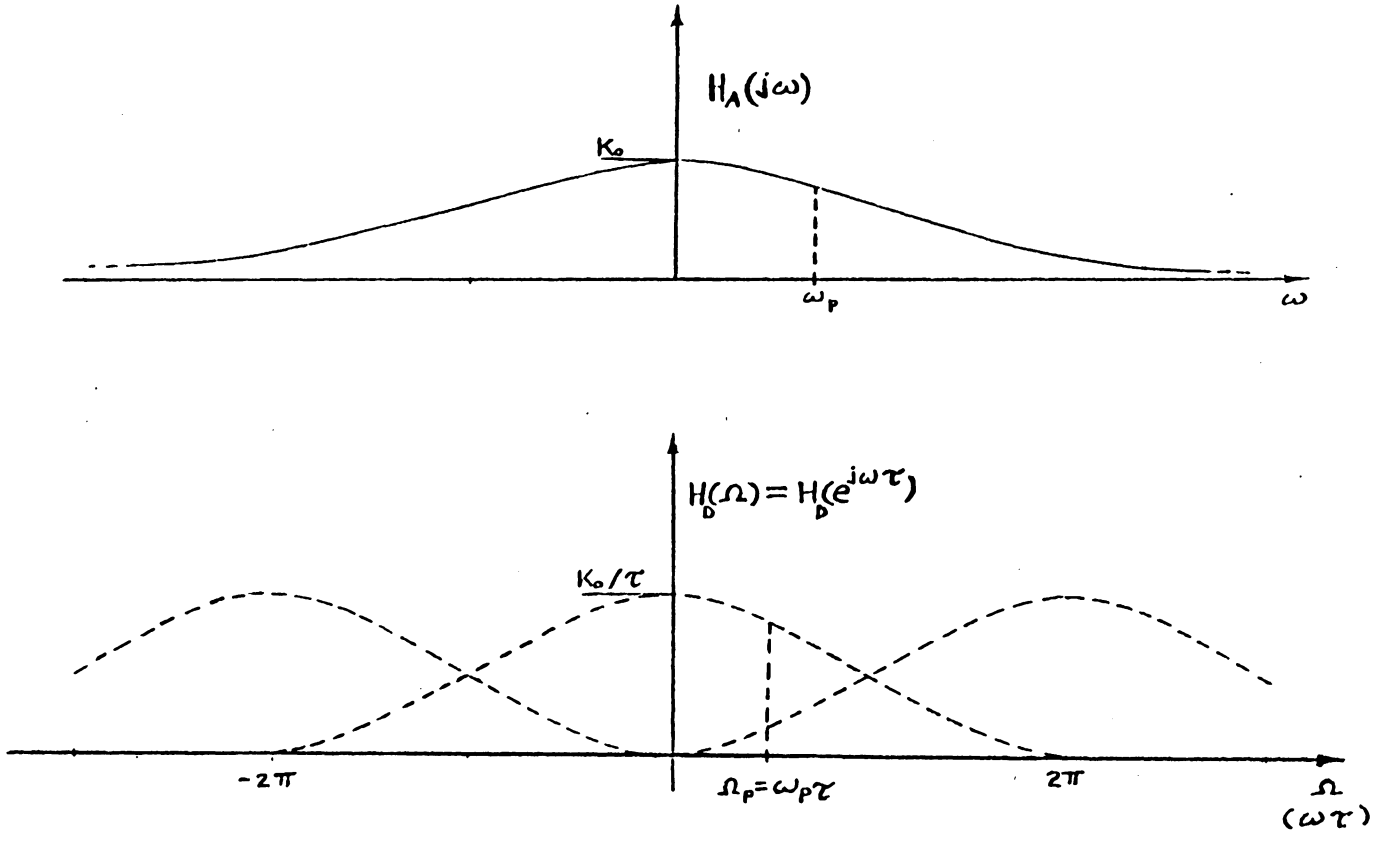

Figure 3.2. Impulse invariant design technique: discrete-time reproduction of an analog attenuation-frequency response with aliasing.

filter is significantly preserved in the digital filter as long as the analog filter is sufficiently bandlimited in the range:

$$-\pi Fs \leq w \leq \pi Fs \qquad \text{(Fs - sampling frequency)}$$

To introduce the concept of impulse invariant (II) filter design, consider an analog filter expressed in the form of a partial fraction expansion.

$$H_A(s) = \sum_{i=1}^{N} \frac{A_i}{s+S_i} \qquad 3.2.9$$

The corresponding impulse response is:

$$H_A(t) = \sum_{i=1}^{N} A_i e^{-S_i \tau} u(t) \qquad 3.2.10$$

For the equivalent digital filter the unit-sample response is:

$$h_D(n) = h_A(n\tau) = \sum_{i=1}^{N} A_i (e^{-S_i \tau n}) u(n\tau) \qquad 3.2.11$$

Taking the z-transform of 3.2.11 yields:

$$H_D(Z) = \sum_{i=1}^{N} \frac{A_i}{1-e^{-S_i \tau} Z^{-1}} \qquad 3.2.12$$

Note that though the theoretical S/Z-transformation was used to obtain equations 3.2.3 and 3.2.12, the impulse in-

variant design procedure does not necessarily correspond to a mapping from the s-domain to the z-domain by that transformation or any other transformation. Note that though the Z-domain poles in equation 3.2.12 could have been obtained from the analog poles with the use of equation 3.2.1 the Z-domain zeroes are a function of both the A_i's and the poles of the analog filter.

Assuming $H_A(jw)$ is sufficiently bandlimited over $-\pi/\tau \leq w \leq \pi/\tau$, by equation 3.2.6 the corresponding digital and analog frequency response amplitudes are related in the following manner:

$$|H_D(e^{jw\tau})| \cong (1/\tau)|H_A(jw)| \qquad 3.2.13$$

To compensate for the above loss in output gain of the digital filter as illustrated in Figure 3.2, the gain in the digital filter can be adjusted by a factor of τ. The resulting equivalent impulse invariant filter of the analog filter of equation 3.2.9 is then expressed as follows:

$$H_D(Z) = \sum_{i=1}^{N} \frac{\tau A_i}{1-e^{-S_i\tau} Z^{-1}} \qquad 3.2.14$$

The following algorithm as developed by Gold and Rabiner[33] and Antoniou[3] can be summarized and extended in the following manner. Consider:

$$H_A(s) = \frac{KN(s)}{D(s)} = K \frac{\prod_{i=1}^{M} (s+S_i)}{\prod_{j=1}^{N} (s+P_j)} \qquad 3.2.15$$

Remark: For a given system to be digitized and to avoid "intolerable" aliasing effects one should assume $M \leq N$ [3].

For any complex pole (P_j) or zero (S_i) in 3.2.15 there exists a corresponding complex conjugate pole (P_c) or zero (S_d) such that:

$$P_c = P_j^*$$
$$S_d = S_i^*$$

Let: $H_A(s) = \frac{KH_{A_1}(s)}{H_{A_2}(s)}$ or $H_A(jw) = \frac{KH_{A_1}(jw)}{H_{A_2}(jw)}$

where: $$H_{A_1}(s) = \frac{1}{D(s)} = \prod_{j=1}^{N} \frac{1}{s+P_j} \qquad 3.2.16(a)$$

$$H_{A_2}(s) = \frac{1}{N(s)} = \prod_{i=1}^{M} \frac{1}{s+S_i} \qquad 3.2.16(b)$$

By partial fraction expansion:

$$H_{A_1}(s) = \sum_{j=1}^{N} \frac{C_j}{S+P_j} \qquad 3.2.17(a)$$

$$H_{A_2}(s) = \sum_{i=1}^{M} \frac{D_i}{s+S_i} \qquad 3.2.17(b)$$

Assuming both $H_{A1}(jw)$ and $H_{A2}(jw)$ are sufficiently band-limited over the interval $-\pi/\tau \leq w \leq \pi/\tau$, then by 3.2.6:

$$H_{D_1}(e^{jw\tau}) \cong (1/\tau)H_{A_1}(jw)$$

$$H_{D_2}(e^{jw\tau}) \cong (1/\tau)H_{A_2}(jw)$$

Therefore:

$$\mathcal{Z}\left[H_A(jw)\right] = K\mathcal{Z}\left[\frac{H_{A_1}(jw)}{H_{A_2}(jw)}\right] \cong K\,\frac{H_{D_1}(e^{jw\tau})}{H_{D_2}(e^{jw\tau})} \qquad 3.2.18$$

Taking then the Z-transform of 3.2.17(a) and 3.2.17(b) yields:

$$H_{D_1}(Z) = \sum_{j=1}^{N} \frac{C_j Z}{Z-e^{-\tau P_j}} = \frac{N_1(Z)}{D_1(Z)} \qquad 3.2.19(a)$$

$$H_{D_2}(Z) = \sum_{i=1}^{M} \frac{D_i Z}{Z-e^{-\tau S_i}} = \frac{N_2(Z)}{D_2(Z)} \qquad 3.2.19(b)$$

Hence: $$H_D(Z)=\mathcal{Z}\left[H_A(s)\right] = \frac{KN_1(Z)D_2(Z)}{N_2(Z)D_1(Z)} \qquad 3.2.20$$

For derivation purposes let:

$$H_{At}(s) = \sum_{i=1}^{Q} \frac{B_i}{s+G_i} \qquad 3.2.21$$

where: $(t,Q,B,G) = \{(1,N,C_i,P_i),(2,M,D_i,S_i)\}$

In taking the Z-transform of 3.2.21 two operations may arise:

1) G_i is a simple root, hence:

$$\mathcal{Z}\left[\frac{B_i}{s+G_i}\right] = \frac{B_i}{1-e^{-G_i\tau}\,Z^{-1}} \qquad 3.2.22$$

2)G_i is a complex root where another root $G_i=G_i^*$, Hence:

$$\mathcal{Z}\left[\frac{B_i}{S+G_i} + \frac{B_i^*}{S+G_i^*}\right] = \frac{B_i}{1-e^{-G_i\tau}\,Z^{-1}} + \frac{B_i^*}{1-e^{-G_i^*\tau}\,Z^{-1}}$$

$$\mathcal{Z}\left[\frac{B_i}{S+G_i} + \frac{B_i}{S+G_i^*}\right] = \frac{(B_i+B_i^*)-Z^{-1}(B_i e^{-G_i^*\tau}+B_i^* e^{-G_i\tau})}{1-Z^{-1}(e^{-G_i\tau}+e^{-G_i^*\tau})+Z^{-2}e^{-(G_i+G_i^*)\tau}} \qquad 3.2.23$$

where: (B_i, B_i^*) and (G_i, G_i^*) are complex conjugate pairs:

Letting:

$$B_i = g_i + jh_i$$
$$G_i = r_i + jw_i$$

Equation 3.2.23 then reduces to:

$$\mathcal{Z}\left[\frac{B_i}{S+G_i} + \frac{B_i^*}{S+G_i^*}\right] = \qquad 3.2.24$$

$$\frac{2g_i - Z^{-1}e^{-r_i\tau}[2g_i\cos(w_i\tau) - 2h_i\sin(w_i\tau)]}{1 - 2Z^{-1}e^{-r_i\tau}\cos(w_i\tau) + Z^{-2}e^{-2r_i\tau}}$$

In summary, both equations 3.2.22 and 3.2.24 apply in taking the Z-transform of (3.2.17(a)) and (3.2.17(b)) before finally computing (3.2.20). There is however one further important point to consider. $H_D(Z)$ may turn out to be unstable since some of the roots of $N_2(Z)$ may be located outside the unit circle. This problem can easily be overcome by replacing the unstable roots in $N_2(Z)$ by their reciprocals. For a proof on how this is so see Antoniou[3]. Below are some important characteristic of the impulse invariant design method:

a) Advantage: Phase as well as attenuation loss characteristics of the analog filter are preserved.

b) Disadvantage: Though it yields good results for lowpass and bandpass filters (at large sampling-to-signal frequency ratios) it may result in unwanted aliasing distortions for highpass and bandstop filters. This last effect is particularly true at low sampling-to-signal frequency ratio operations. To counter this problem in highpass and bandstop designs, the analog normalized lowpass filter may first be transformed to a digital <u>normalized</u> lowpass filter by this method. The filter is then denormalized with the use of the Constantinides transformations (see section 3.5)

3.3 Prewarped Denormalized Frequency Effects and Aliasing Analysis of LDI and Bilinear filters.

Frequency warping distortion effects which are to be accounted for in any discrete-time filter design depend not only on the S/Z-transformation used, but also on the adopted operating sampling-to-reference frequency ratio. The reference frequency is the cutoff frequency for lowpass and highpass filters and the upper cutoff frequency for bandpass and bandstop filters. As discussed in section 3.2 there is no frequency warping distortion with the impulse invariant (II) filter, and for a sufficiently bandlimited analog filter the frequency response of the corresponding II digital filter is an aliased version of the analog filter's frequency response as depicted in figure 3.2. The phase and the attenuation loss characteristic of the analog filter will be preserved with the corresponding II digital filter as long as the analog filter is sufficiently bandlimited in the range:

$$-\pi Fs \leq w \leq \pi Fs \qquad 3.3.1$$

For impulse invariant designs, equation (3.3.1) defines a design constraint on the operating sampling-to-reference frequency ratio of the eventual digital filter.

In constrast, the LDI and the bilinear transformations create frequency warping distortions which must be accounted

for and which can affect the required order of the digital filter along with its attenuation response. The LDI and the bilinear prewarping relations as derived in chapter 2 can be normalized in the following manner:

Bilinear: $G_1(K) = Fw/Fs = (1/\pi)\tan(K\pi)$

LDI: $G_2(K) = Fw/Fs = (1/\pi)\sin(K\pi)$

where: $K = F_\Omega/Fs$

F_Ω = discrete-time frequency (Hz)

Fw= prewarped analog frequency (Hz)

Functions $G_1(K)$ and $G_2(K)$ are plotted in figure 3.3 along with a reference line of a 1/1 slope. Suppose one were to design a digital filter with a passband-stopband transition frequency width, d, and with the frequency response characteristic defined by the unbroken line in figure 3.4. With the bilinear S/Z-transformation, the characteristic frequencies F_{sc} and F_{pc} are prewarped to higher frequencies while, with the LDI transformation, they are prewarped to lower frequencies. The prewarped passband-stopband transition, to which the analog prewarped filter must correspond, is smaller than the transition of the digital filter in the LDI design and larger in the bilinear design. This is depicted by d_1 and d_2 in figures 3.3 and 3.4. As a rule, for a fixed passband loss, higher order specifications are required for

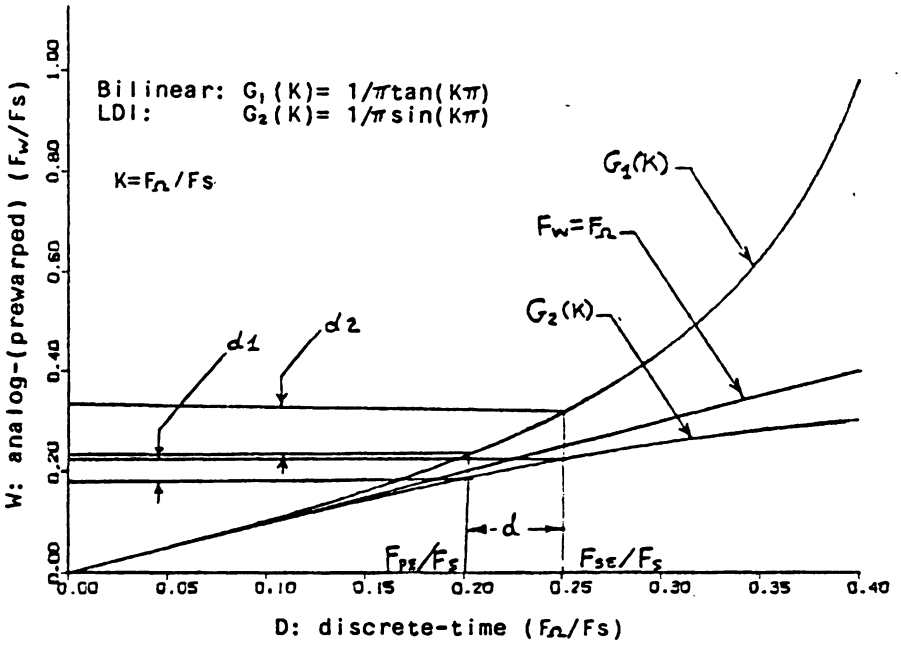

Figure 3.3. Bilinear and LDI normalized frequency prewarping curves with prewarped representations of a typical passband-stopband transition (see Figure 3.4).

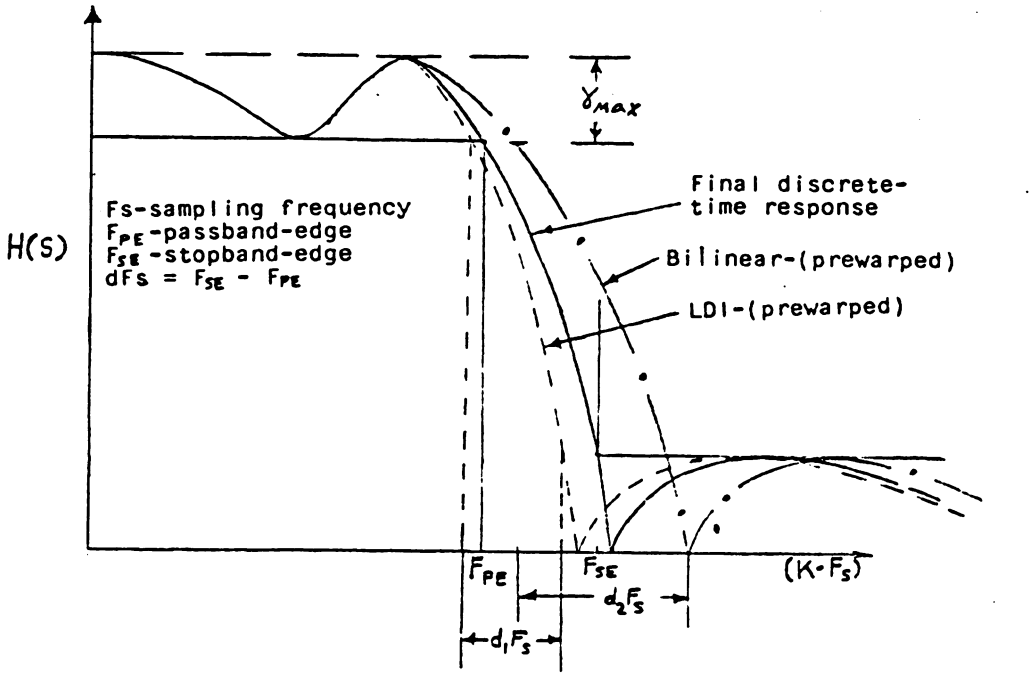

Figure 3.4. Desired discrete-time filter response and LDI/Bilinear prewarped filter response.

shorter passband-stopband transitions. Hence, for a fixed passband loss, LDI designs require higher order filter specifications to meet shorter passband-stopband transitions than corresponding bilinear designs. In actual filter implementations where the filter order must obviously be an integer number, an LDI filter design may be of higher order than its corresponding bilinear design. Figure 3.5 depicts more graphically the changes in the characteristic prewarping curves at different sampling frequencies, Fs, for a fixed operating frequency window. Note that the region of frequencies at wich a digital filter can be prewarped decreases for lower sampling-to-characteristic frequency ratios. It is tempting to conclude from the results of figures 3.3 and 3.5 that the bilinear design is the best design approach since, unlike the LDI design, the required filter order decreases to meet larger prewarped passband-stopband transitions for smaller sampling-to-characteristic frequency ratios. However, in actual implementations, the lower the required filter order the more difficult it is to meet a desired passband loss criteria.

With classical prewarping the digital filter is obtained by first deriving the corresponding prewarped analog filter which is denormalized to the desired (prewarped) frequency.

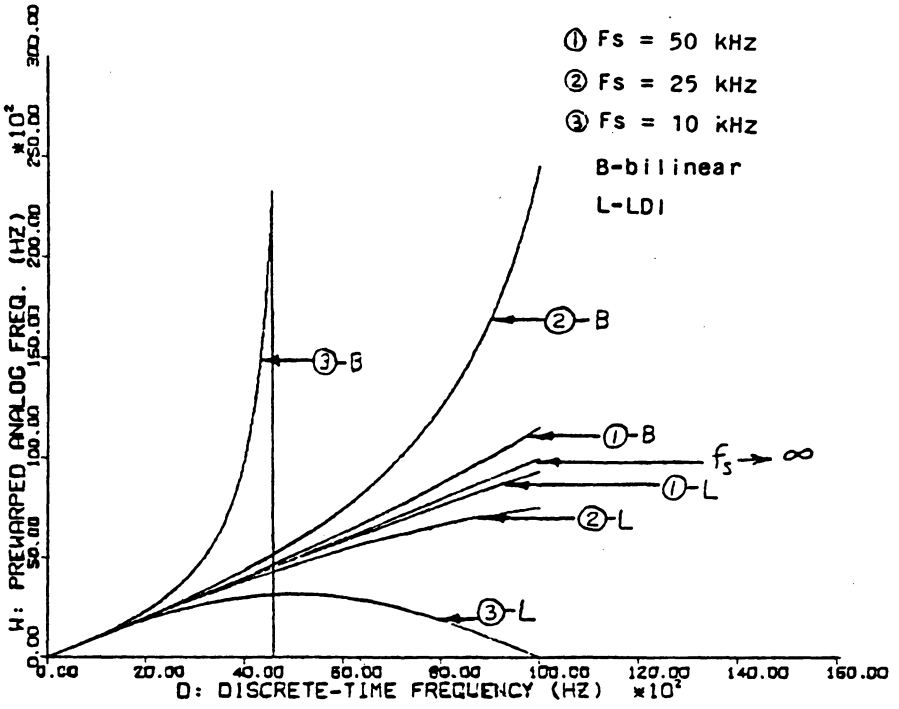

Figure 3.5. Bilinear and LDI frequency prewarping curves for sampling frequencies (Fs) of 50, 25, and 10 Khz.

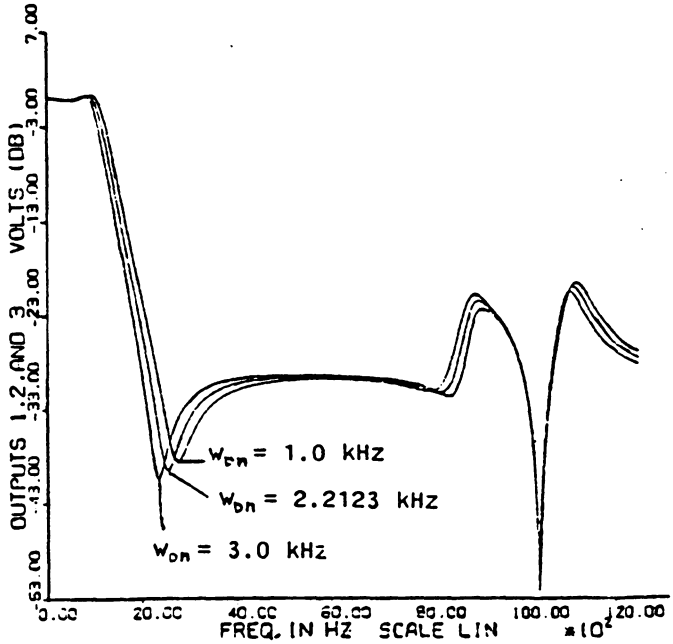

Figure 3.6. Frequency response of an LDI 3rd-order elliptic lowpass switched-capacitor filter denormalized at three seperate prewarped frequencies (W_{on}) and operating at a 10 Khz sampling frequency.

The prewarped analog filter is then S/Z-transformed into the desired digital filter. The chosen denormalizing frequency critically determines the shape of the final digital filter's frequency response. Figure 3.6 illustrates the effect on the frequency response of an elliptic 3rd-order lowpass SC filter denormalized at three different frequencies. For this particular example denormalizing at 3kHz provided the best emulation of the corresponding analog filter's frequency response with a near-perfect location of the notch. At two sucessive lower denormalizing frequencies, the frequency response progressively degrades. This is manifested by a shift to higher frequencies of the notch and cutoff frequencies along with a slight increase of the stopband loss. This is not a consistent response for all filter designs. In chapter 4 a similar analysis is performed for a BDS 7th-order filter whose passband-stopband transition deteriorates at larger denormalizing frequencies. It is because of this inconsistency of classical prewarping that it is always preferable to adopt the alternative approach of prewarping the passband-stopband transition edge frequencies and then determining the order and the filter approximation which best meets the prewarped transition. After S/Z-transforming, the desired passband-stopband transition is ensured. The

Antoniou filter design formulations discussed in the next section are based on this design criteria.

An important topic to consider is the aliasing effects incurred in digital filters or any other type of digital systems operating with different time-varying input signals. Aliasing effects, as applied to SC filters, are best demostrated with the aid of an example. Figure 3.7 illustrates the effect on the frequency response of a 3rd order elliptic SC lowpass filter as the aliasing point shifts to lower frequencies for smaller clock-to-cutoff frequency ratios (Fs/Fco) of 25, 10, and 5. The greatest attenuation degradation occurs at the stopband which shifts to smaller values of attenuation loss for lower Fs/Fco ratios. At the same time, the notch shifts in position and eventually disappears while the passband losses its equiripple characteristic.

A conclusion that can be drawn from the above prewarped denormalizing frequency and aliasing effects analysis is that it is always better to design for high clock-to-operating frequency ratios. In realizing an active filter design there are nonetheless upperbound limitations on the Fc/Fco ratio. Dynamic characteristics such as slew rate and settling time of circuit components (i.e. opamps, switches, etc.) can limit the operating frequency of the clock. This

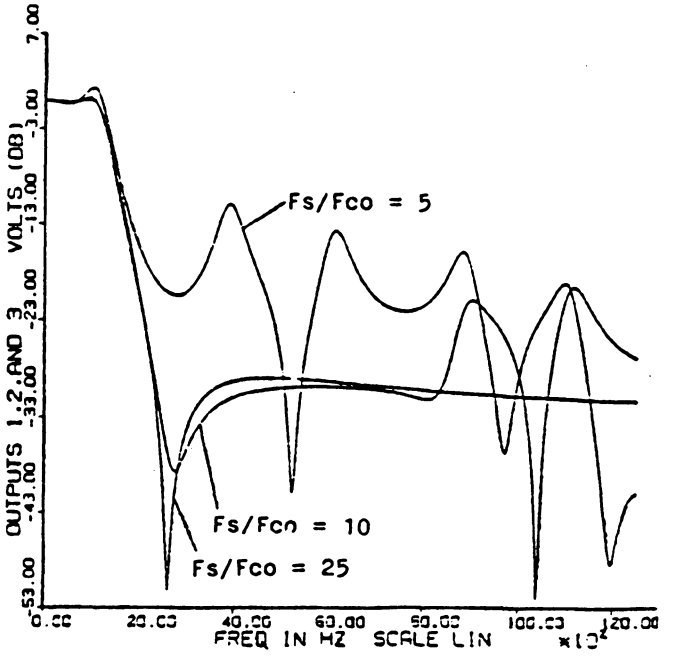

Figure 3.7. Frequency response of an LDI 3rd-order elliptic lowpass switched-capacitor filter operating at three seperate Fs/Fco ratios.

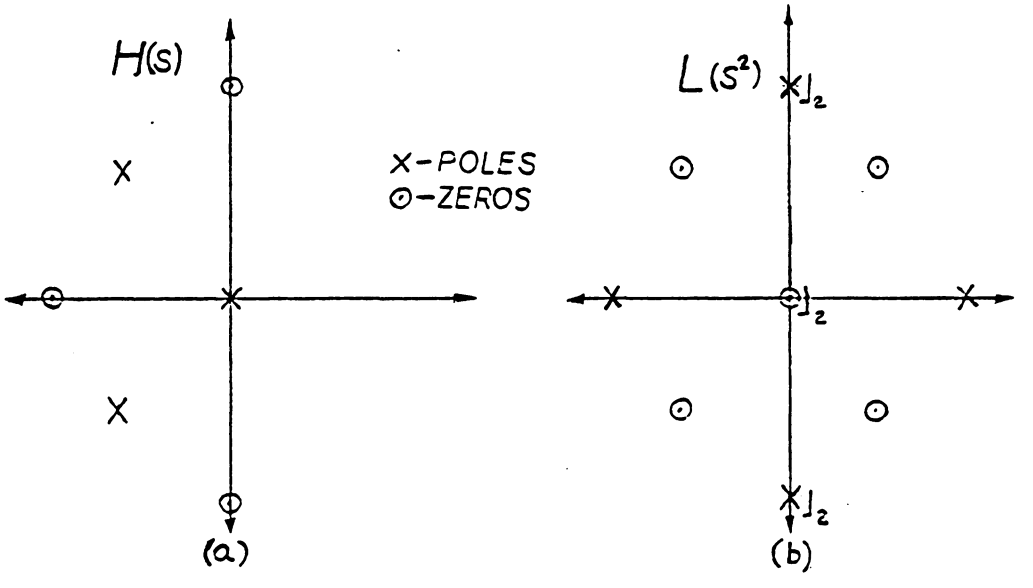

Figure 3.8. Zero and Pole locations of a representative transfer function (H(S)) and corresponding loss function (L(S)).

is particularly true when the operating frequency window of the filter is in the megahertz range for example.

3.4 Extended Antoniou Design Formulations by Prewarping Passband-Stopband Edge Frequencies.

Antoniou [3] reviewed formulations for digital filter design based on prewarping passband-stopband edge frequencies using the bilinear transformation. Here the formulations are extended to include the LDI and the impulse-invariant filter designs as well.

3.4.1 Basic Concepts

The following concepts are of fundamental importance:

a.Transfer Function (H):

Vo-output ; Vi-input

s-domain: $H(s)=Vo(s)/Vi(s)=N(s)/D(s)$; $s=\sigma+jw$

z-domain: $H(z)=Vo(z)/Vi(z)=N(Z)/D(Z)$; $z=e^{sT}$

Ts-sampling period

b.Loss function(L):

s-domain: $L(-s^2) = \frac{D(s)D(-s)}{N(s)N(-s)}$; Z-domain: $L(Z) = \frac{D(Z)D(Z^{-1})}{N(Z)N(Z^{-1})}$

In the frequency domain:

s-domain: $L(w^2) = \frac{1}{H(jw)H(-jw)}$

$$\text{Z-domain: } L(e^{jw\tau}) = \frac{D(e^{jw\tau})D(e^{-jw\tau})}{N(e^{jw\tau})N(e^{-jw\tau})}$$

Remark: zero-pole s-domain plots of H and L for a typical system are depicted in figures 3.8(a) and 3.8(b).

c.Loss attenuation (A):

$$\text{s-domain: } A(w)=20\log\left|\frac{Vi(jw)}{Vo(jw)}\right| = 20\log\left|\frac{1}{H_A(jw)}\right| = 20\log L(w^2)$$

$$\text{Z-domain: } A(e^{jw\tau}) = 20\log\left|\frac{Vi(e^{jw\tau})}{Vo(e^{jw\tau})}\right| = 20\log\left|\frac{1}{H_D(e^{jw\tau})}\right|$$

$$= 20\log|L(e^{jw\tau})|$$

d.Phase shift (θ) and group delay (τ):

s-domain: $\theta(w)=\arg\{H_A(jw)\}$

$\tau=-d\theta(w)/dw$

z-domain: $\theta(w)=\arg\{H_A(jw)\}$

$\tau=-d\theta(w)/dw$

Figure 3.9 illustrates the typical attenuation (-A) versus frequency (ϕ) characteristics of lowpass (LP), highpass (HP), bandpass (BP), and bandstop (BS) filters and with them lets define the following characteristic frequencies and loss magnitudes:

s-domain: $\phi=w$; Z-domain: $\phi=\Omega$

passband edge: $\phi_{pe} = w_{pe}; \Omega_{pe}$

stopband edge: $\phi_{se} = w_{se}; \Omega_{se}$

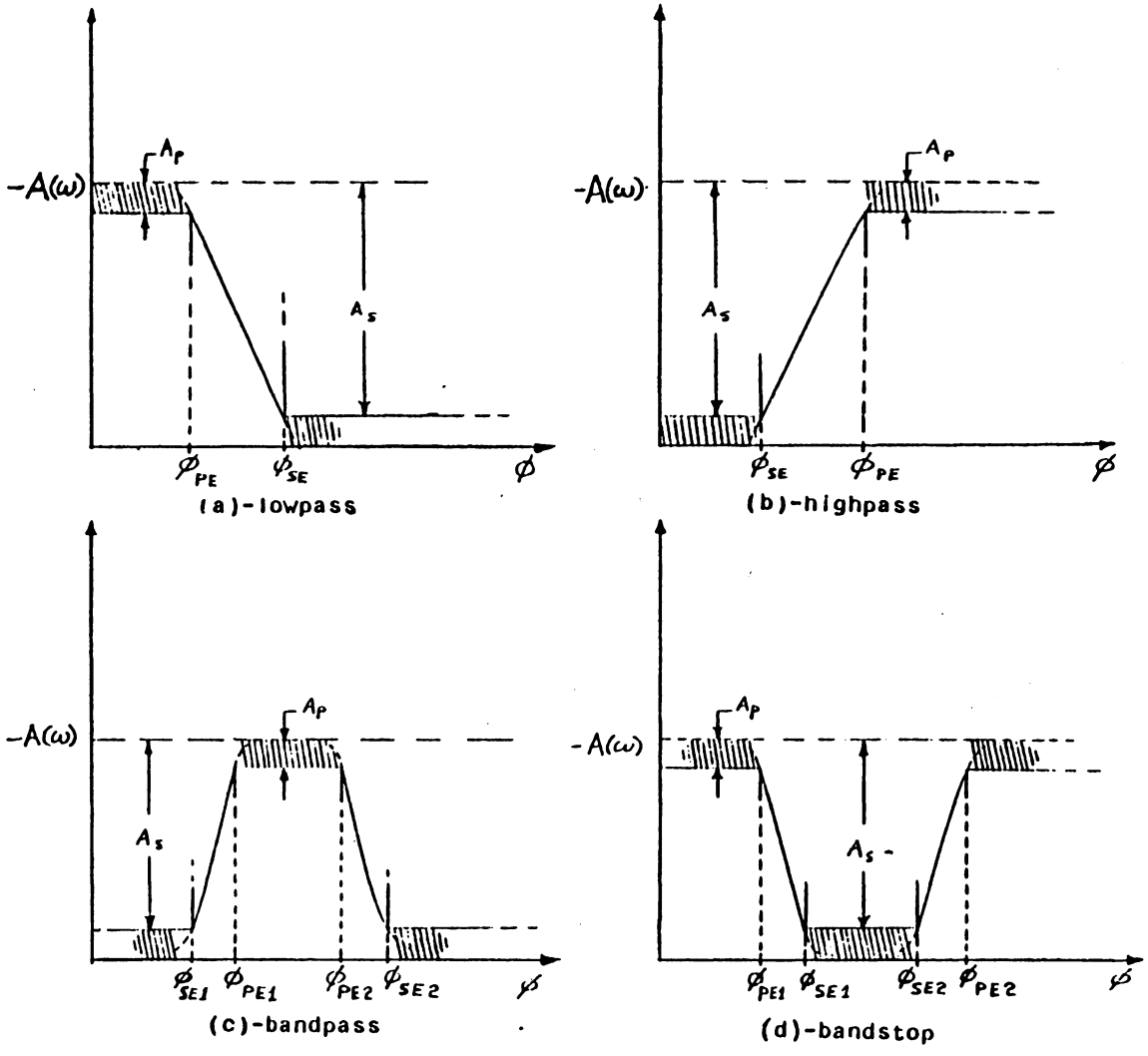

Figure 3.9. Characteristic frequencies and attenuation losses of lowpass, highpass, bandpass, and bandstop filters. (see section 3.4 for definitions of ϕ)

(For Butterworth and Tschebyscheff filter approximations the cutoff frequency is the passband edge frequency. For Jacobi-Elliptic filter approximations the cutoff frequency (ϕ) is defined as: $\phi = \sqrt{\phi_{pe}\phi_{se}}$

passband loss: A_p

stopband loss: A_s

Any transfer function (analog or digital) will characterize a stable, causal, and realizeable network if the following constraints are satisfied:

1. It must be a rational function of S (or Z) with real coefficients.
2. Poles must lie in the left-half S-plane (or inside the Z-plane unit circle).
3. The degree of the numerator polynomial must be equal to or less than that of the denominator polynomial.

3.4.2 Digital Filter Design Formulations

Figure 3.9(a)-(d) depicts together with the passband and stopband attenuation loss parameters Ap and As the characteristic frequencies used in any type of filter design. There are certain upper bound restrictions on the normalized lowpass stopband edge frequency (w_{sen}) with respect to the normalized lowpass passband edge frequency (w_{pen}) and these are listed on tables 3.1 and 3.2 for all four types of

TABLE 3.1. Lowpass and Highpass Filter Parameters [3].

($\omega_{PE}|_n$ relations are presented in Tables 3.3, 3.4, and 3.5).

Filter Type	$\omega_{SE}\|_n$	λ and K_o for Both LP and HP Filters		Impulse Invariant
		LDI	Bilinear	
LP	$\omega_{SE}\|_n \le \frac{\omega_{PE}\|_n}{K_o}$	$\lambda = \frac{\omega_{PE}\|_n \cdot T_s}{2\sin(\Omega_{PE} \cdot T_s/2)}$	$\lambda = \frac{\omega_{PE}\|_n \cdot T_s}{2\tan(\Omega_{PE} \cdot T_s/2)}$	$\lambda = \frac{T_s \omega_{PE}\|_n}{\Omega_{PE}}$
HP	$\omega_{SE}\|_n \le \omega_{PE}\|_n \cdot K_o$	$K_o = \frac{\sin(\Omega_{PE} \cdot T_s/2)}{\sin(\Omega_{SE} \cdot T_s/2)}$	$K_o = \frac{\tan(\Omega_{PE} \cdot T_s/2)}{\tan(\Omega_{SE} \cdot T_s/2)}$	$K_o = \frac{\Omega_{PE}}{\Omega_{SE}}$

TABLE 3.2. Bandpass and Bandstop Filter Parameters [3].

($\omega_{PE}|_n$ relations are presented in Tables 3.3, 3.4, and 3.5).

Filter Type	ω_o	$\omega_{SE}\|_n$	B
BP	$\omega_o = \frac{2\sqrt{K_B}}{T_s}$	$\omega_{SE}\|_n \leq \begin{cases} \omega_{PE}\|_n/K_1 & \text{if } K_C \geq K_B \\ \omega_{PE}\|_n/K_2 & \text{if } K_C < K_B \end{cases}$	$B = \frac{2K_a}{T_s \omega_{PE}\|_n}$
BS	$\omega_o = \frac{2\sqrt{K_B}}{T_s}$	$\omega_{SE}\|_n \leq \begin{cases} \omega_{PE}\|_n \cdot K_2 & \text{if } K_C \geq K_B \\ \omega_{PE}\|_n \cdot K_1 & \text{if } K_C < K_B \end{cases}$	$B = \frac{2K_a \omega_{PE}\|_n}{T_s}$

Parameters	Impulse Invariant	LDI	Bilinear
K_a	$(\Omega_{PE2}-\Omega_{PE1})/2$	$\sin\left(\frac{\Omega_{PE2}\cdot T_s}{2}\right) - \sin\left(\frac{\Omega_{PE1}\cdot T_s}{2}\right)$	$\tan\left(\frac{\Omega_{PE2}\cdot T_s}{2}\right) - \tan\left(\frac{\Omega_{PE1}\cdot T_s}{2}\right)$
K_b	$(\Omega_{PE1}\cdot\Omega_{PE2})/4$	$\sin\left(\frac{\Omega_{PE1}\cdot T_s}{2}\right) \times \sin\left(\frac{\Omega_{PE2}\cdot T_s}{2}\right)$	$\tan\left(\frac{\Omega_{PE1}\cdot T_s}{2}\right) \times \tan\left(\frac{\Omega_{PE2}\cdot T_s}{2}\right)$
K_c	$(\Omega_{SE1}\cdot\Omega_{SE2})/4$	$\sin\left(\frac{\Omega_{SE1}\cdot T_s}{2}\right) \times \sin\left(\frac{\Omega_{SE2}\cdot T_s}{2}\right)$	$\tan\left(\frac{\Omega_{SE1}\cdot T_s}{2}\right) \times \tan\left(\frac{\Omega_{SE2}\cdot T_s}{2}\right)$
K_1	$\frac{2K_a\Omega_{SE1}}{4K_b - \Omega_{SE1}^2}$	$\frac{K_a \sin(\Omega_{SE1}\cdot T_s/2)}{K_b - \sin^2(\Omega_{SE1}\cdot T_s/2)}$	$\frac{K_a \tan(\Omega_{SE1}\cdot T_s/2)}{K_b - \tan^2(\Omega_{SE1}\cdot T_s/2)}$
K_2	$\frac{2K_a\Omega_{SE2}}{\Omega_{SE2}^2 - 4K_b}$	$\frac{K_a \sin(\Omega_{SE2}\cdot T_s/2)}{\sin^2(\Omega_{SE2}\cdot T_s/2) - K_b}$	$\frac{K_a \tan(\Omega_{SE2}\cdot T_s/2)}{\tan^2(\Omega_{SE2}\cdot T_s/2) - K_b}$

filters. Also listed in these table are the denormalizing coefficients λ (for LP and HP) and B (for BP and BS) whose use will be explained shortly. These tables by Antoniou [3] have been extended to include not only the original bilinear transformation design case but the LDI and the impulse invariant transformation designs as well.

For the Butterworth, Tschebyscheff, and Jacobi-Elliptic filters, design formulations of required filter order (n), selectivity factor (k), and normalized lowpass passband edge frequencies (w_{pen}) are presented in tables 3.3 through 3.5. With the use of n,k, and w_{pen} Butterworth, Tschebyscheff, and Jacobi-Elliptic normalized lowpass filter approximations can be derived with the use of algorithms presented in Appendix A. Table 3.6 lists the transformations necessary for obtaining any denormalized lowpass transfer function with the use of parameters λ and B as defined in tables 3.1 and 3.2. The denormalizing operation is defined below:

$$Hx(s) = Hn(\bar{s})\Big|_{\bar{s}=Fx(s)}$$

where: x= LP,HP,BP,BS

Table 3.7 summarizes the transformations necessary for obtaining any denormalized discrete-time transfer function from the denormalized analog transfer function (Hx(S)) by means of:

TABLE 3.3. Butterworth Filter Design [3]

$$n \geq \frac{\text{Log } D}{2\text{Log}(1/K)}$$

$$\omega_{PE}|_n = (10^{0.1A_p} - 1)^{1/2n}$$

LP	$K = K_o$
HP	$K = 1/K_o$
BP	$K = \begin{cases} K_1 & \text{if } K_C \geq K_B \\ K_2 & \text{if } K_C < K_B \end{cases}$
BS	$K = \begin{cases} 1/K_2 & \text{if } K_C \geq K_B \\ 1/K_1 & \text{if } K_C < K_B \end{cases}$

where $D = \dfrac{10^{0.1A_s} - 1}{10^{0.1A_p} - 1}$

TABLE 3.4. Tschebyscheff Filter Design [3].

$$n \geq \frac{\cosh^{-1}(\sqrt{D})}{\cosh^{-1}(1/K)} \quad ; \quad D = \frac{10^{0.1A_s} - 1}{10^{0.1A_p} - 1}$$

$$\omega_{PE}|_n = 1$$

LP	$K = K_o$
HP	$K = 1/K_o$
BP	$K = \begin{cases} K_1 & \text{if } K_C \geq K_B \\ K_2 & \text{if } K_C < K_B \end{cases}$
BS	$K = \begin{cases} 1/K_2 & \text{if } K_C \geq K_B \\ 1/K_1 & \text{if } K_C < K_B \end{cases}$

TABLE 3.5. Jacoby-Elliptic Filters [3].

$$n \geq \frac{\text{Log } 16D}{\text{Log } 1/q} \quad ; \quad D = \frac{10^{0.1A_s} - 1}{10^{0.1A_p} - 1}$$

$$K' = \sqrt{1 - K^2}$$

$$q_o = \frac{1}{2}\left[\frac{1 - \sqrt{K'}}{1 + \sqrt{K'}}\right]$$

$$q = q_o + 2q_o^5 + 15q_o^9 + 150q_o^{13}$$

	K	$\omega_{PE}\|_n$
LP	K_o	$\sqrt{K_o}$
HP	$1/K_o$	$1/\sqrt{K_o}$
BP	K_1 if $K_C \geq K_B$ K_2 if $K_C < K_B$	$\sqrt{K_1}$ $\sqrt{K_2}$
BS	$1/K_2$ if $K_C \geq K_B$ $1/K_1$ if $K_C < K_B$	$1/\sqrt{K_2}$ $1/\sqrt{K_1}$

TABLE 3.6. Denormalizing Relations [3].

x	fx(S)
LP	$\lambda \bar{S}$
HP	$\lambda / \bar{S}$
BP	$\frac{1}{B}\left(\bar{S} + \frac{\omega_o^2}{\bar{S}}\right)$
BS	$\frac{B\bar{S}}{\bar{S}^2 + \omega_o^2}$

TABLE 3.7. S/Z-Transformations.

W	$P_W(Z)$
LDI	$\frac{1}{T_s} \frac{1 - Z^{-1}}{Z^{-1/2}}$
Bilinear	$\frac{2}{T_s} \frac{1 - Z^{-1}}{1 + Z^{-1}}$

$$H_{Dx}(Z) = H_x(s)\Big|_{s=Pw(Z)}$$

where: w= LDI, Bilinear

x= LP,HP,BP,BS

(Section 3.2 discusses the impulse invariant S/Z-domain transformation.)

3.5 Constantinides Transformations

A.G. Constantinides [6] proposed a set of Z-domain relationships for transforming any normalized lowpass discrete-time filter with a passband-edge frequency Ω_{pen} into a denormalized lowpass, highpass, bandpass, or bandstop digital filter. The classical digital filter design procedure as depicted in design path (a) in figure 3.10 starts with the normalized analog lowpass filter ($H_{An}(S)$) which is denormalized to a LP, HP, BP, or BS analog filter and which in turn is transformed into its equivalent digital filter. By Constantinides approach (design path (b)) the normalized analog lowpass filter is first transformed by whatever S/Z-transformation is selected into a normalized digital lowpass filter ($H_{Dn}(Z)$): $H_{Dn}(Z)$ is then transformed into the desired denormalized digital filter.

Table 3.8 presents Constantinides [3] transformations that can be used to obtain the denormalized LP, HP, BS, and

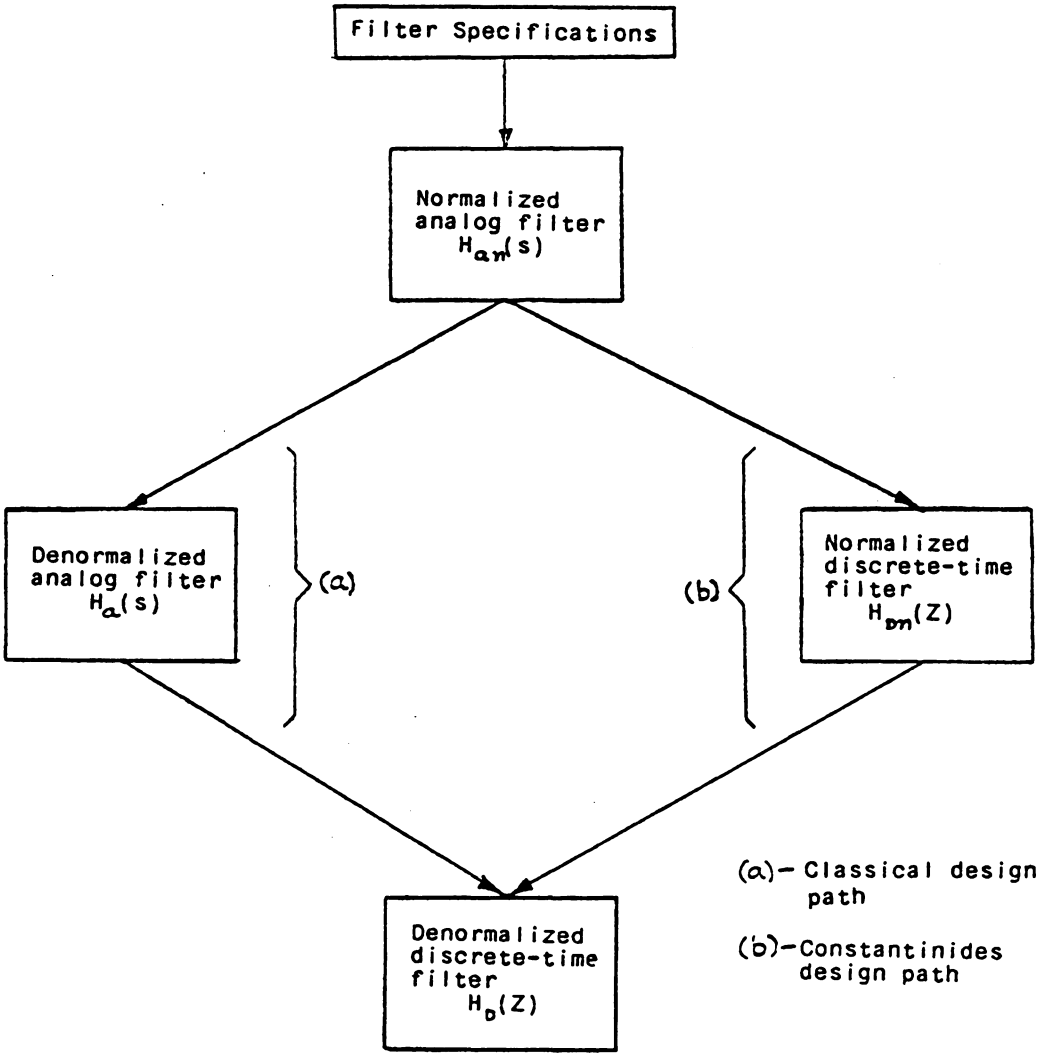

Figure 3.10. Classical and Constantinides discrete-time filter design strategies.

TABLE 3.8. Constantinides Transformations [6].

Filter Type	Transformation $\bar{Z}^{-1} = f_x(Z^{-1})$	Transformation Parameters (α,K)
Lowpass	$\bar{Z}^{-1} = \dfrac{Z^{-1} - \alpha}{1 - \alpha Z^{-1}}$	$\alpha = \dfrac{\sin\left\{\dfrac{(\Omega_{PE}\|_n - \Omega_{PE})T_s}{2}\right\}}{\sin\left\{\dfrac{(\Omega_{PE}\|_n + \Omega_{PE})T_s}{2}\right\}}$
Highpass	$-\left[\dfrac{Z^{-1} + \alpha}{1 + \alpha Z^{-1}}\right]$	$\alpha = -\dfrac{\cos\left\{\dfrac{(\Omega_{PE}\|_n - \Omega_{PE})T_s}{2}\right\}}{\cos\left\{\dfrac{(\Omega_{PE}\|_n + \Omega_{PE})T_s}{2}\right\}}$
Bandpass	$-\left[\dfrac{Z^{-2} - \frac{2\alpha K}{K+1} Z^{-1} + \frac{K-1}{K+1}}{\frac{K-1}{K+1} Z^{-2} - \frac{2\alpha K}{K+1} Z^{-1} + 1}\right]$	$\alpha = \dfrac{\cos\left\{\dfrac{(\Omega_{PE2} + \Omega_{PE1})T_s}{2}\right\}}{\cos\left\{\dfrac{(\Omega_{PE2} - \Omega_{PE1})T_s}{2}\right\}} = \cos\omega_o T_s$ $K = \cot\left\{\dfrac{(\Omega_{PE2} - \Omega_{PE1})T_s}{2}\right\} \tan\left\{\dfrac{\Omega_{PE}\|_n \cdot T_s}{2}\right\}$
Bandpass	$\dfrac{Z^{-2} - \frac{2\alpha}{1+K} Z^{-1} + \frac{1-K}{1+K}}{\frac{1-K}{1+K} Z^{-2} - \frac{2\alpha}{1+K} Z^{-1} + 1}$	$\alpha = \dfrac{\cos\left\{\dfrac{(\Omega_{PE2} + \Omega_{PE1})T_s}{2}\right\}}{\cos\left\{\dfrac{(\Omega_{PE2} + \Omega_{PE1})T_s}{2}\right\}} = \cos\omega_o T_s$ $K = \tan\left\{\dfrac{(\Omega_{PE2} - \Omega_{PE1})T_s}{2}\right\} \tan\left\{\dfrac{\Omega_{PE}\|_n \cdot T_s}{2}\right\}$

where: Ω_{PE} = desired cutoff frequency

Ω_{PE1} = lower cutoff frequency

Ω_{PE2} = upper cutoff frequency

$\Omega_{PE}|_n$ = normalized digital lowpass cutoff frequency

BP Z-domain transfer function from the normalized Z-domain lowpass transfer function by means of:

$$H_{Dx}(Z^{-1}) = H_{Dn}(Z^{-1})\Big|_{Z^{-1} = F_x(Z^{-1})}$$

where: x= LP,HP,BP,BS

The advantage of the Constantinides transformation procedure are:

1. It can be applied regardless of the design procedure used in obtaining the digital normalized lowpass filter.
2. In transforming denormalized s-domain highpass and bandpass filters to their Z-domain equivalent by the impulse invariant design technique (section 3.2) aliasing distortions are acute. By Oppenheim and Schafer [28] this effect is best compensated with the use of Constantinides transformations.
3. It offers a fine-tuning feature for adjusting the denormalized passband edge frequencies of lowpass and highpass filters by varying α, while for bandpass and bandstop filters the lower and upper passband edge frequencies can be fine-tuned by varying α and K [6].

3.6 Bilinear and LDI S/Z-Transformation Realization Using the Leapfrog Design Technique

In the construction of bilinear and LDI filters various techniques have been developed for realizing the S/Z-transformation. The leapfrog design technique, first developed by Girling and Good [12], is the most popular approach for realizing bilinear and LDI S/Z-transformations. This technique generates a signal flow diagram, composed of signal gain and integration branches, of a passive LC filter. These signal integration branches can then be replaced by corresponding SC integration circuits such as those depicted in Figure 2.8 ; thus realizing the desired S/Z-transformed digital filter. What this technique requires is a passive LC prototype of the prewarped analog filter. The Leapfrog design technique will be presented here for a lowpass design case. This filter design method cannot be implemented in switched capacitor impulse invariant filter designs unless impulse invariant integration circuits are first developed.

A normalized 3rd-order lowpass passive LC filter corresponding to the frequency response of figure 3.11 is depicted in figure 3.12. Suppose a denormalized LDI SC lowpass filter with similar attenuation frequency response characteristics is desired but denormalized at a cutoff frequency (Fco)

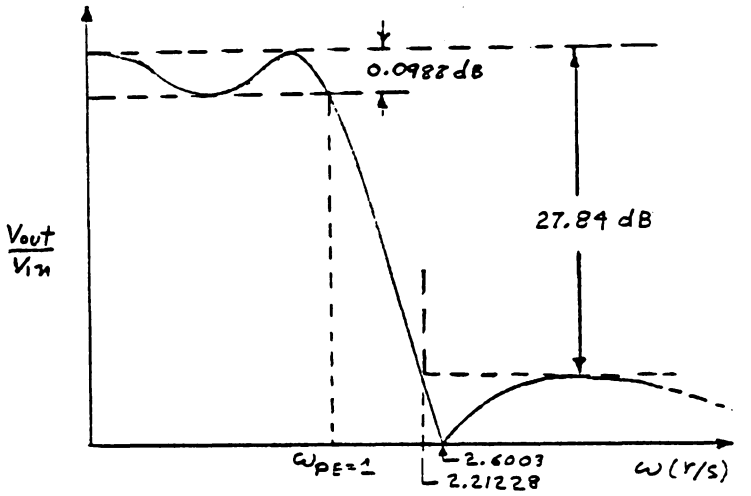

Figure 3.11. 3rd-order elliptic normalized lowpass filter attenuation-frequency response.

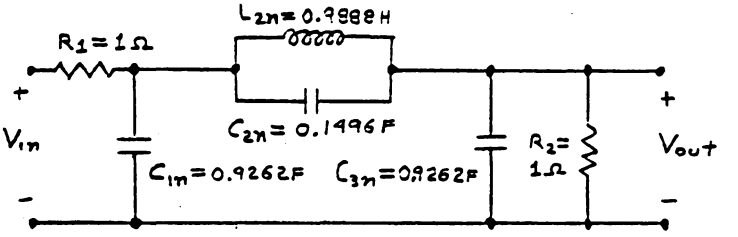

Figure 3.12. Normalized 3rd-order elliptic lowpass LC filter.

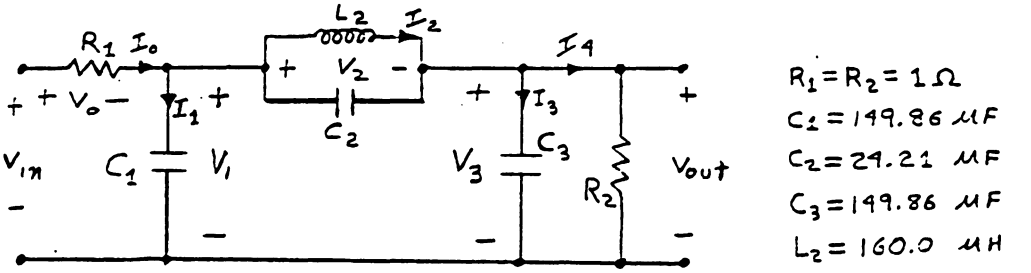

Figure 3.13. Denormalized 3rd-order elliptic lowpass LC filter.

of 1Khz and operating with a clock frequency (Fc) of 10Khz. For LDI circuit realizations, the effective sampling frequency (Fs) equals the clock frequency ; hence the effective sampling-to-cutoff frequency ratio is:

$$Fs/Fc = 10$$

A denormalized prewarped analog lowpass filter must first be derived having prewarped characteristic frequencies corresponding to the discrete-time characteristic frequencies of the final digital lowpass filter. To achieve this the classical approach of prewarping the filter attenuation characteristic at one frequency is arbitrarily selected. From the frequency analysis presented in section 3.3., the filter is chosen to be prewarped and denormalized at the cutoff frequency. The prewarped denormalizing frequency value is computed as follows:

Given Fs = 10kHz ; Fco = 1.0kHz : w_{nco} = 1r/s

$$Ts = 10^{-4}$$

$$w_{Dn} = w_{Pw}/w_{nco} = (2/Ts)\sin[(2\pi FcoTs)/2]/w_{nco} \qquad 3.6.1$$

$$w = 6180.4 \qquad 3.6.2$$

With the use of well known element denormalization relations, the following denormalized element values of the denormalized prewarped LC prototype of figure 3.13 are obtained:

$$C1=149.862\ \mu F$$

C2=24.205 μF

C3=149.862 μF

L2=159.991 μH

A node voltage analysis of figure 3.13 yields the following equations:

$$I_0 - I_2 - (V_1-V_3)SC_2 - V_1SC_1 = 0$$

$$V_1 = \frac{(I_0-I_2)}{S(C_1+C_2)} + \frac{C_2}{C_1+C_2} V_3 \qquad 3.6.3$$

$$I_2 + (V_1-V_3)SC_2 - V_3SC_3 - I_4 = 0$$

$$V_3 = \frac{(I_2-I_4)}{S(C_2+C_3)} + \frac{C_2}{C_2+C_3} V_1 \qquad 3.6.4$$

$$I_2 = (V_1-V_3)/SL_2 \qquad 3.6.5$$

$$I_0 = (V_{in}-V_1)/R_1 \qquad 3.6.6$$

$$I_4 = V_3/R_2 \qquad 3.6.7$$

Equation 3.6.3 and 3.6.4 can be modeled as branches of capacitors and voltage-controlled voltage sources in series as depicted in figure 3.14. The Leapfrog signal flow diagram representing equations 3.6.3 through 3.6.7 above is depicted in figure 3.15. Here parameters X_1 and X_2 are defined as:

$$X_1 = \frac{C_2}{C_1+C_2} = \qquad X_2 = \frac{C_2}{C_2+C_3} = 0.13906$$

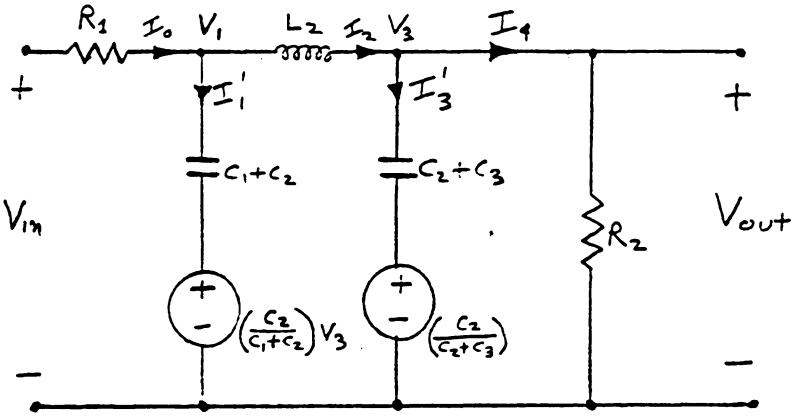

Figure 3.14. Circuit equivalence diagram corresponding to equations 3.6.3 - 3.6.7.

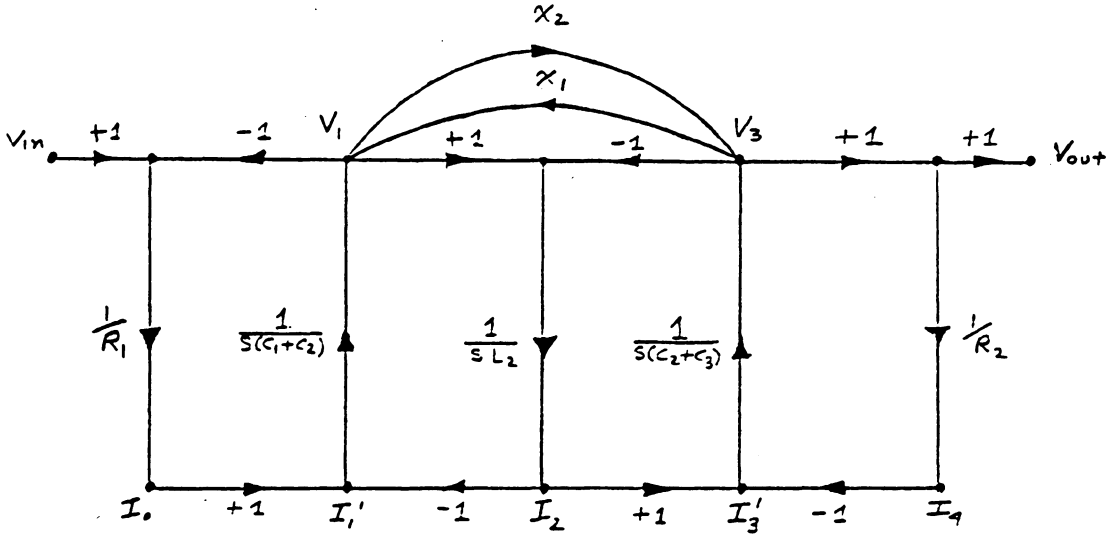

Figure 3.15. Leapfrog signal flow diagram of figure 3.14.

For SC filter construction purposes the bottom current-specified nodes of figures 3.15 must be converted to voltage-specified nodes. This is readily achieved by multiplying and dividing incident branches to these nodes by an arbitrary resistor, Rs, as shown in figure 3.16 while maintaining gain equivalence throughout. Rs (along with R_1 and R_2) is then set to 1Ω. Before replacing the integrating branches of figure 3.16 by the LDI SC integrating/summation stage of figure 2.8(III) there is the problem of positive summation branches which the LDI SC circuit cannot implement without the need of inverters. Unlike the inverting summer in figure 2.8(III) the integrating branches incident on nodes V_1 and V_3 receive positive summing signals through gain paths X_1 and X_2. This problem may be solved by negating a node in contact with the summing paths X_1 and X_2, thereby making these paths negative summing signals. In this example, node V_3 was negated and the resulting leapfrog flow diagram is shown in figure 3.17. The resulting voltage equations for nodes V_1, V_2, and V_2 are:

$$V_1 = \frac{V_0 - V_2}{S(C_1+C_2)} - \frac{C_2}{C_1+C_2} V_3^* \qquad 3.6.8$$

$$V_3^* = \frac{V_2 - V_4}{S(C_2+C_3)} - \frac{C_2}{C_2+C_3} V_1 \qquad 3.6.9$$

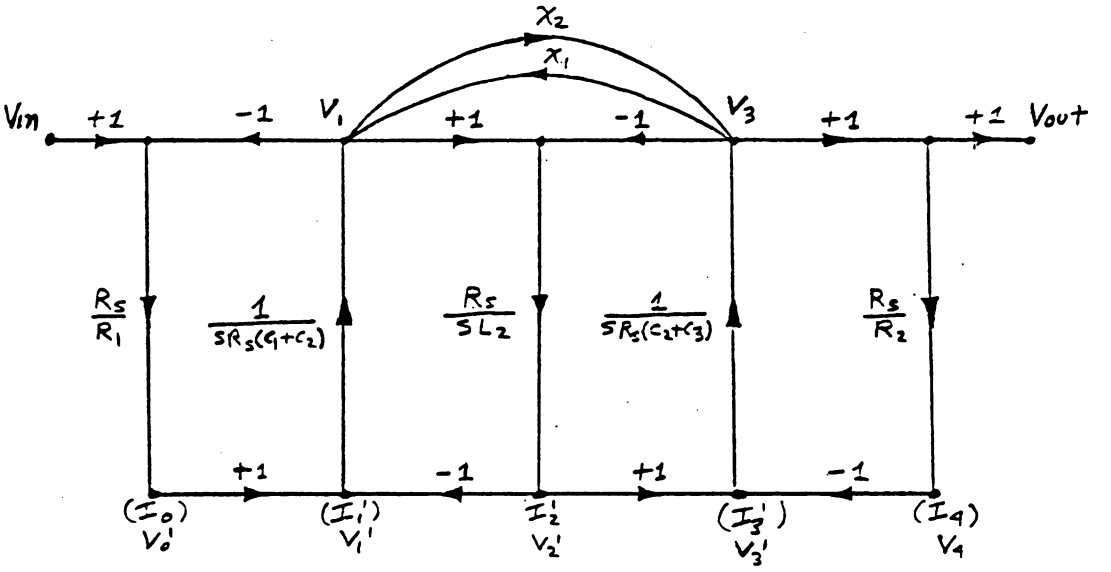

Figure 3.16. Leapfrog signal flow diagram of figure 3.15 with bottom current nodes converted into voltage nodes.

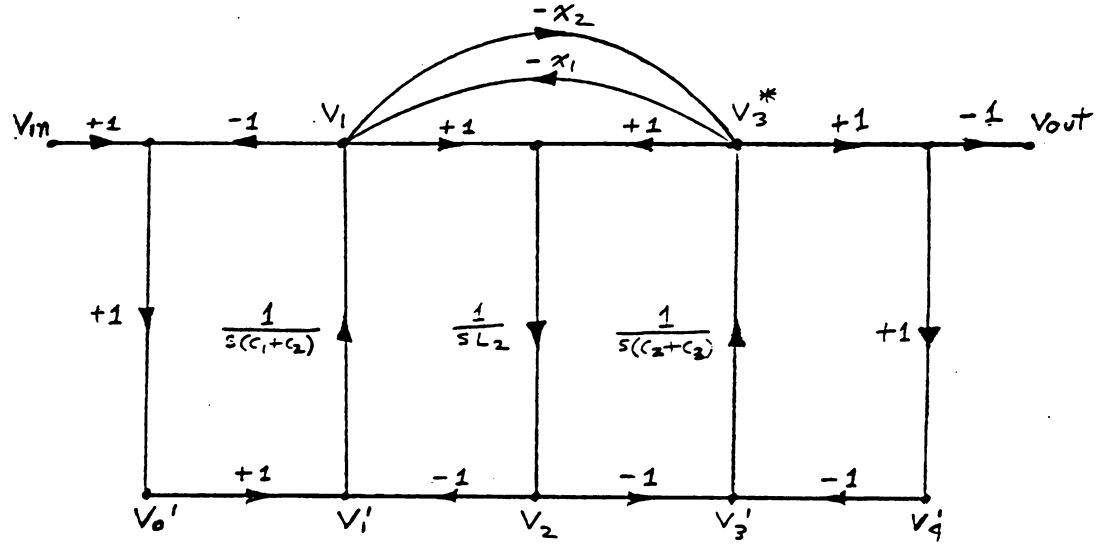

Figure 3.17. Leapfrog signal flow diagram of figure 3.16 with node V3 negated.

$$V_2 = (V_1 + V_3^*)/SL_2 \qquad 3.6.10$$

Note that since the path to Vout from V_3 is negative, Vout is now 180 degrees out of phase with respect to Vin. For filtering purposes this is not relevant, but if need be Vin can always be negated to compensate for this phase shift. To do this Vin can simply be sampled as a negative signal. Taking the LDI S/Z-transformation of 3.6.8 through 3.6.10 and comparing to the LDI integration/summation format of equation 2.5.16 the following capacitor relations for each of the integration stages of the final digital filter are obtained:

$$\frac{Cu_1}{Ck_1} = \frac{Ts}{C_1 + C_2} = 0.5745 \quad ; \quad \frac{Cx_1}{Ck_3} = X_1 = 0.139$$

$$\frac{Cu_2}{Ck_2} = \frac{Ts}{L_2} = 0.625$$

$$\frac{Cu_3}{Ck_3} = \frac{Ts}{C_2 + C_3} = 0.5745 \quad ; \quad \frac{Cx_2}{Ck_3} = X_2 = 0.139$$

An inherent advantage of switched capacitor circuits is now evident in that the capacitor values can be made small while maintaining the desired capacitor ratios. Arbitrarily selecting all the sampling capacitors (Cu's) to be 1.0nf results in the follwing capacitor values:

$Cu_1 = 1.0nf$ $\quad Ck_1 = 1.7407nf$ $\quad Cx_1 = 0.24205nf$

$Cu_2 = 1.0nf$ $\quad Ck_2 = 1.60nf$ $\quad Cx_2 = 0.24205nf$

Cu_3 = 1.0nf Ck_3 = 1.7407nf

A clock-phased signal sampling scheme must now be chosen for the filter of figure 3.17 and, in addition, all sampling capacitors of each integrating stage must discharge and transmit signals to the opamps at the same time. Both signal sampling Schemes I and II (see chapter 2) were adopted for the filter of figure 3.17 and identical attenuation frequency responses for both case were obtained when simulated on DIANA [36] as depicted figure 3.18. Arbitrarily applying Scheme I to figure 3.17 results in the circuit of figure 2.12(b)for which a DIANA simulation is depicted in figure 3.19. Notice the aliasing effect which occurs at 10kHz. One final note: due to the equally terminated resistances (R_1 and R_2) in figure 3.13, the dc gain of both the analog and the digital filter is 0.5 (-6.0db). To compensate for this loss in gain the magnitude of the sampled signal from Vin can be doubled by doubling the value of Cu_2 in the circuit of figure 2.12(b) from 1 to 2 nf.

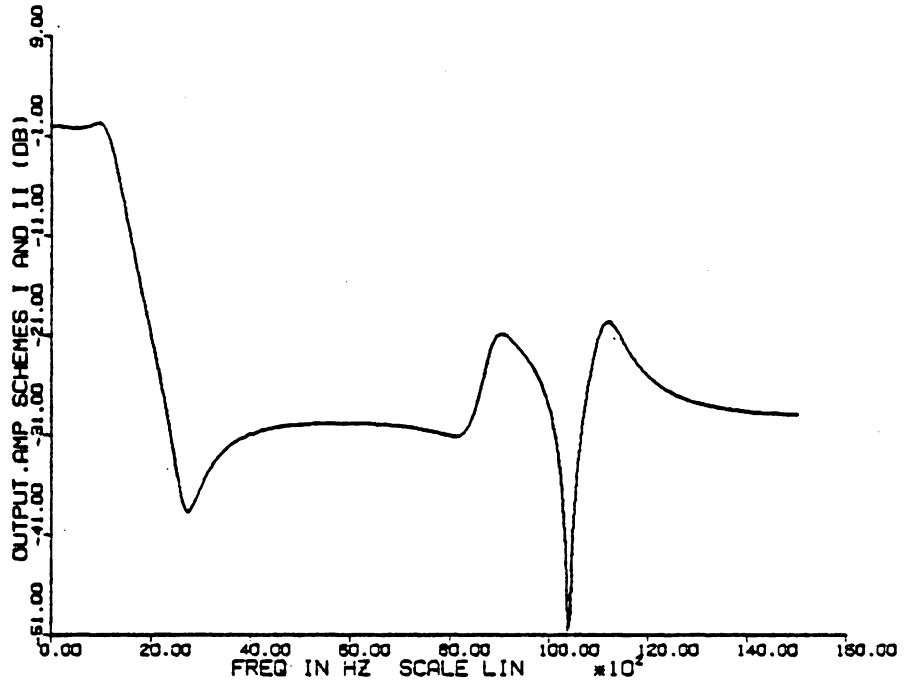

Figure 3.18. Attenuation-frequency response of the switched capacitor filter corresponding to the leapfrog signal flow diagram of figure 3.17 when implementing clock-phased signal-sampling schemes I or II.

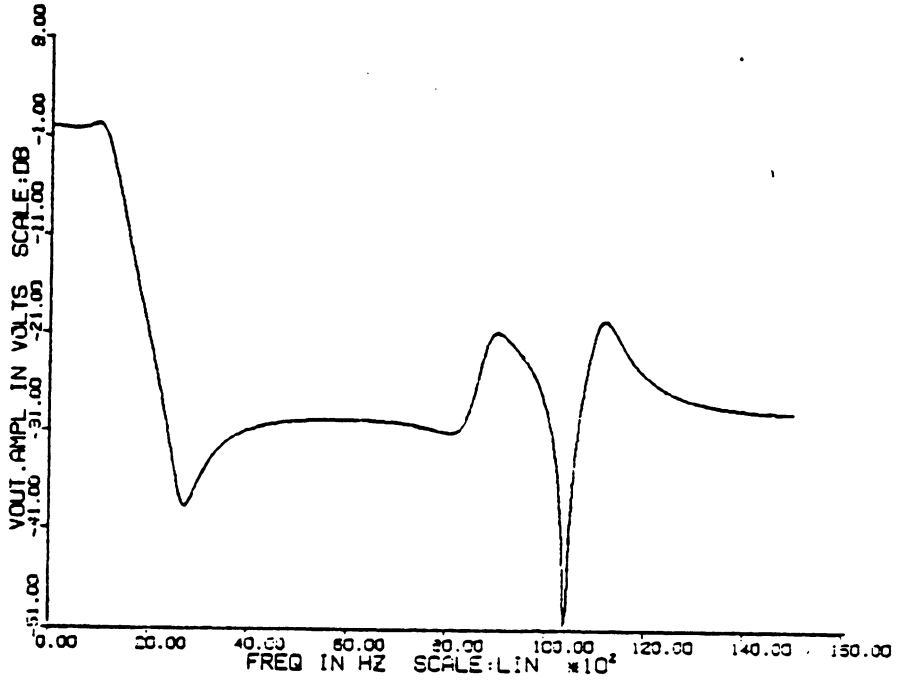

Figure 3.19. Attenuation-frequency response of the 3rd-order switched capacitor elliptic lowpass filter of figure 2.12(b).

Chapter IV

BILINEAR 7TH-ORDER AND LDI 8TH-ORDER SWITCHED CAPACITOR LOWPASS FILTER COMPUTER AND TEST RESULTS

4.1 Introduction: Objectives and Design Strategies

The experimental performance of the bilinear and the LDI switched capacitor (SC) filter design in meeting an arbitrary elliptic lowpass attenuation-frequency response were compared by means of computer simulations and test results. Both a BSS and a BDS filter design were evaluated and compared by means of computer simulation with the intent of selecting a bilinear filter for experimental testing alongside the LDI filter.

For the BSS and the BDS designs the following design steps were taken:

1. Select a normalized lowpass passive LC filter with an attenuation frequency response that best matches the desired attenuation frequency response of the final digital filter. (Nominally it is the prewarped frequency response of the digital filter which should be matched. Nonetheless, no readily available algorithm was available at the time for obtaining the prewarped frequency response during the bilinear filter design stage.)

2. Obtain the denormalized lowpass passive LC filter by means of inductor and capacitor denormalization using prewarped denormalizing frequencies.
3. Derive the leapfrog signal flow diagram (LSFD) of the denormalized analog filter.
4. Obtain the equivalent switched capacitor filter by replacing the integration/summation branches in the LSFD with equivalent SC integration/summation stages.

For the LDI design the following design steps were adopted:

1. Prewarp the desired passband-stopband transition edge frequencies Ω_{pe} and Ω_{se} (see figure 3.9).
2. Obtain the required elliptic filter approximation and filter order which meets the desired passband loss and prewarped passband-stopband transition edge frequencies. (Even in the remote case where the required filter order is an integer, the resulting stopband loss of the filter approximation is unlikely to match the desired stopband loss.)
3. Select a normalized lowpass passive LC filter with an attenuation frequency response that best matches the attenuation frequency response of the computed prewarped filter approximation.

4. Adopt design steps 2 through 4 as applied to the BSS and BDS filter designs above.

For the LDI and bilinear filter designs the following clock-phased signal-sampling schemes were evaluated with the intention of selecting one for implementation:

1. Scheme I: Alternate SC integration/summation stages in the ladder filter structure connect and receive signal charge for processing from their input switched capacitors at a common clock phase.
2. Scheme II: All SC integration/summation stages in the ladder filter structure connect and receive signal charge for processing from their input switched capacitors at a common clock phase.

As will be explained in section 4.3, no clock-phased signal-sampling scheme was necessary for the BDS filter design.

4.2 Elliptic Lowpass Digital Filter Specifications, Required Order, and Prewarped Analog Filter Approximations

The following specifications were selected to be met by BSS, BDS, and LDI SC filter designs.

a) Filter type: Jacobi-elliptic

b) Passband attenuation loss (Ap) = 0.03 dB

c) Stopband attenuation loss (As) = 82.11 dB

d) Passband-edge frequency (Fpe),(cutoff) = 1.0 kHz

e) Stopband-edge frequency (Fse) = 1.8361 kHz

f) Clock frequency (Fc) = 10 kHz

Hence: Clock period (Tc) = 10^{-4} sec

The effective sampling period (Ts), and the sampling-to-cutoff frequency ratio (Fs/Fco) of the BSS, BDS, and LDI designs are listed below.

(BSS): Ts = 10^{-4} sec ; Fs/Fco = 10

(BDS): Ts = (0.5)x10^{-4} sec ; Fs/Fco = 20

(LDI): Ts = 10^{-4} sec ; Fs/Fco = 10

With specified values of Ts, Ωpe, and Ωse, values of denormalizing constants (λ) and required filter order (n) were obtained by means of tables 3.1 and 3.5. With n defaulted to an integer, and with the specified stopband loss (Ap), the normalized transfer function (Hn(s)) (in biquadratic sections) corresponding to the required prewarped filter approximation was derived using the elliptic filter algorithm presented in Appendix A. With the use of the computer program ANT (see Appendix A) values of λ, n, and parameter values of Hn(s) (as defined below) were computed and the results are listed in table 4.1.

$$Hn(s) = \frac{K_0}{D_0(s)} \prod_{i=1}^{r} \frac{s + A_{0_i}}{S + B_{1_i}s + B_{0_i}} \qquad 4.2.1$$

Table 4.1. Required and Adopted Order, Denormalizing Constant, and Parameter Values of the Analog Normalized Lowpass Transfer Function of the BDS, BSS, and LDI SCF Elliptic Lowpass Filter.

Component	Single-Sample	Double-Sample	LDI
Order			
Required	6.6266	6.8947	7.1601
Adopted	7	7	8
Denormalizing Constant (λ)	0.0010875	0.0011533	0.0001218
Hn(S) Parameters			
Ko	0.0003418	0.0005647	0.00001643
σ_o	0.3623649	0.3801434	-------
A01	9.4952748	8.7180491	38.677578
A02	3.1051775	2.8797424	5.027823
A03	2.0926430	1.9554543	2.412923
A04	------	------	1.822132
B01	0.2333963	0.2549870	0.143306
B02	0.4349581	0.4682642	0.309524
B03	0.5732057	0.6107634	0.507527
B04	------	------	0.626183
B11	0.6180851	0.6420791	0.663891
B12	0.3795791	0.3863048	0.509158
B13	0.1235172	0.1238044	0.296805
B14	------	------	0.094930

$$Hn(S) = \frac{Ko}{Do(S)} \prod_{i=1}^{r} \frac{S + A0i}{S + B1i*S + B0i}$$

$$r = \begin{cases} 3 & \text{Bilinear (BDS and BSS)} \\ 4 & \text{LDI} \end{cases}$$

$$Do(S) = \begin{cases} S + \sigma_o & \text{Bilinear (BDS and BSS)} \\ 1 & \text{LDI} \end{cases}$$

$$\text{where:} \quad r = \begin{cases} 3 & \text{BDS} \\ 4 & \text{LDI} \end{cases} \quad \text{and} \quad D_0(s) = \begin{cases} s + \sigma_0 & \text{BDS} \\ 1 & \text{LDI} \end{cases}$$

As expected from the analysis presented in section 3.3, the required filter order of the LDI design is larger than the other two equivalent bilinear designs. Note that despite the fact that the sampling frequency of the BDS design is twice that of the BSS design, the latter design requires a lower order filter. Recall that in most digital systems a high clock operation ensures a better approximation of equivalent analog systems. Considering the shape of the characteristic bilinear frequency prewarping curve in figure 3.3 as a function of Fs/F it is to be expected that by having a Fs/F ratio twice that of the BDS design, for all frequencies F, the BSS design will require larger passband-stopband transition widths than the BDS design. Hence, the required theoretical order of the BSS design to meet large transition widths is smaller than the BDS design.

The prewarped denormalized lowpass analog filter, $H_A(s)$, from which the digital switched capacitor filter is obtained is derived as follows:

$$H_A(s) = Hn(\bar{s})\Big|_{\bar{s} = \lambda s} \qquad 4.2.2$$

To obtain the switched capacitor equivalent of $H_A(s)$, by means of the leapfrog design technique and analog-to-SC integration/summation stage substitution, $H_A(s)$ must first be synthesized to a passive LC circuit. No readily available synthesis computer program was present at the time for the BSS and BDS design stage; hence, the design strategy presented in section 4.1 was adopted instead. When a circuit synthesis design package did become available during the LDI filter design stage, it entailed increasing the width of the prewarped passband-stopband transition, due to the even order of the filter approximation, so as to realize a resistance terminated LC ladder passive filter [4].

4.3 BSS and BDS 7th-Order Lowpass Filter Computer Comparisons

As discussed in section 4.2 no circuit systhesis program was available for obtaining the passive analog denormalized prototype from the denormalized prewarped analog transfer function as defined by equation 4.2.2. If the denormalized passive prototype is obtained, an SC filter design can be developed having a frequency response that best matches the specifications of section 4.2. Instead, a passive normalized lowpass filter was adopted which best met these specifica-

tions. This filter was then denormalized to a classically prewarped analog lowpass filter which was then S/Z- transformed to an equivalent SC filter. The S/Z-transformation was performed by first deriving the leapfrog signal flow diagram of the prewarped filter and then making analog-to-SC integration/summation stage substitutions. The selected 'best-match' normalized analog 7th-order elliptic lowpass filter upon which the adopted denormalized discrete-time lowpass specifications of section 4.2 were based is depicted in figure 4.1. Normalized component values are tabulated in table 4.2. The denormalized prewarped analog filter is depicted in figure 4.2 and its component values are also tabulated in table 4.2. The normalized frequency response is depicted in figure 4.3.

The leapfrog signal flow diagram of figure 4.2, containing denormalized integrating constants (K_i) and signal summation path gains (X_i), is depicted in figure 4.4. As discussed in chapter 3, positive summation paths, such as those in figure 4.4, cannot be directly implemented by any SC integrating stage and must be negated either by negating circuit nodes of by adding inverting buffers. For the BSS filter design nodes V_3 and V_7 where negated resulting in the signal flow graph of figure 4.5. For the BDS filter design

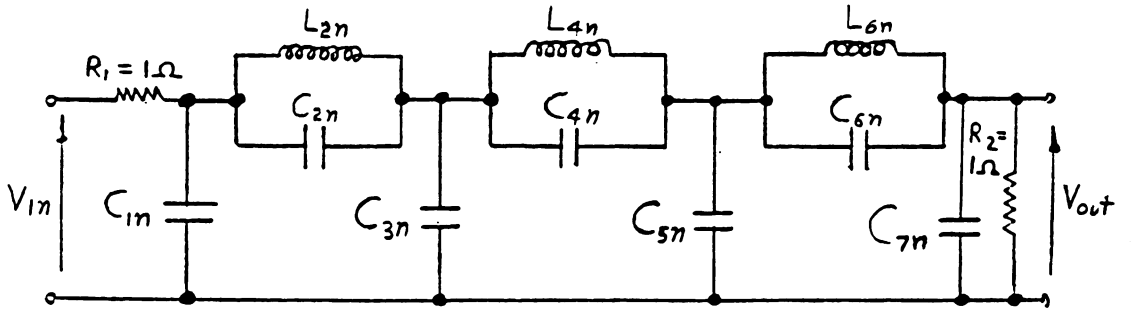

Figure 4.1. Normalized 7th-order elliptic lowpass LC filter.

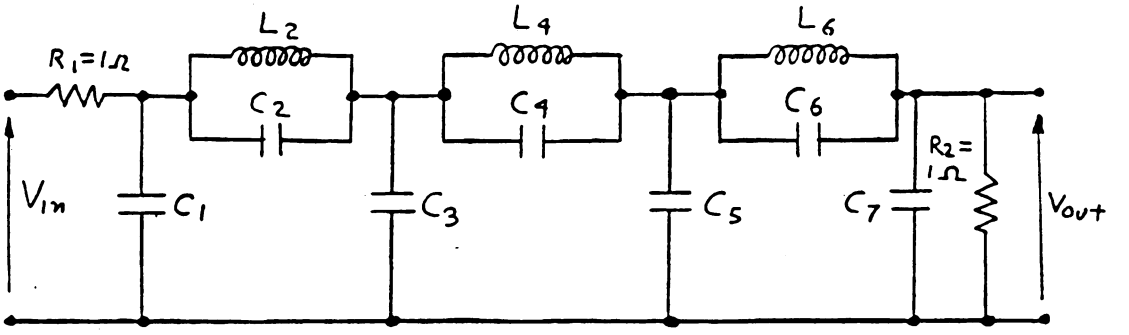

Figure 4.2. Prewarped-denormalized 7th-order elliptic lowpass LC filter.

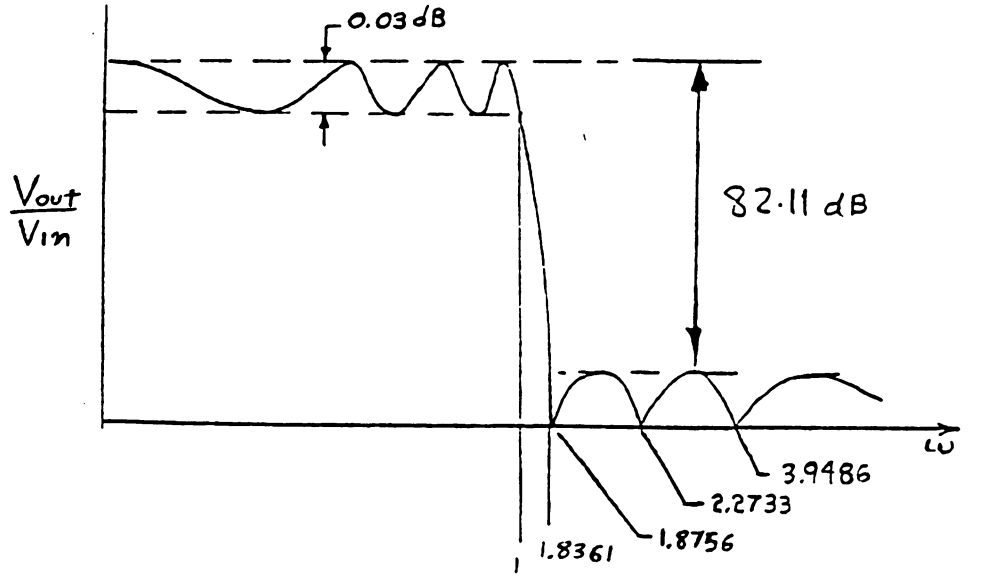

Figure 4.3. Attenuation-frequency response of 7th-order elliptic lowpass analog filter.

TABLE 4.2. Normalized and Denormalized Components of Passive LC Networks for the Bilinear and the LDI Design Cases.

	Bilinear 7th Order		LDI 8th Order	
Component	Normalized*	Denormalized	Normalized**	Denormalized
C_1	0.89703 F	$1.4159(10)^{-4}$ F	1.0070875 F	$1.6295(10)^{-4}$ F
C_2	0.04663 H	$7.36023(10)^{-6}$ H	0.0795947 H	$1.28787(10)^{-5}$ H
C_3	1.67701 H	$2.64705(10)^{-4}$ H	1.647433 H	$2.6656(10)^{-4}$ H
C_4	0.21124 H	$3.33428(10)^{-5}$ H	0.23217 H	$3.756614(10)^{-5}$ H
C_5	1.60770 H	$2.53765(10)^{-4}$ H	1.521333 H	$2.46158(10)^{-4}$ H
C_6	0.15766 H	$2.48856(10)^{-5}$ H	0.157865 H	$2.5543(10)^{-5}$ H
C_7	0.79759 H	$1.259(10)^{-4}$ H	1.4014335 H	$2.26758(10)^{-4}$ H
L_2	1.37533 H	$2.17087(10)^{-4}$ H	1.442074 H	$2.3333(10)^{-4}$ H
L_4	1.34563 H	$2.124(10)^{-4}$ H	1.4658171 H	$2.37176(10)^{-4}$ H
L_6	1.22740 H	$1.93737(10)^{-4}$ H	1.6064 H	$2.599(10)^{-4}$ H
L_8	-	-	1.0830 H	$1.75234(10)^{-4}$ H
R_1	1.0	1.0	1.0	1.0
R_2	1.0	1.0	1.0	1.0

* A. I. Zverev, "Handbook of Filter Synthesis," Wiley, New York, 1967.

** P. E. Allen and L. P. Huelsman, "Introduction to the Theory and Design of Active Filters," McGraw-Hill, New York, 1980.

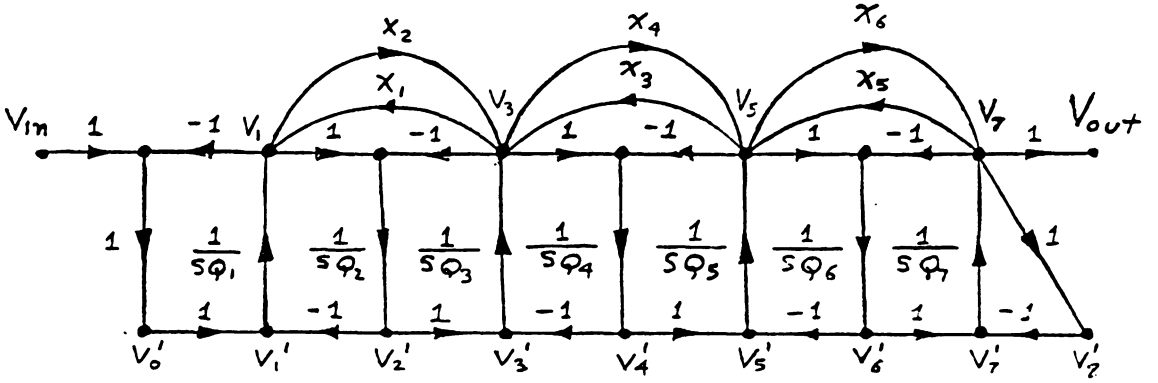

Figure 4.4. Leapfrog signal flow diagram of 7th-order elliptic lowpass analog filter.

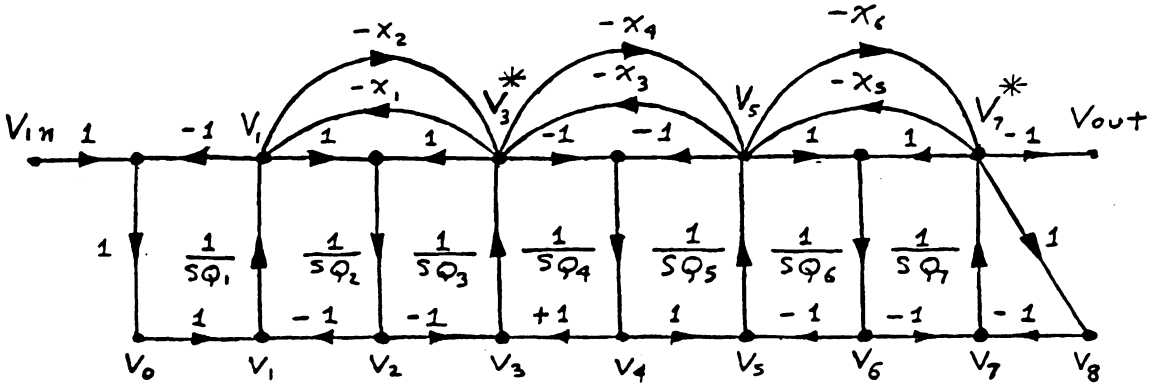

Figure 4.5. Leapfrog signal flow diagram of 7th-order elliptic lowpass analog filter with nodes v3 and v7 negated.

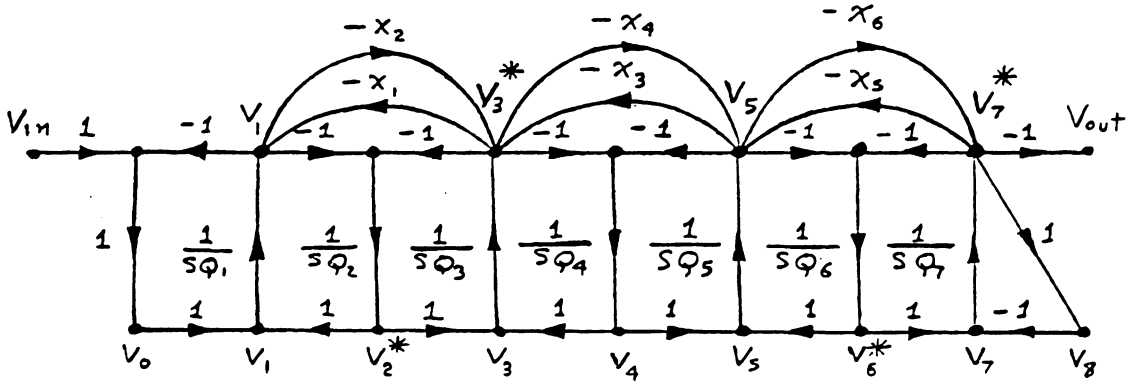

Figure 4.6. Leapfrog signal flow diagram of 7th-order elliptic lowpass analog filter with nodes v2, v3, v6, and v7 negated.

nodes V_2, V_3, V_6, and V_7 were negated resulting in the diagram in figure 4.6 where all internal stages have their inputs either all negative or all positive. The BDS filter was designed in this fashion so as to make it compatible for construction and testing purposes with the LDI structure of section 4.4.

Due to its signal double-sampling operation, the BDS design does not require any particular clock-phased signal-sampling scheme. This, however, is not the case for the BSS design. Both phasing schemes I and II were tested on the BSS design for a clock-to-cutoff frequency ratio of 10 and the resulting frequency response of both are plotted in figure 4.7. Scheme II which offered the best performance was adopted and the resulting BSS elliptic lowpass SC filter is depicted in figure 4.8. For the BDS elliptic lowpass filter design the SC filter is depicted in figure 4.9.

The BSS and the BDS lowpass filter designs were tested to compare their performance at clock-to-cutoff ratios (Fc/Fco) of 50, 25, 12.5, and 8. Simulation was performed by means of DIANA [36], and the frequency response results are plotted in figures 4.10 and 4.11. The most obvious difference between the two designs is evident from their stopband performance. For lower Fc/Fco ratios, the BDS design exhibits

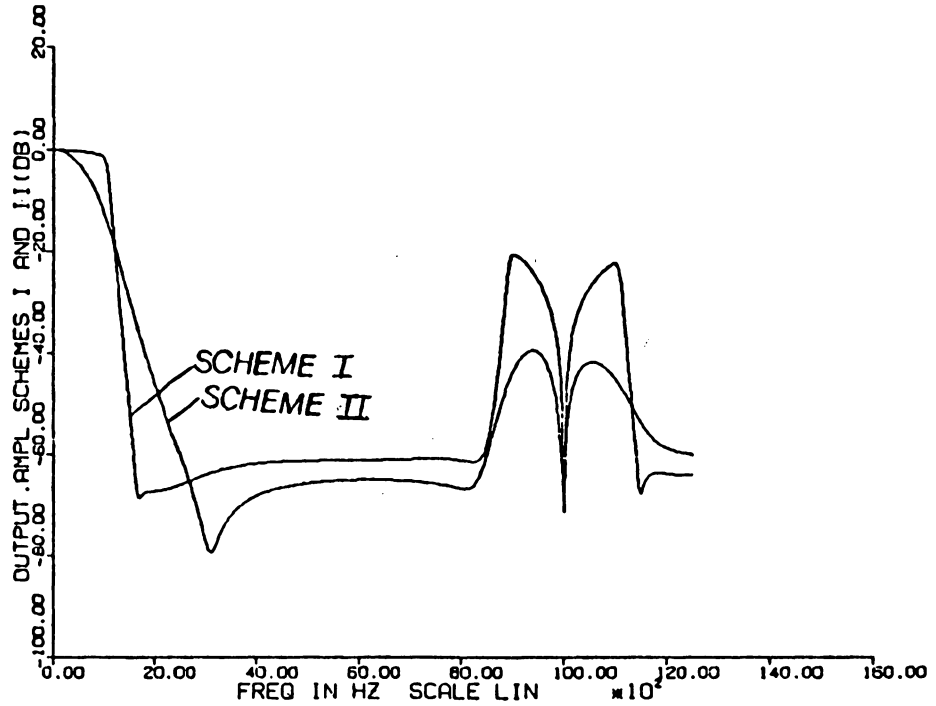

Figure 4.7. BSS filter: Clock-phased signal-sampling schemes I and II (filter attenuation-frequency response).

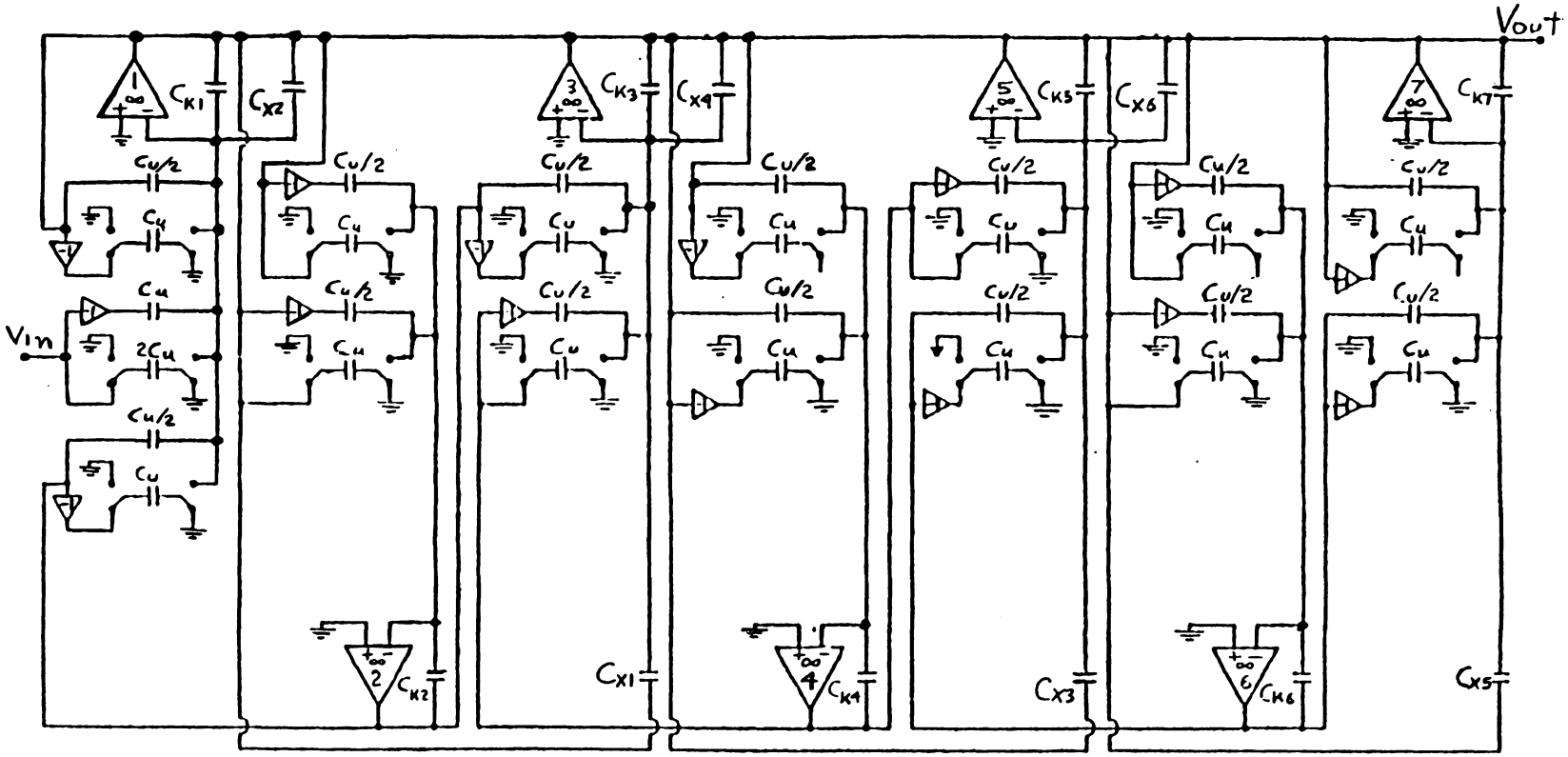

Figure 4.8. BSS 7th-order elliptic lowpass SCF leapfrog circuit (scheme I implementation).

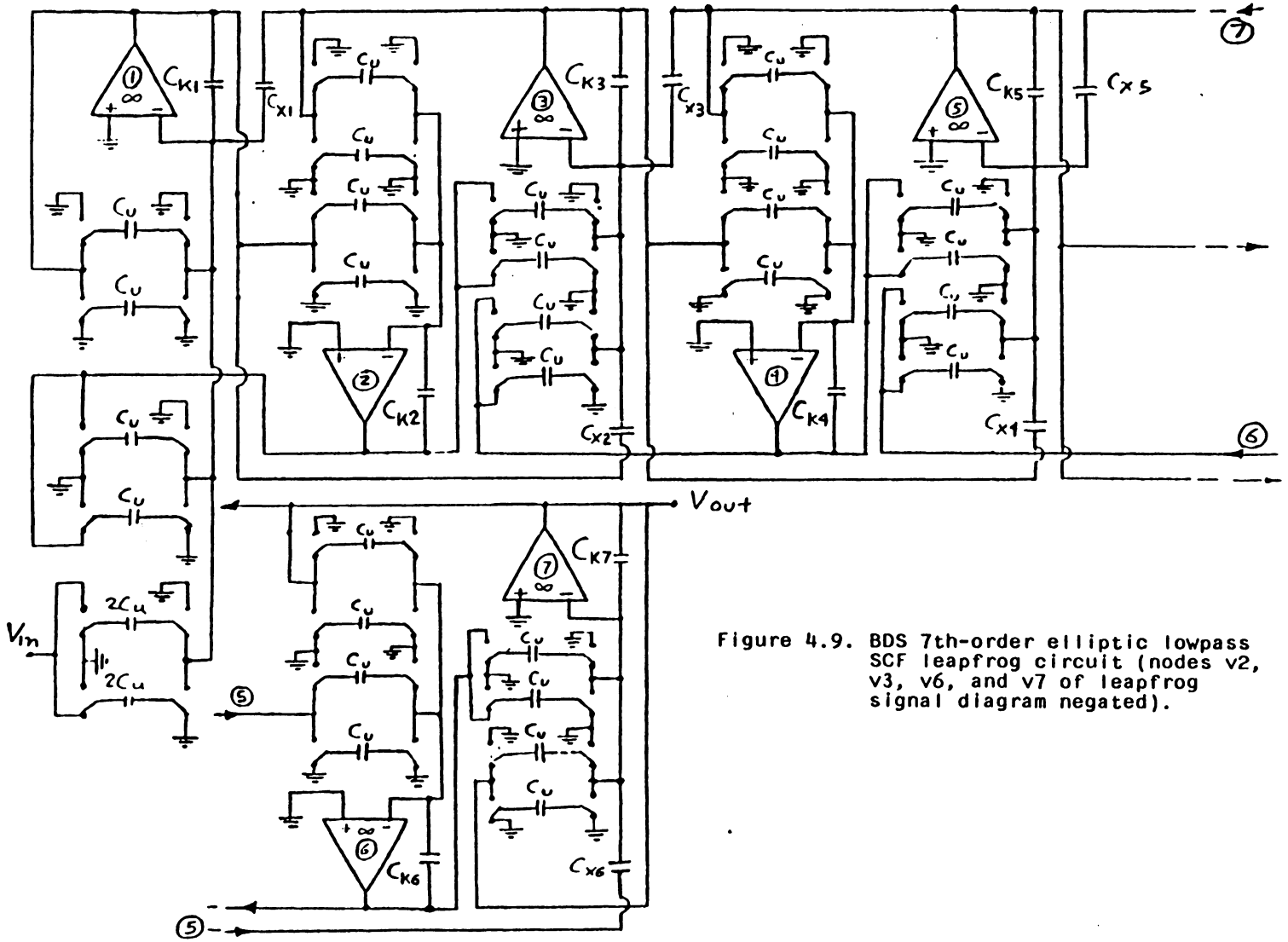

Figure 4.9. BDS 7th-order elliptic lowpass SCF leapfrog circuit (nodes v2, v3, v6, and v7 of leapfrog signal diagram negated).

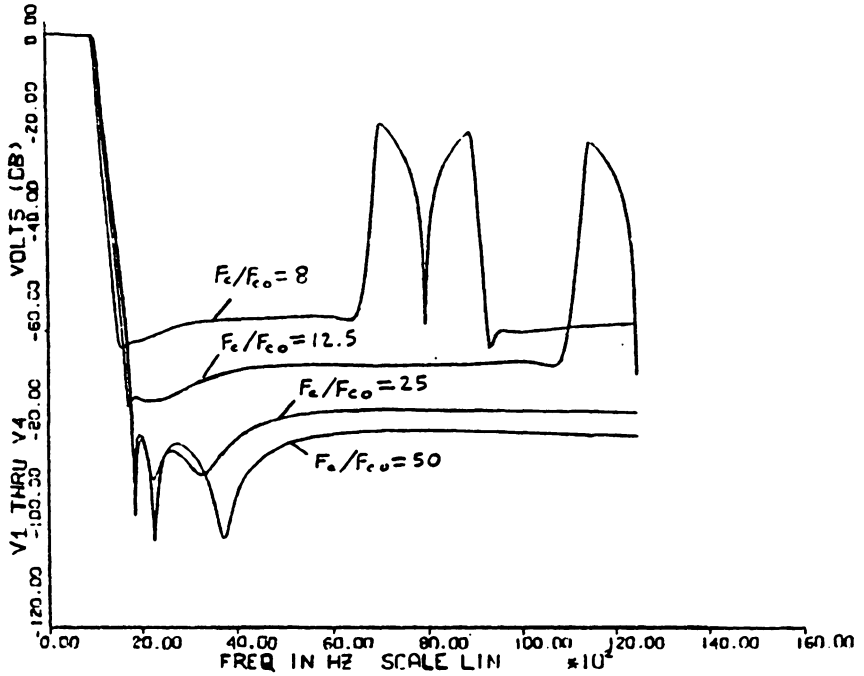

Figure 4.10. BSS 7th-order elliptic lowpass SCF leapfrog circuit attenuation-frequency response at Fc/Fco ratios: 50, 25, 12.5, and 8.

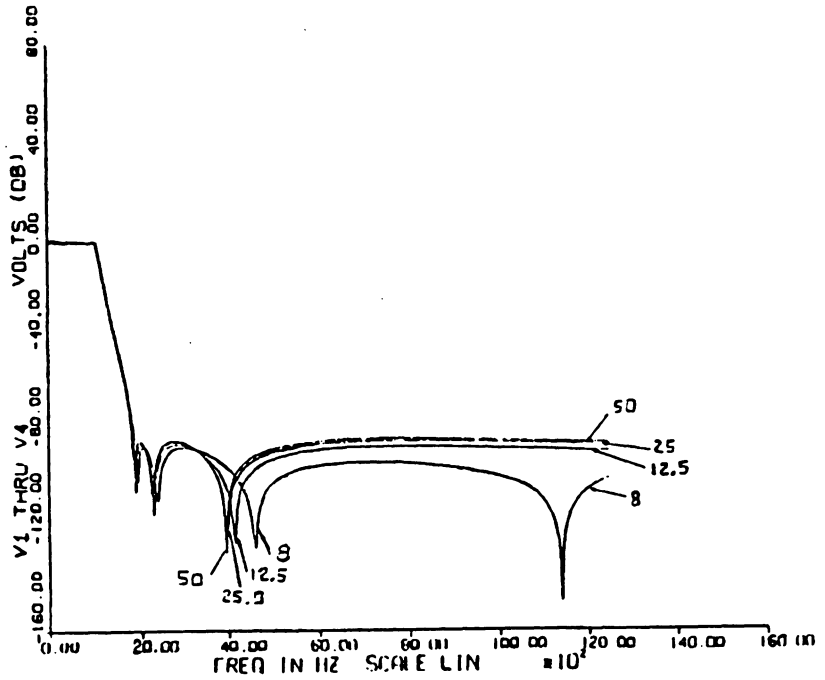

Figure 4.11. BDS 7th-order elliptic lowpass SCF leapfrog circuit attenuation-frequency response at Fc/Fco ratios: 50, 25, 12.5, and 8.

relatively small changes in stopband loss as illustrated in figure 4.11. By constrast, the BSS design deteriorates significantly in this respect as seen in figure 4.10, where the notches disappear at lower Fc/Fco ratios. Figure 4.12 illustrates the difference between the two designs for a Fc/Fco ratio of 12.5.

Although the above results suffice to demonstrate the superior performance of the BDS design, consideration may also be given to comparing the number of circuit components as listed in table 4.3. Thus, although requiring more capacitors and switches, the BDS design uses fewer inverters. With this comparative analysis of the BSS and BDS design in mind, it was thus decided to develop the BDS filter with a prewarped denormalizing frequency at 1kHz and operating with a Fc/Fco ratio of 10.

To provide data for a suitable choice of prewarped denormalizing frequency, the BDS design using a Fc/Fco ratio of 8 was simulated at three frequencies: 500Hz, 1000Hz, and 1836.1Hz (first notch location). The results of the simulations are shown in figure 4.13 and may be summarized as follows:

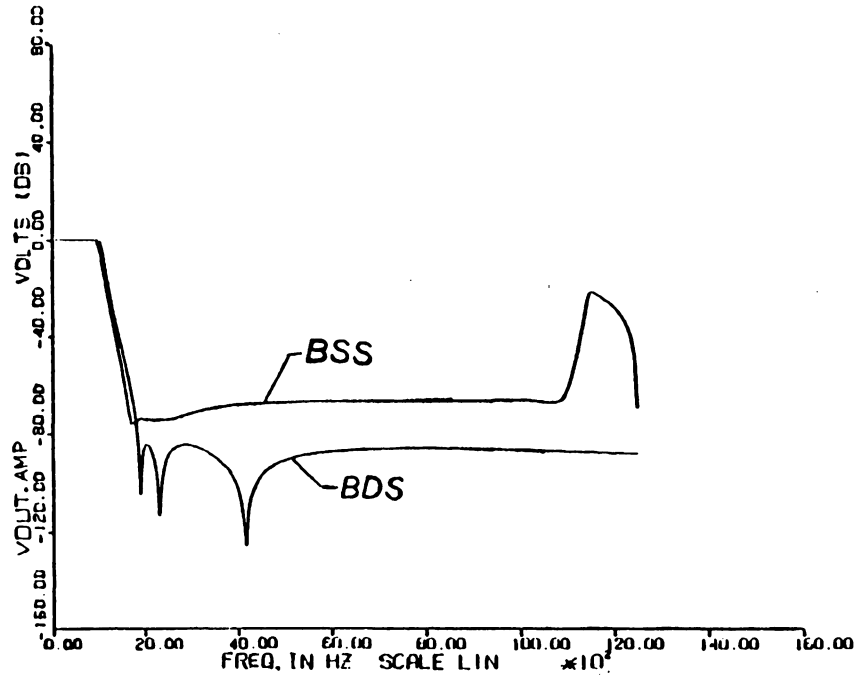

Figure 4.12. BSS and BDS 7th-order elliptic lowpass SCF leapfrog circuit attenuation-frequency response at Fc/Fco ratio of 12.5.

Table 4.3. Number of Components of 7th-Order Bilinear and 8th-Order LDI Elliptic SCR Lowpass Filters.

Component Type	Single-Sample Bilinear	Double-Sample Bilinear	LDI
	Fig. 4.8	Fig. 4.9	Fig. 4.19
Op-Amp	7	7	7
Switched-Capacitor	15	30	17
Switch	15	30	17
Inverter	14	0	0

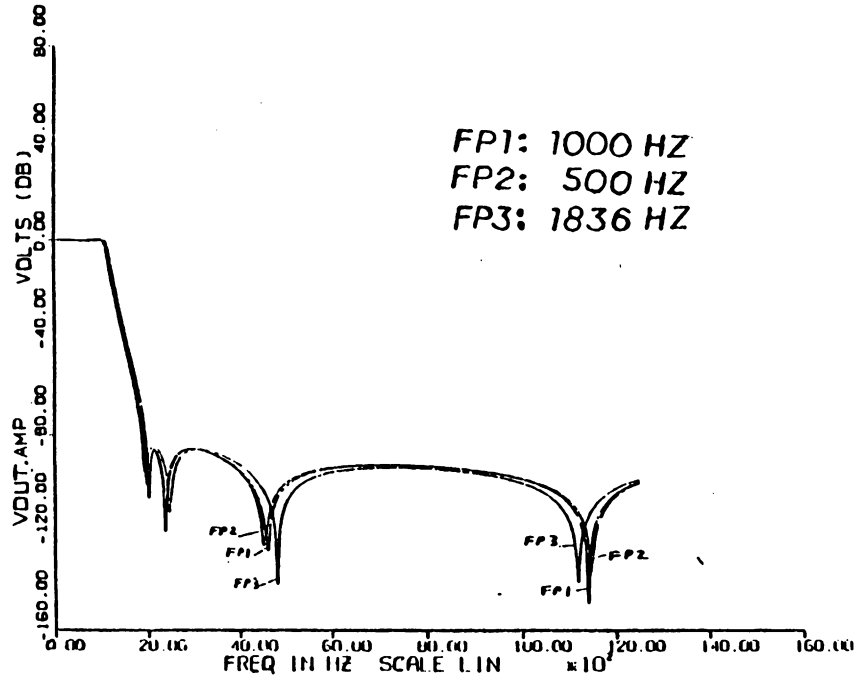

Figure 4.13. BDS 7th-order elliptic lowpass SCF leapfrog circuit attenuation-frequency response; prewarped-denormalized at frequencies: 1836.1Hz, 1000Hz, and 500Hz.

i) FP3 (1836.1Hz): This causes the notches to shift to higher frequencies.

ii) FP2 (500Hz): This causes the notches to shift to slightly lower frequencies.

iii) FP1 (1000Hz): The notches are located very close to their desired positions.

4.4 LDI 8th-Order Elliptic Lowpass Filter Design

A similar problem to that of the bilinear design case was encountered for the LDI filter in deriving the passive analog denormalized circuit prototype form the denormalized prewarped analog transfer function (defined by equation 4.2.2). Though a passive circuit synthesis program did became available, it entailed expanding the frequency width of the prewarped passband-stopband transition in order to realize a resistance terminated LC ladder network (due to the even order of the filter [4]). Instead, a passive normalized lowpass LC filter was selected with an attenuation-frequency response that best matched the attenuation-frequency response of the prewarped filter approximation as defined by 4.2.1. This filter was then denormalized to a classically prewarped analog filter that was then S/Z-transformed to its corresponding LDI SC filter.

The selected normalized lowpass filter is depicted in figure 4.14 which has the following attenuation characteristic:

a) Passband loss (Ap): 0.177 dB

b) Stopband loss (As): -101.0 dB

c) Passband-edge frequency (Fpe), (cutoff): 1 kHz

d) Stopband-edge frequency (Fse): 1780 kHz

Normalized component values of figure 4.14 are listed in table 4.2. The denormalized filter is depicted in figure 4.15 and its component values are tabulated in table 4.2.

This filter along with the LDI normalized biquadratic sections of section 4.2 was denormalized for a cutoff frequency of 1kHz and their frequency response outputs plotted in figure 4.16. Note that the 6dB difference between two responses is due to the equal resistance terminations of the denormalized highpass prototype of figure 4.15. Note also that the last zero of the best fit design is located at infinity.

The final leapfrog signal flow graph of the LDI design with nodes V_2, V_3, V_6, and V_7 negated is depicted in figure 4.17. Both clock-phased signal-sampling schemes I and II were simulated giving identical frequency response results as shown in figure 4.18. Phasing scheme I was arbitrarily

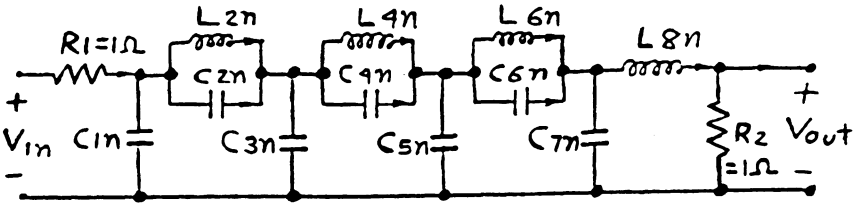

Figure 4.14. 8th-order normalized elliptic lowpass LC filter.

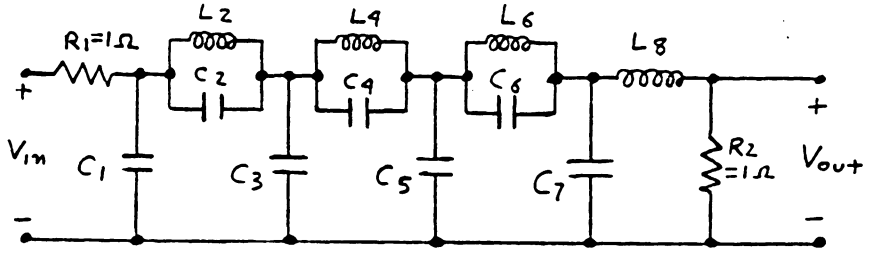

Figure 4.15. Prewarped-denormalized 8th-order elliptic lowpass LC filter.

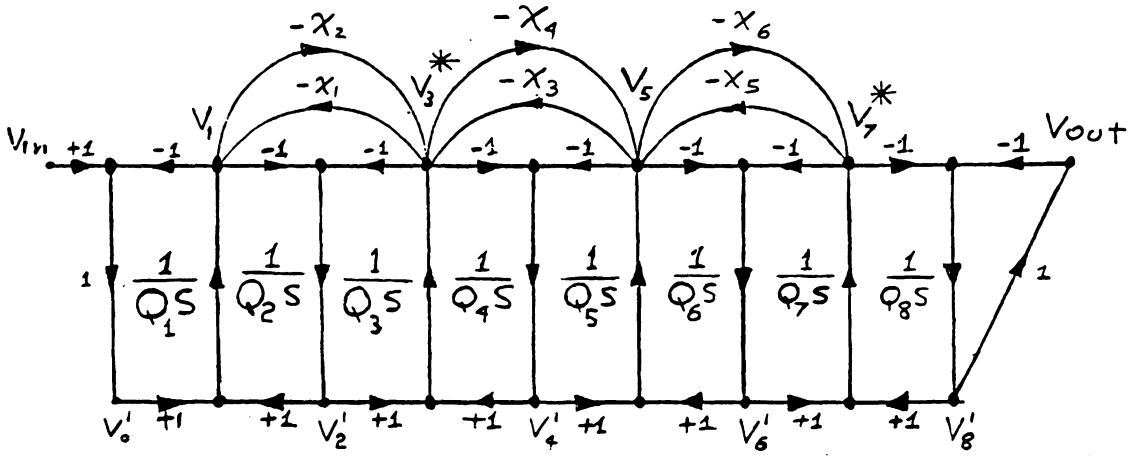

Figure 4.17. Leapfrog signal flow diagram of 8th-order elliptic lowpass filter with nodes v2, v3, v6, and v7 negated.

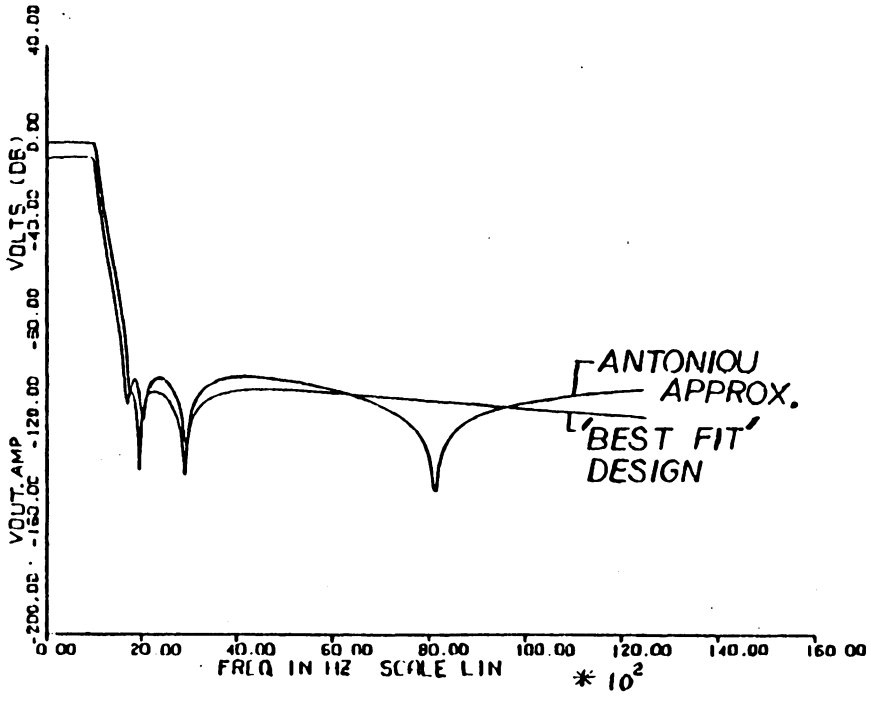

Figure 4.16. 8th-order denormalized prewarped elliptic analog lowpass attenuation-frequency response: Antoniou and 'best-fit' designs.

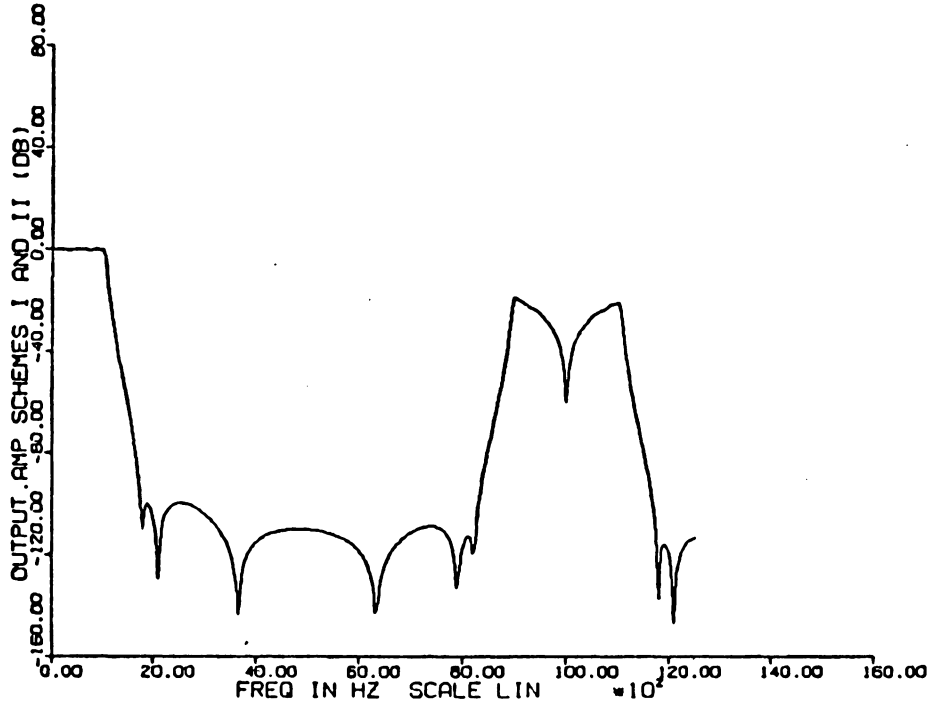

Figure 4.18. LDI 8th-order SCF elliptic lowpass filter attenuation-frequency response: clock-phased signal-sampling schemes I and II implementation.

selected resulting in the SC filter of figure 4.19. A minor phasing mistake was incurred in the construction of the LDI filter and this involved a 180 degrees phase shift between the sampling of opamp 1 and the sampling of the input Vin and opamp 2 by the first stage as illustrated in figure 4.19. As it turns out, for an operating Fc/Fco ratio of 10, this sampling mistake in the implemented LDI design (LDI I) did not affect the overall computer predicted performance of the filter when compared to the response of the proper LDI design (LDI II) as depicted in figure 4.20.

4.5 Computer and Experimental Results of the BDS and the LDI Elliptic Lowpass Filters

For both the BDS and the LDI designs, the passive normalized lowpass filters of figures 4.1 and 4.14 were denormalized to analog lowpass filters (figures 4.2 and 4.15) which are the prewarped analog equivalent of the BDS and the LDI digital filters of figures 4.9 and 4.19. Both the BDS and the LDI filters were designed to operate for a 10kHz clock frequency. The prewarped denormalizing frequencies (w_{Dn}) are listed below.

BDS: $Ts = Tc/2 = (0.5)\times10^{-4}$; $Fco = 1000$ Hz

$$w_{Dn} = [2/((0.5)(10)^{-4})]\{\tan(\pi Fco(0.5)(10)^{-4})\}$$

$$w_{Dn} = 6391.256 \qquad 4.5.1$$

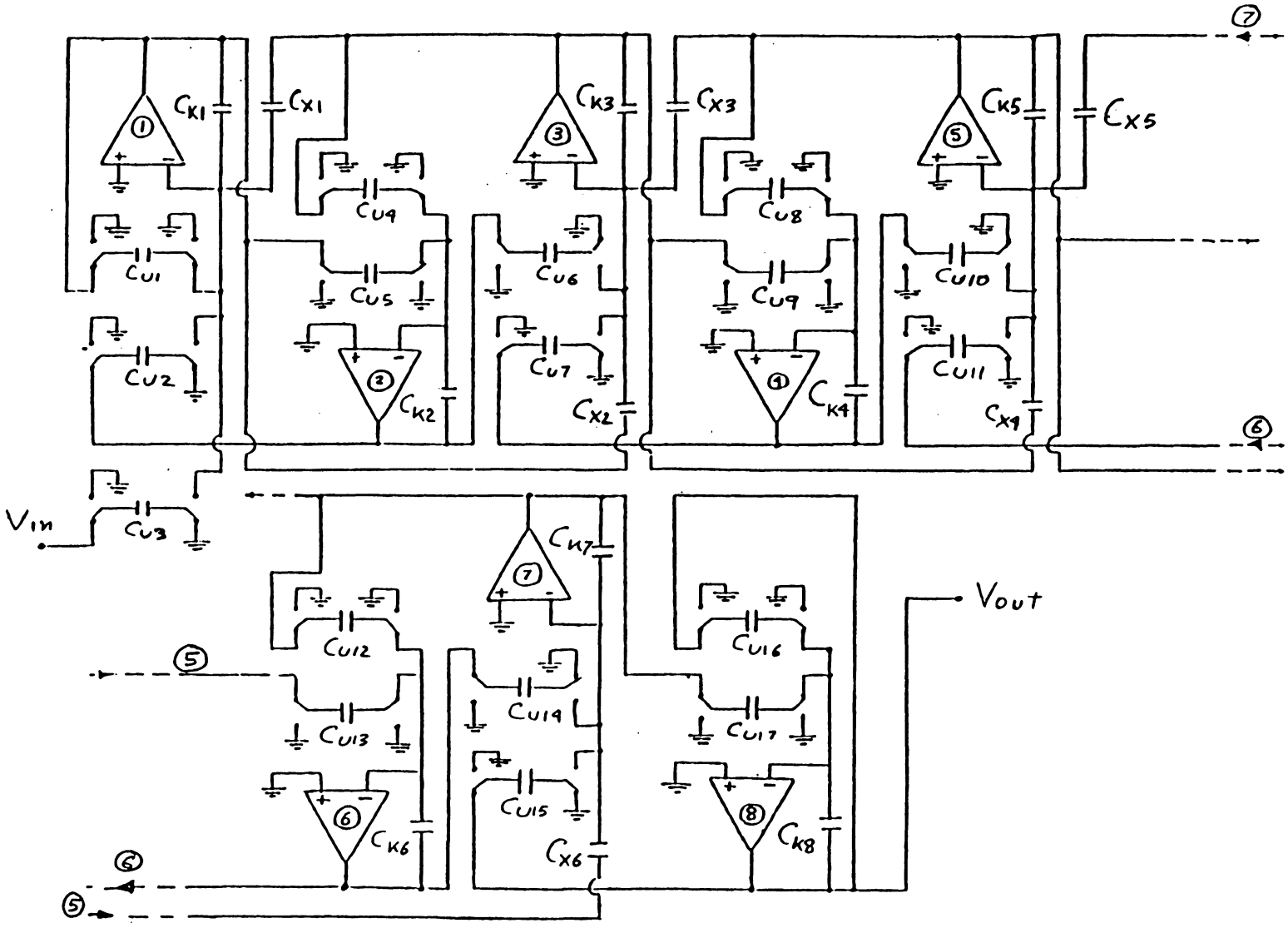

Figure 4.19. LDI 8th-order elliptic lowpass SCF circuit diagram (clock-phased signal-sampling scheme I implementation).

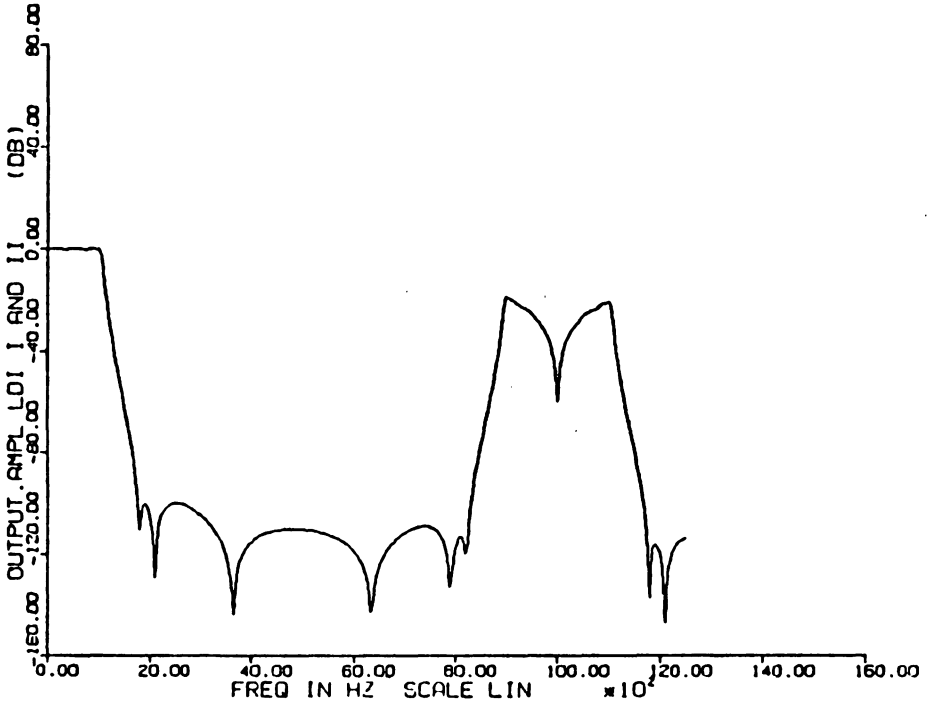

Figure 4.20. LDI 8th-order elliptic lowpass SCF attenuation-frequency response: LDI I- implemented design; LDI II- proper design.

$$\text{LDI: } Ts = Tc = 10^{-4} \quad ; \quad Fco = 1000 \text{ Hz}$$

$$w_{Dn} = [2/(10^{-4})]\{\sin(\pi Fco 10^{-4})\}$$

$$w_{Dn} = 6232.92 \qquad 4.5.2$$

The denormalized capacitor and inductor components of figures 4.2 and 4.15 were computed by the following element denormalization relations:

$$L = Ln/w_{Dn} \quad ; \quad C = Cn/w_{Dn} \qquad 4.5.3$$

The values of normalized and denormalized capacitor and inductor values for the BDS and LDI design cases are tabulated in table 4.2.

The adopted leapfrog signal flow diagram of figures 4.2 and 4.14 are depicted in figures 4.6 and 4.17 respectively. the output ($Vo_i(s)$) for a typical integration/summation stage of figures 4.6 and 4.17 have the following relationship format:

$$Vo_i(s) = \frac{1}{Q_i s} \sum_j vin_j(s) + \sum_k X_k \, Vin_k(s) \qquad 4.5.4$$

Where for some stages there are no summing input signals ($Vin_k(s)$). Denormalized integrating constants (Q_i) and summing signal gain constants (X_k) in figures 4.6 and 4.17 are functions of denormalized capacitor and inductor values of figures 4.2 and 4.14. Q_i and X_i relationships and values for

the bilinear design case are tabulated in table 4.4. Likewise, table 4.5 lists relationships and values of Q_i and X_i for the LDI design case.

A typical SC integration and summation stage (figure 2.8) can be defined to have the following output ($Vo_i(Z)$) relationship format:

$$Vo_i(Z) = G \frac{Cu_i}{Ck_i} \sum_j \frac{Xin_j(Z)}{Pw(Z)} + \sum_k \frac{Cx_k}{Ck_i} Vin_k(Z) \qquad 4.5.5$$

$G = 1/Ts(LDI) ; = 2/Ts(Bilinear ; Pw(Z)$ - (see Table 3.7)

When SC integration-summation stages are eventually replaced for the analog integration stages of figures 4.6 and 4.17 the Cxk capacitors become the notch-forming capacitors of the resulting BDS and LDI elliptic filters of figures 4.9 and 4.19. Taking the bilinear and the LDI S/Z-transformation of equation 4.5.4 and then equating the results to the relationship format of equation 4.5.5 produces the following Cui, Cki, and Cxk capacitor equations for the BDS and the LDI filter integration/summation stages:

$$(BDS): \quad Cki = \frac{QiCui}{Ts} = \frac{2QiCui}{Tc} \qquad 4.5.6$$

$$Cxk = Xk(Cki) \qquad 4.5.7$$

$$(LDI): \quad Cki = \frac{QiCui}{Ts} = \frac{QiCui}{Tc} \qquad 4.5.8$$

TABLE 4.4. BDS 7th-Order Leapfrog Lowpass Analog Integrating Constants (Qi) and Summation Gain Constants (Xi): Relationships and Values.

Stage (i)	Qi Relationship	Qi Value
1	$C_1 + C_2$	0.94366
2	L_2	1.37533
3	$C_2 + C_3 + C_4$	1.93488
4	L_4	1.34563
5	$C_4 + C_5 + C_6$	1.9766
6	L_6	1.22740
7	$C_6 + C_7$	0.95525

(xi)	Xi Relationship	Xi Value
i=1	$C_2/(C_1+C_2)$	0.0494
2	$C_2/(C_2+C_3+C_4)$	0.0241
3	$C_4/(C_2+C_3+C_4)$	0.1092
4	$C_4/(C_4+C_5+C_6)$	0.1069
5	$C_6/(C_4+C_5+C_6)$	0.0798
6	$C_6/(C_6+C_7)$	0.1650

where: $C_{Ki} = \frac{2Q_i C_{ui}}{T_c}$ $\quad i = 1, \ldots, 7$

$C_{x1} = x_1 C_{K1}$ | $C_{x4} = x_4 C_{K5}$

$C_{x2} = x_2 C_{K2}$ | $C_{x5} = x_5 C_{K5}$

$C_{x3} = x_3 C_{K3}$ | $C_{x6} = x_6 C_{K7}$

TABLE 4.5. LDI 8th-Order Leapfrog Lowpass Analog Integrating Constants (Qi) and Summation Gain Constants (Xi): Relationships and Values.

Stage (i)	Qi Relationship	Qi Value
1	$C_1 + C_2$	1.0866822
2	L_2	1.442074
3	$C_2 + C_3 + C_4$	1.9591977
4	L_4	1.442074
5	$C_4 + C_5 + C_6$	1.911368
6	L_6	1.6064
7	$C_6 + C_7$	1.5593005
8	L_8	1.08300

(xi)	Xi Relationship	Xi Value
i=1	$C_2/(C_1+C_2)$	0.0732456
2	$C_2/(C_2+C_3+C_4)$	0.0406262
3	$C_4/(C_2+C_3+C_4)$	0.1185026
4	$C_4/(C_4+C_5+C_6)$	0.121468
5	$C_6/(C_4+C_5+C_6)$	0.0825927
6	$C_6/(C_6+C_7)$	0.1012409

where: $C_{Ki} = \frac{Q_i C_{ui}}{T_c}$; $i = 1, \ldots, 8$

$C_{x1} = x_1 C_{K1}$ | $C_{x4} = x_4 C_{K4}$

$C_{x2} = x_2 C_{K2}$ | $C_{x5} = x_5 C_{K5}$

$C_{x3} = x_3 C_{K3}$ | $C_{x6} = x_6 C_{K6}$

$$Cxk = Xk(Cki) \qquad 4.5.9$$

where: Ts-sampling period

Tc-clock period

By selecting Cui as 1000pf (which is large enough to avoid the adverse effects of stray capacitance yet small enough to allow a reasonably high clock rate), by using the tabulated values of Qi and Xi, and by designing for a clock perod of 10^{-4} sec, the design values of Cki and Cxi for the BDS and the LDI filters were obtained. Design and implemented values of Cui, Cki, and Cxi for the bilinear and the LDI filters of figures 4.9 and 4.19 are listed in tables 4.6 and 4.7 respectively. The LDI filter was dynamically ranged at the 1kHz cutoff frequency (see Appendix C); thus, the implemented values in table 4.7 are dynamically ranged capacitor values. Due to the equally terminated resistances (R_1 and R_2) of the prewarped denormalized analog circuits, there is an unwanted 6dB passband loss which would appear in the SC filters. To compensate for this, the effective input signal for both the BDS and LDI filters was magnified by a factor of 2 by simply doubling the value of the Vin-sampling capacitors Cu (BDS) and Cu3 (LDI). The implemented capacitor values were measured on an ESL Model 253 Impedance Bridge (accuracy: 0.25%).

TABLE 4.6. BDS 7th-Order SCF Capacitor Values.

Capacitor	Design Value (nF)	Actual Value (nF)
C_{K1}	2.8420	2.829
C_{K2}	4.1250	4.124
C_{K3}	5.8760	5.920
C_{K4}	4.0441	4.060
C_{K5}	6.4896	6.530
C_{K6}	4.0529	4.067
C_{K7}	2.8890	2.885
C_{x1}	0.1398	0.137
C_{x2}	0.1427	0.142
C_{x3}	0.6463	0.654
C_{x4}	0.6979	0.706
C_{x5}	0.5209	0.519
C_{x6}	0.4762	0.479
C_u	1.0000	{0.950 → 1.047 mean = 0.981}

TABLE 4.7. LDI-8th Order SCF Capacitor Values.

Capacitor	Design Value (nF)	Actual Value (nF)
C_{K1}	1.7583	1.858
C_{K2}	2.3333	2.34
C_{K3}	3.170	3.45
C_{K4}	2.3333	2.36
C_{K5}	3.0927	3.22
C_{K6}	2.5992	2.66
C_{K7}	2.523	2.65
C_{K8}	1.7523	1.792
C_{x1}	0.1275423	0.137
C_{x2}	0.1300452	0.135
C_{x3}	0.3427922	0.372
C_{x4}	0.4116963	0.477
C_{x5}	0.20804	0.287
C_{x6}	0.31362	0.511
C_{u1}	1.0	1.002
C_{u2}	1.162	1.174
C_{u3}	0.8704	0.884
C_{u4}	0.8522	0.859
C_{u5}	0.8606	0.859
C_{u6}	1.1734	1.174
C_{u7}	1.1686	1.166
C_{u8}	0.7808	0.778

TABLE 4.7. LDI 8th-Order SCF Capacitor Values (Continued).

Capacitor	Design Value (nF)	Actual Value (nF)
C_{u9}	0.8557	0.857
C_{u10}	1.2807	1.301
C_{u11}	1.0698	1.063
C_{u12}	0.7613	0.768
C_{u13}	0.934728	0.938
C_{u14}	1.313545	1.328
C_{u15}	0.591302	0.572
C_{u16}	1.0	1.001
C_{u17}	1.7523	1.792

The following circuit components were used in the construction of the BDS and the LDI filters:

Op-amp: Harris HA4605

Switch: Harris HI2201

For the operation of the switched capacitor driving switches above two clocks were used, ϕ_1 and ϕ_2, operating at a 60-40% duty cycle. The duty cycle waveform of the clocks is illustrated in figure 4.21 along with a representative SC integration stage depicting the ϕ_1 and ϕ_2 phasing of the input switched capacitor.

The DIANA computer simulation of the BDS and the LDI filters for idealized component values and operating with a single clock having a 60-40 % duty-cycle is presented in figures 4.22 and 4.23 respectively. Practical results obtained with an HP Model 3580A spectrum analyzer are presented in figures 4.24-4.27 for the BDS filter and figures 4.28-4.33 for the LDI filter. All laboratory tests were performed with a 60-40% duty cycle clock operation. A 1 volt amplitude input signal was used for all BDS filter tests and for some of the LDI filter tests. The input signal to the LDI filter was at one point magnified by a factor of 7.0795 so as to obtain a better resolution of the stopband characteristic which had an attenuation loss almost equal to that

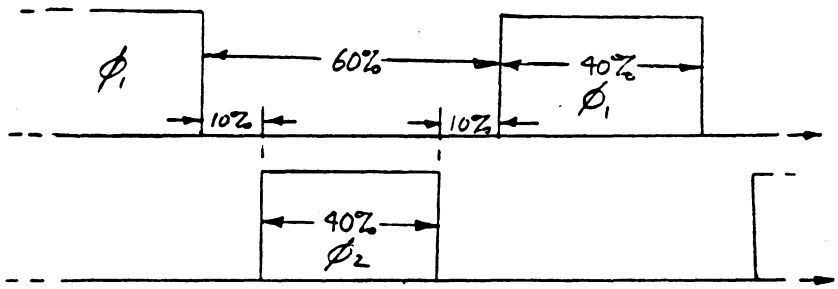

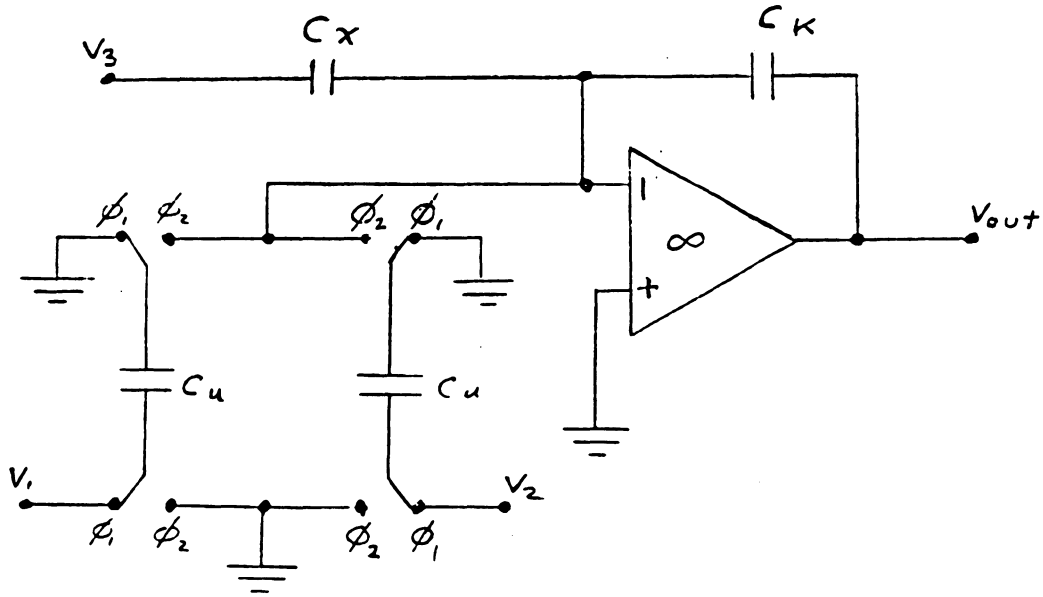

Figure 4.21. 60-40% dual-clock duty cycle implementation on a typical switched capacitor integration/summation stage.

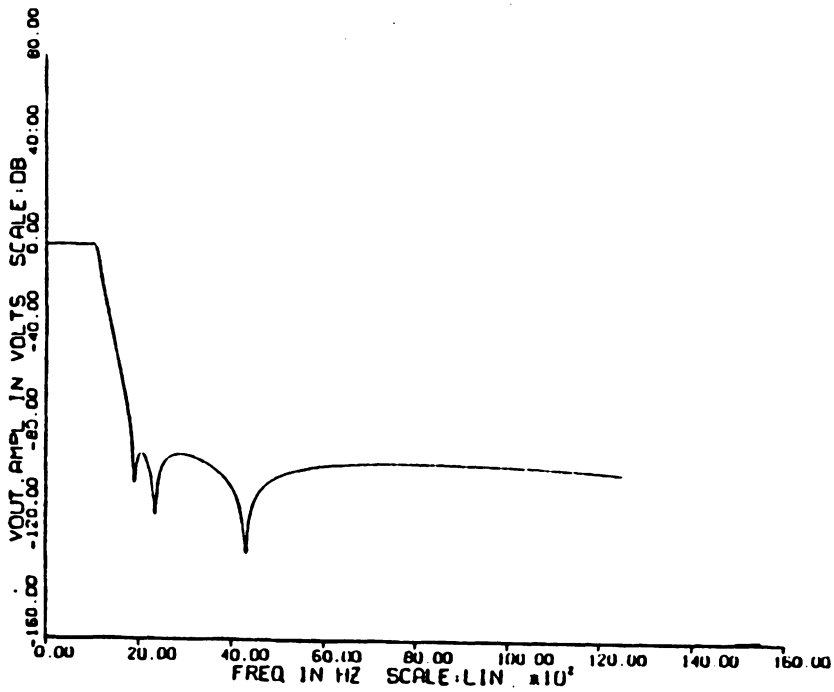

Figure 4.22. BDS 7th-order SCF elliptic lowpass filter attenuation-frequency response (idealized components).

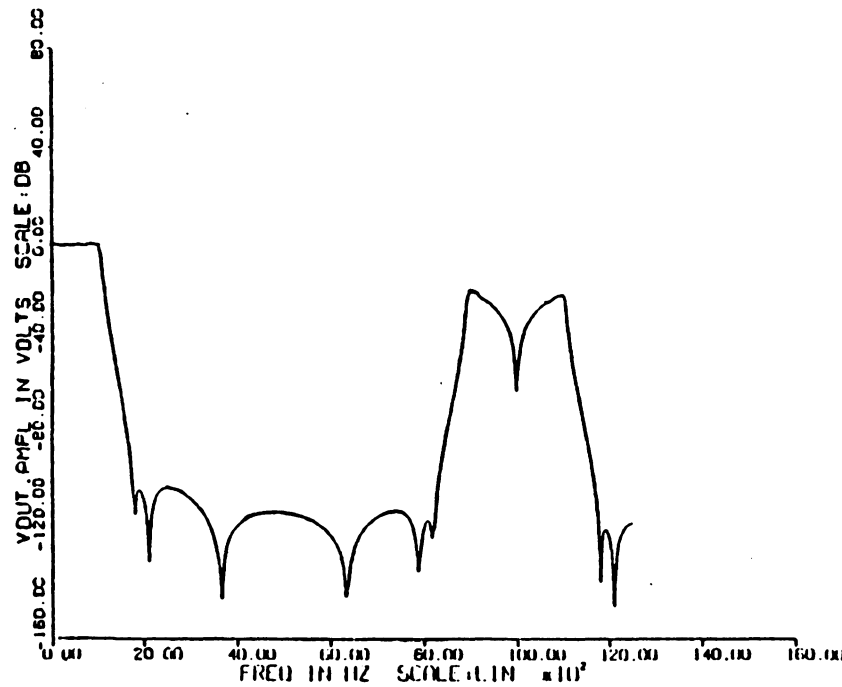

Figure 4.23. LDI 8th-order SCF elliptic lowpass filter attenuation-frequency response (idealized components).

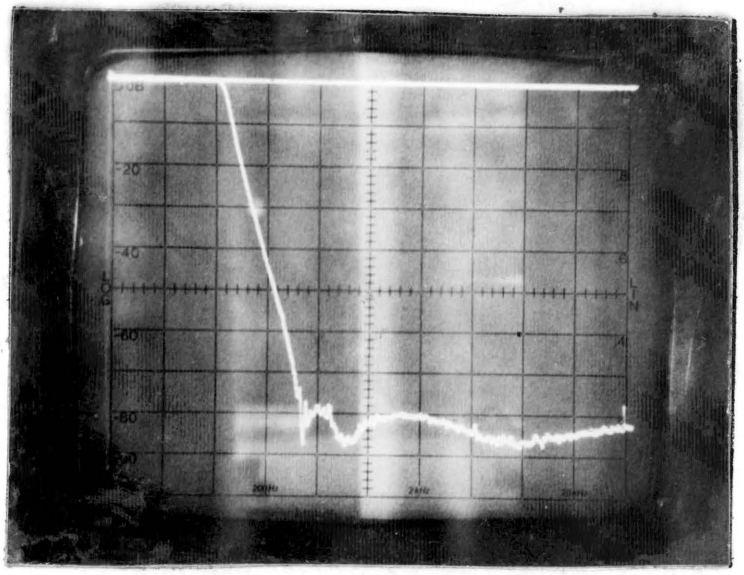

Figure 4.24. BDS filter test results (passband & stopband)
vertical: 10 dB/div duty cycle: 40-60%
horizontal: 0.5 Khz/div Fc/Fco: 10

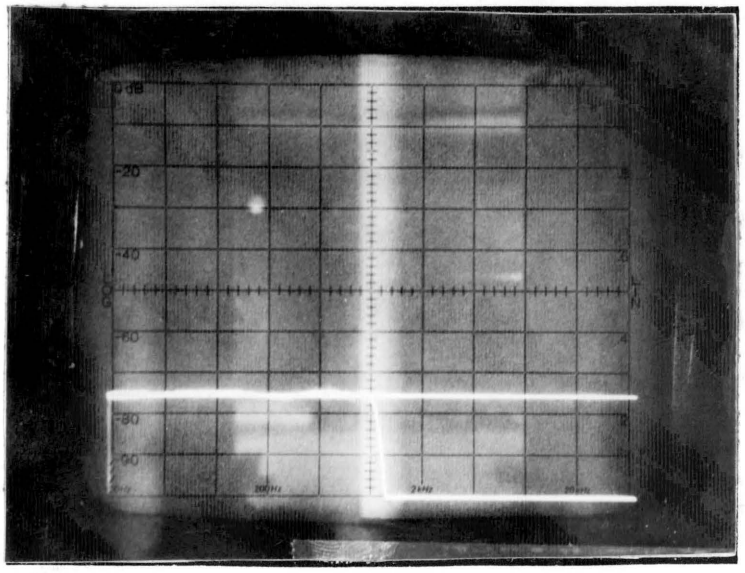

Figure 4.25. BDS filter test results (passband)
vertical: 1 dB/div duty cycle: 40-60%
horizontal: 0.2 Khz/div Fc/Fco: 10

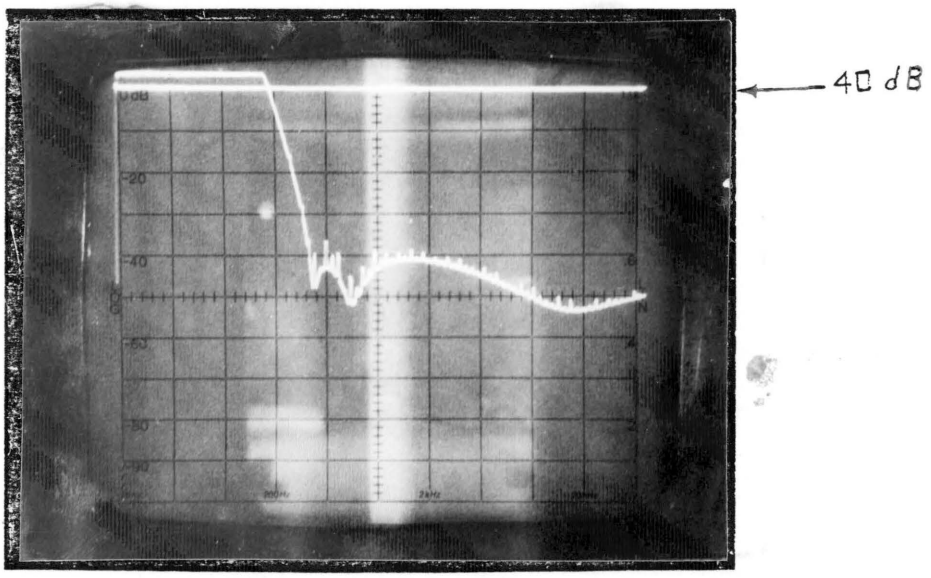

Figure 4.26. BDS filter test results (stopband).
vertical: 10 dB/div duty cycle: 40-60%
horizontal: 0.5 Khz/div Fc/Fco: 10

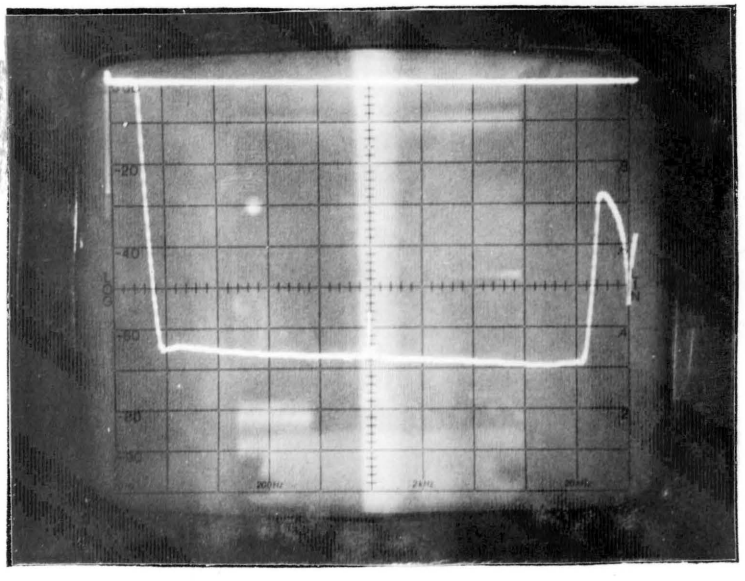

Figure 4.27. BDS filter test results (passband & stopband)
vertical: 10 dB/div duty cycle: 40-60%
horizontal: 2 Khz/div Fc/Fco: 10

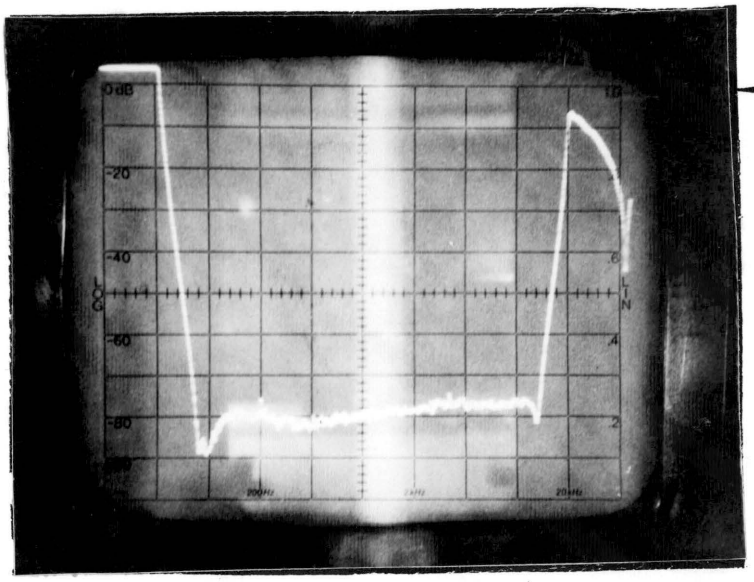

Figure 4.28. LDI filter test results (stopband).
vertical: 10 dB/div duty cycle: 40-60%
horizontal: 1 Khz/div Fc/Fco: 10

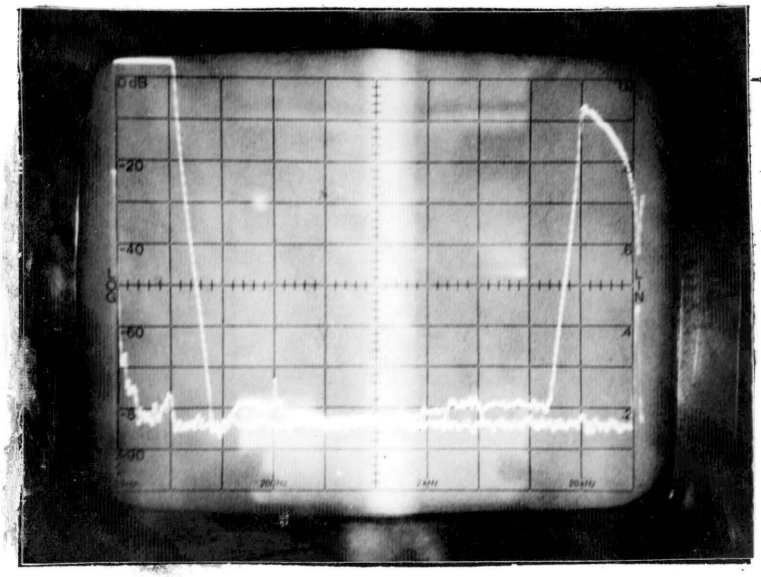

Figure 4.29. LDI filter test results (stopband & noise level)
vertical: 10 dB/div duty cycle: 40-60%
horizontal: 1 Khz/div Fc/Fco: 10

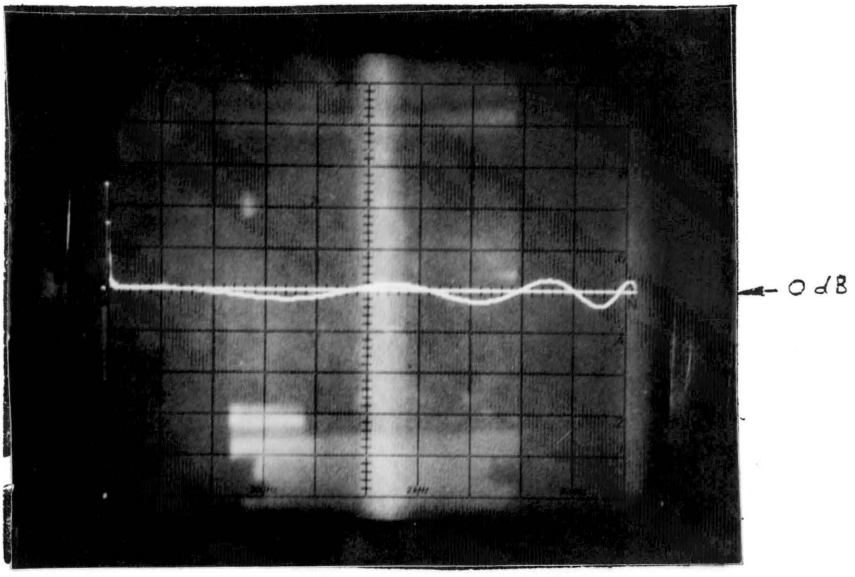

Figure 4.30. LDI filter test results (passband)
vertical: 1 dB/div duty cycle: 40-60%
horizontal: 0.1 Khz/div Fc/Fco: 10

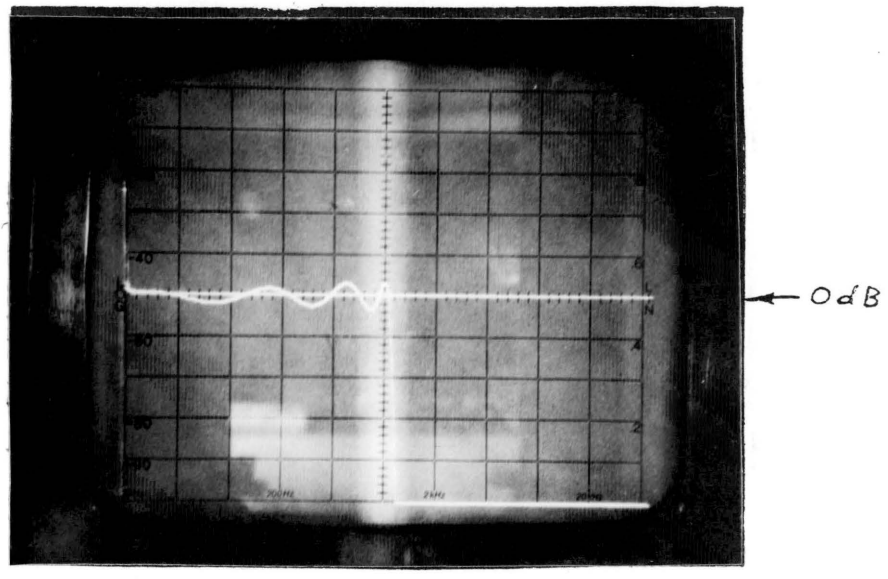

Figure 4.31. LDI filter test results (passband)
vertical: 1 dB/div duty cycle: 40-60%
horizontal: 0.2 Khz/div Fc/Fco: 10

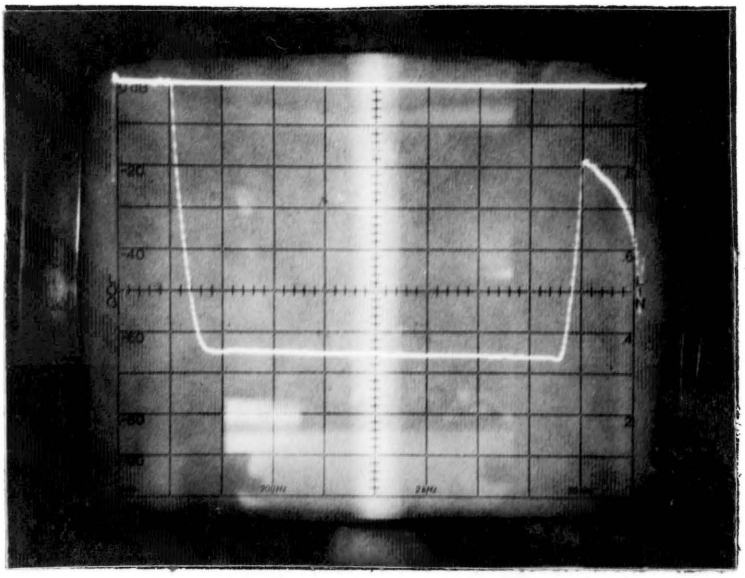

Figure 4.32. LDI filter test results (passband & stopband).
vertical: 10 dB/div duty cycle: 40-60%
horizontal: 1 Khz/div Fc/Fco: 10

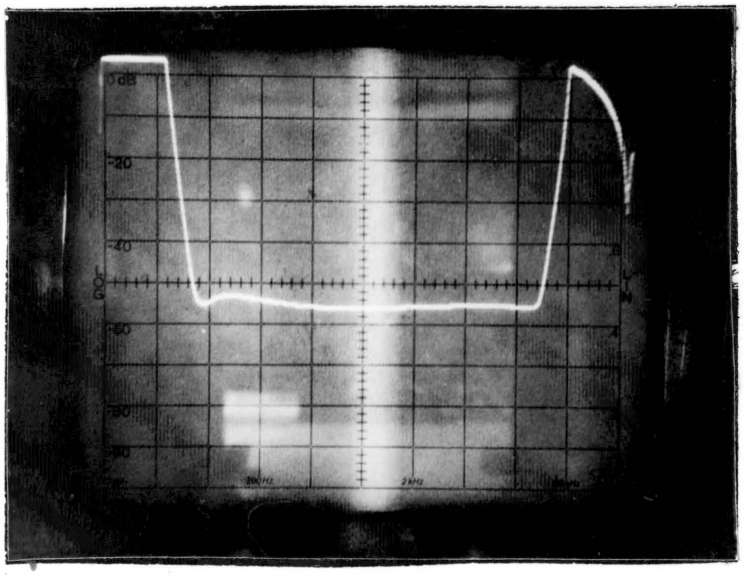

Figure 4.33. LDI filter test results (stopband).
vertical: 10 dB/div duty cycle: 40-60%
horizontal: 1 Khz/div Fc/Fco: 10

of the noise level (-84 dB), (see figure 4.29). Without this input signal amplification the stopband characteristic of the LDI filter degrades as depicted in figures 4.32 and 4.33. The test results show the notches clearly in figures 4.24 and 4.26 for the BDS filter and the first stopband notch for the LDI filter in figures 4.28 and 4.29. There is slight evidence of passband ripple for the BDS filter (figure 4.25) while there is a clear ripple waveform in the passband of the LDI filter in figure 4.30 and 4.31. Comparative values of passband and stopband characteristics from DIANA computer simulations and from test results are presented in table 4.8 for the BDS filter and table 4.9 for the LDI filter.

Theoretically, an increased clock frequency should yield an appropiately scaled frequency response curve for both the LDI and the bilinear filters. This is evident from figures 4.34(a) and 4.35(a) for the BDS filter in which the effect of increasing the clock frequency to 20kHz and 30kHz yields excellent replication of the output. An excellent replication of the output is also evident for the LDI filter operating at 20, 30, 40, and 50 kHz as depicted in figures 4.34(b), 4.35(b), 4.36(b), and 4.37(b). However, for the BDS filter, operating at 40 kHz clock, the notches are lost

Table 4.8. Comparative design, computer, and experimental results for the BDS 7th-order elliptic lowpass filter.

Parameter	Design Specification	DIANA Simulation	Experimental Result
Peak amplitude	0dB	0.053dB	0.1db
Cut-off frequency	1000Hz	1054Hz	1000Hz
Passband loss	0.03dB	0.03dB	0.1dB
1st notch	1876Hz	1908Hz	1875Hz
2nd notch	2273Hz	2359Hz	2250Hz
3rd notch	3949Hz	4317Hz	4400Hz
1st "flyback"	-82.11dB	-84.49dB	-83dB
2nd "flyback"	-82.11dB	-84.85dB	-81dB
3rd "flyback"	-82.11dB	-87.83dB	-

Table 4.9. Comparative design, computer, and experimental results for the LDI 8th-order elliptic lowpass filter.

Parameter	Design Specification	DIANA Simulation	Experimental Result
Peak amplitude	0dB	0.1967dB	0.45dB
Cut-off frequency	1000Hz	1005Hz	1010Hz
Passband loss	0.177dB	0.405dB	0.07dB
1st notch	1876Hz	1808Hz	1800Hz
2nd notch	2273Hz	2109Hz	----
3rd notch	3949Hz	3665Hz	----
4th notch	----	6326Hz	----
1st "flyback"	-101.0dB	-100.06dB	-99dB
2nd "flyback"	-101.0dB	-99.652dB	---
3rd "flyback"	-101.0dB	-109.97dB	---
4th "flyback"	----	-108.89dB	---

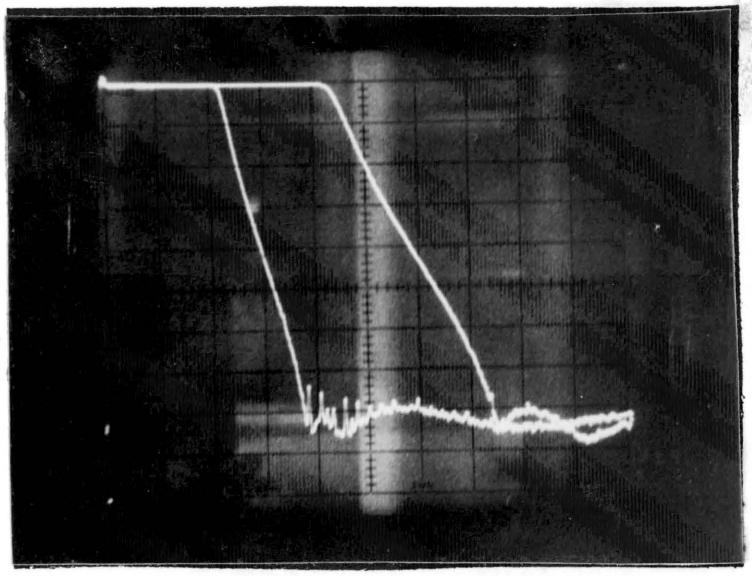

(a) BDS filter: vertical: 10 dB/div duty cycle: 40-60%
horizontal: 0.5 Khz/div

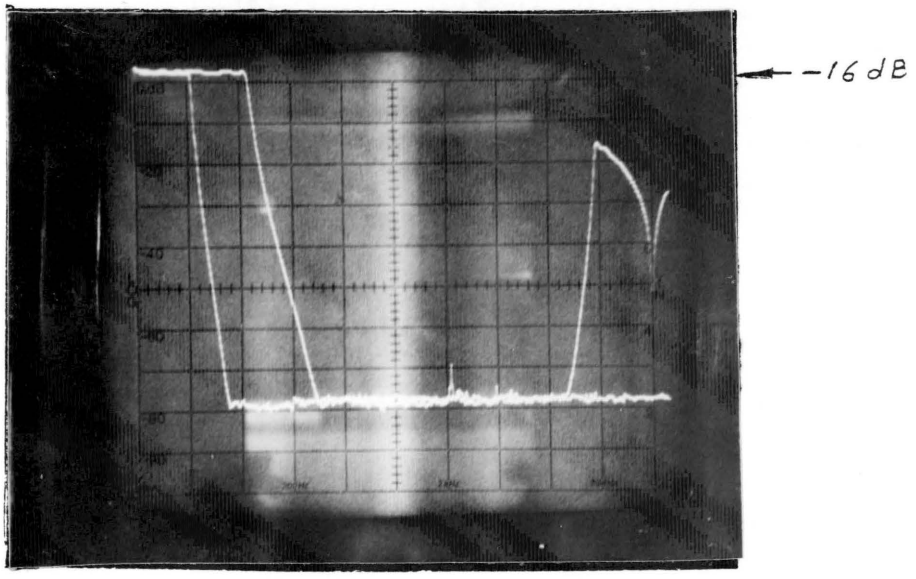

(b) LDI filter: vertical: 10 dB/div duty cycle: 40-60%
horizontal: 1 Khz/div

Figure 4.34. BDS and LDI filter test results.
clock (Fc): 10 Khz & 20 Khz.

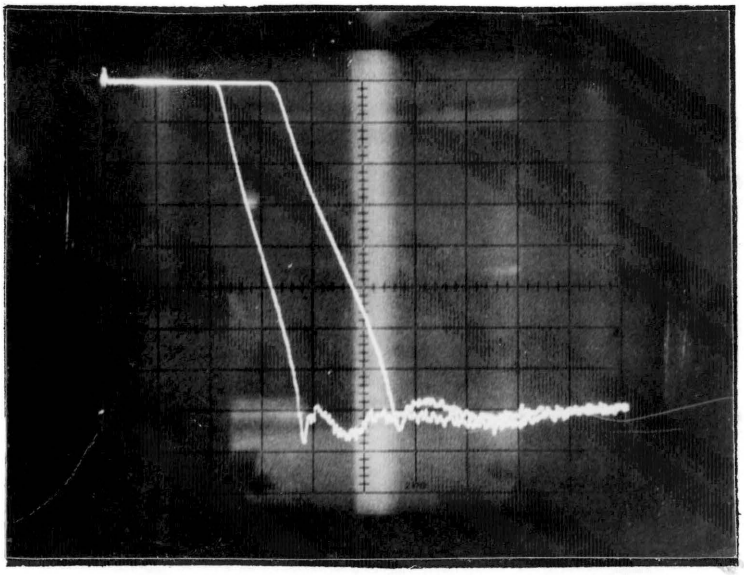

(a) BDS filter: vertical: 10 dB/div duty cycle: 40-60%
horizontal: 1 Khz/div.

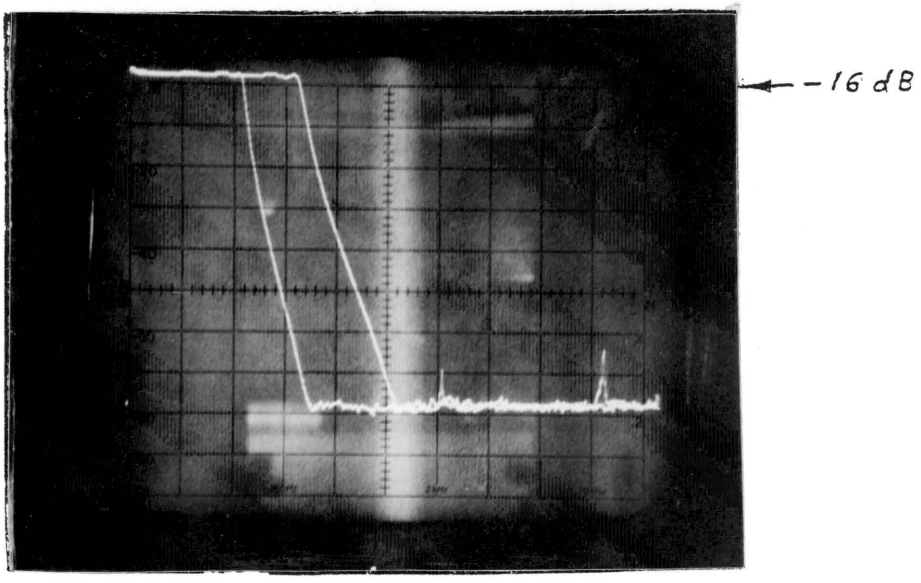

(b) LDI filter: vertical: 10 db/div duty cycle: 40-60%
horizontal: 1 Khz/div

Figure 4.35. BDS and LDI filter test results.
clock (Fc): 20 Khz and 30 Khz.

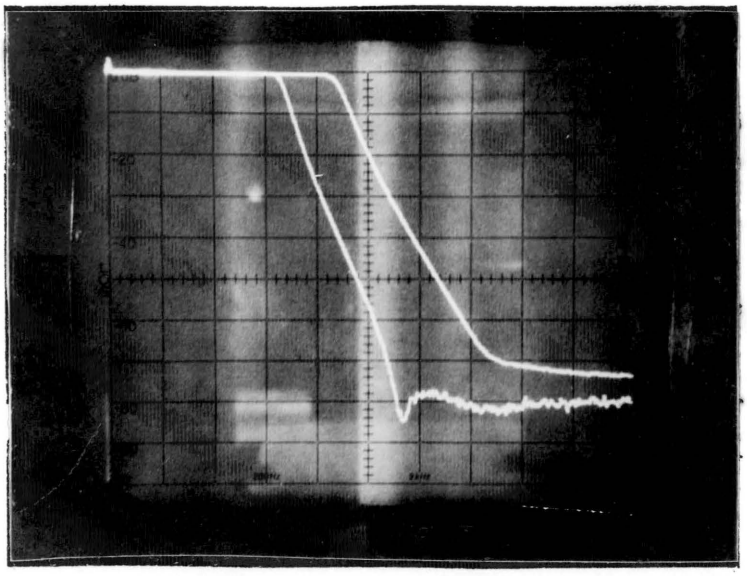

(a) BDS filter: vertical: 10 dB/div duty cycle: 40-60%
horizontal: 1 Khz/div

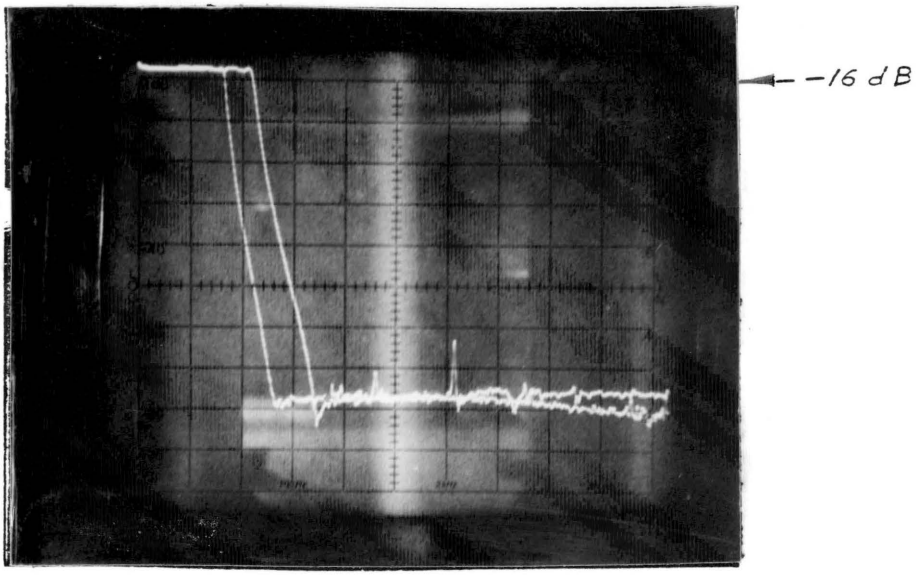

(b) LDI filter: vertical: 10 dB/div duty cycle: 40-60%
horizontal: 2 Khz/div

Figure 4.36. BDS and LDI filter test results
clock (Fc): 30 Khz and 40 Khz

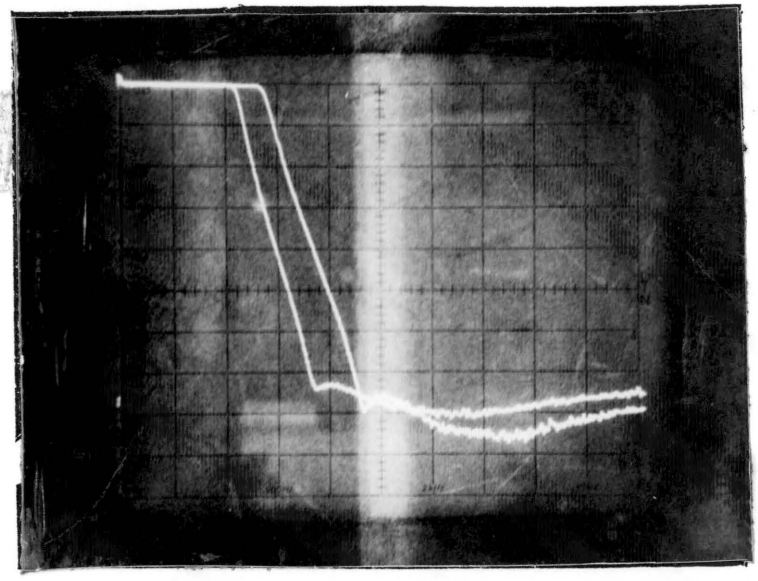

(a) BDS filter: vertical: 10 dB/div duty cycle: 50-50%
horizontal: 2 Khz/div

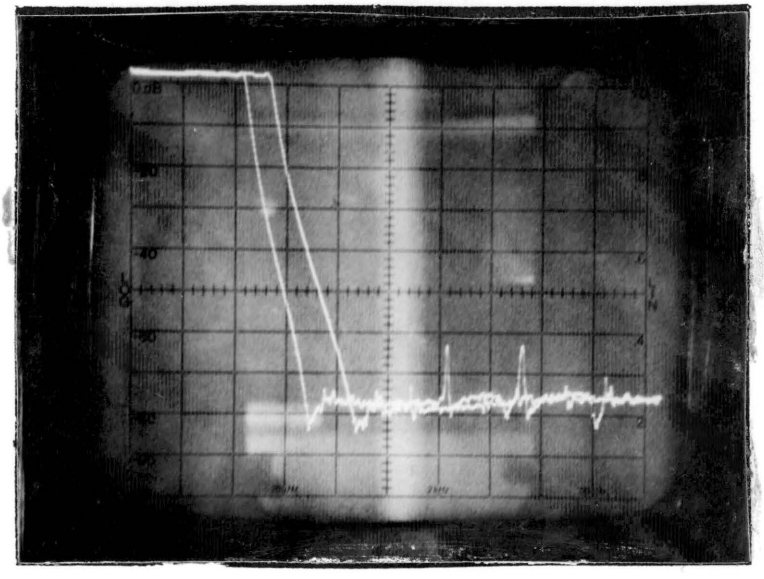

(b) LDI filter: vertical: 10 dB/div duty cycle: 40-60%
horizontal: 2 Khz/div

Figure 4.37. BDS and LDI filter test results
clock (Fc): 40 Khz and 50 Khz

and the stopband loss is reduced from 80 dB to 70 dB as seen in figure 4.36(a). Slight improvement in the stopband characteristic is produced by altering the duty-cycle to 50-50%. From figure 4.37(a), it is seen that the first notch reappears and the stopband loss increases to 74 dB. A slightly improved result is seen at Fc=50 kHz but the frequency response is no longer a good reproduction of the original response. For the LDI filter there is a faithful reproduction and even improvement of the output where the first stopband notch becomes more pronounced at higher clock operations. It should be noted that unlike the LDI filter, no dynamic ranging or amplification of the input signal was done for the BDS filter during these tests.

Chapter V

SWITCHED CAPACITOR CIRCUIT NOISE ANALYSIS USING POWER SPECTRUM ESTIMATION TECHNIQUES

5.1 Introduction

The purpose of this chapter is to introduce and review certain power spectrum estimation techniques which can be used in power spectrum analysis of switched capacitor (SC) circuits. The primary intention is to provide an alternative aproach for analyzing the power spectrum of SC circuits without the need of complicated and tedious analytical spectrum analysis. Two distinct power spectrum estimation techniques will be discussed: the windowed periodogram and the AR-system modeling. The windowed periodogram technique is usually employed to determine the asymptotic behavior of the system's power spectrum frequency response and subsequently the AR-system modeling technique is used to reproduce the power spectrum. The basic references to this chapter are Beex [5], Oppenheim and Schafer [28], and Kay and Marple [18].

5.2 Switched Capacitor Noise Models and Foundation of Noise Power Spectrum Estimation

5.2.1 Introduction

Figure 5.1 depicts the equivalent noise model for a switched capacitor element with one mos switch. The noise source (Ns) is defined as a white noise with a spectral density given by:

$$S_{Ns}(f) = 2K\theta R \qquad -\infty \leq f \leq \infty \qquad 5.4.1$$

where: K - absolute temperature in Kelvin (K)

θ - Boltzmann's constant

R - switch resistance

The overall noise model for a typical parasitic sensitive switched capacitor SC integrator is presented in figure 5.2 where the LDI differential input integrator is adopted. This circuit as analyzed by Gobet and Knob [13] in the s-domain will be computer modeled and various estimates of its output noise spectrum will be analyzed and compared in section 5.4 with the analytical results of Gobet and Knob. The noise source of the op-amp (Noa) is defined by Furrer and Guggenbuhl [10] as a white noise with a spectral density of:

$$S_{OA}(f) = 2K\theta Req \qquad -\infty \leq f \leq \infty \qquad 5.2.2$$

where: Req - equivalent noise resistance

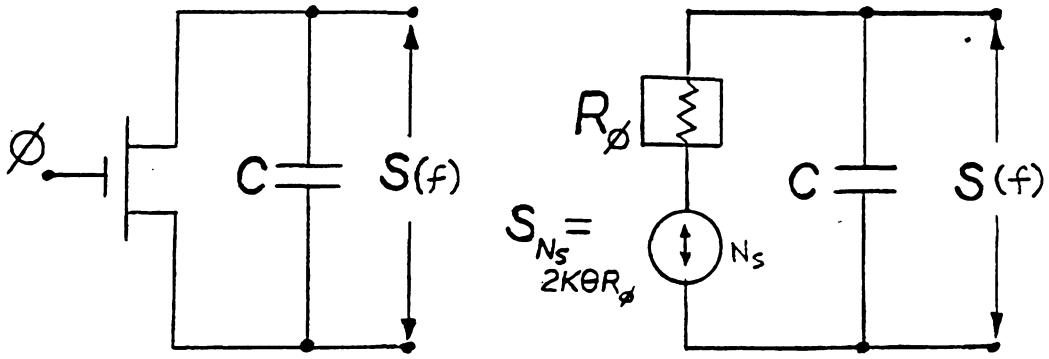

Figure 5.1. Noise model of a switched capacitor with one MOS switch.

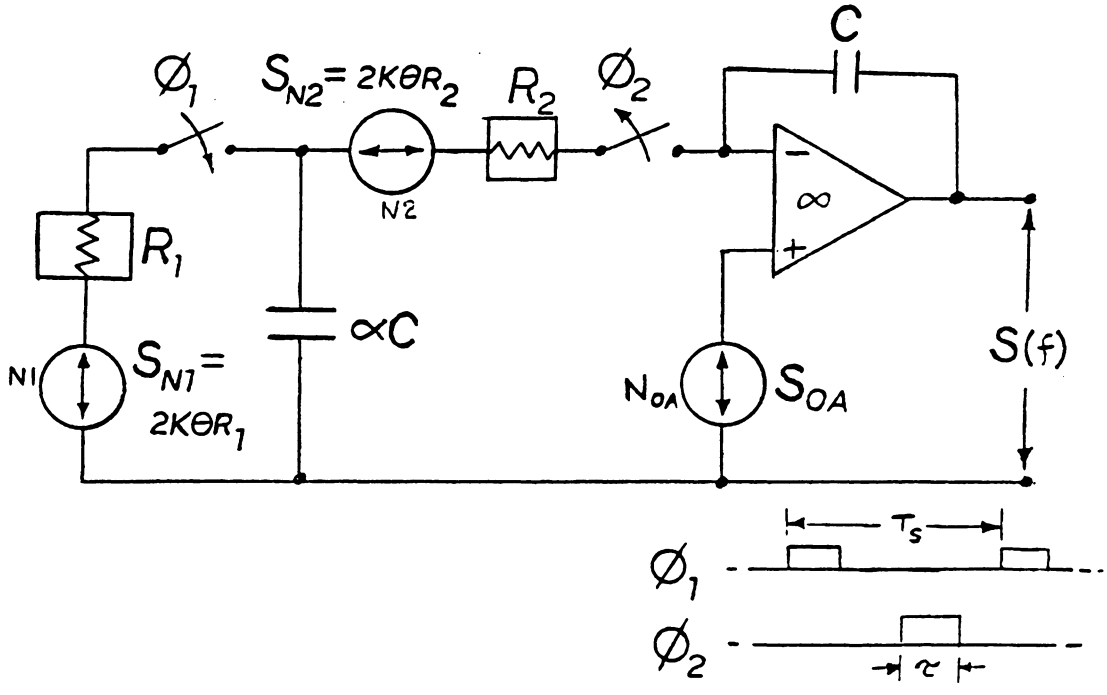

Figure 5.2. Noise model of a parasitic sensitive LDI switched capacitor integration circuit.

The value of 5.2.2 varies with the type of op-amp used. Gobet and Knob in their analytical noise spectrum analysis of figure 5.2 used a value of $2.512(10)^{-14}$ V^2/Hz. The basic noise model structure of figure 5.2 can readily be applied to other types of SC integrators. Other noise models such as those which account for the 1/f noise of op-amps can readily be included in the overall noise model of a SC circuit such as that of figure 5.2 or any other larger ladder SC network.

Figure 5.3 depicts a typical system with internal noise sources (Ni) and transfer functions between the noise sources and the output (Hi(w)). The power spectral density of the noise sources are labeled as Si(w) while the power spectral density and the autocorrelation of the output of the system are labeled Sout(w) and Rxx(τ) respectively. Figure 5.3 is applicable to the internal structure of any SC system. Wether analyzed in the s-domain or the Z-domain two distinct approaches can be adopted in computing the analytical output power spectrum of any SC system. These two approaches become particularly suitable when the noise sources of the system are uncorrelated. One approach involves computing by superposition time-domain output functions of the system due to each of the internal noise sources and then summing all these functions. The resulting time-domain system output

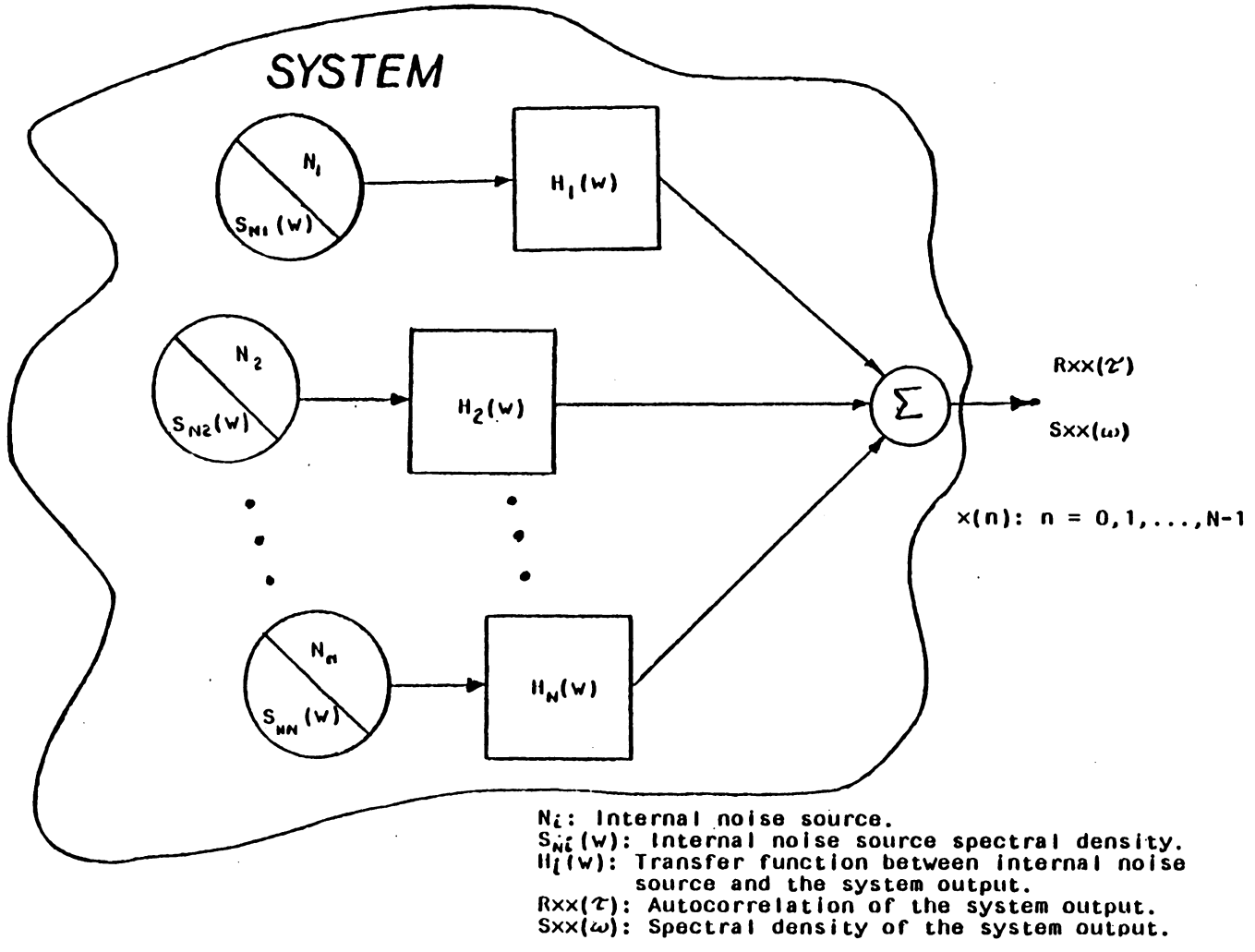

Figure 5.3. Generalized system noise model.

function is given below:

$$X(t)=\sum_{i=1}^{N} X_i(t) \qquad 5.2.3$$

where $X_i(t)$ is the output function due to the ith internal noise source. The autocorrelation of X(t) (Rxx(τ)) is then obtained and the output noise power spectrum is computed by taking the fourier transform of the autocorrelation.

$$Sout(w)=\mathcal{F}\{Rxx(\tau)\} \qquad 5.2.4$$

The other approach involves computing first the transfer function between each uncorrelated noise source and the output of the system. The output noise power spectrum for a system with N noise sources is then computed by the following formulation:

$$Sout(w)=\sum_{i=1}^{N} |H_i(w)|^2 S_i(w) \qquad 5.2.5$$

For both approaches the analytical computation involved becomes more difficult to carry out when some or all the noise sources are correlated. In which case, superposition cannot be adopted in the first approach when computing the output time-domain function due to two or more correlated sources. For the second approach cross-spectral density functions between two or more correlated noise sources must be computed, and the output spectral density components due

to these noise cross-spectral densities must be added to the formulation for Sout(w) given in 5.2.5. Even in the case where all internal noise sources are uncorrelated the computation of time-domain output functions and transfer functions can become a tedious and cumbersome task, particularly for high order SC filters. For example, if the noise model of figure 5.2 is implemented for the 3rd-order elliptic low-pass SC filter of figure 2.12 the number of noise source-to-output transfer functions required is 17. Such difficulties involved in analytical power spectrum computations makes the alternative approach of power spectrum estimation more attractive and suitable.

There are many power spectrum estimation techniques developed over the last 200 years and all involve analyzing a finite record length of output time-domain samples (X(n) in figure 5.3). The fundamental advantage of power spectrum estimation over analytical spectrum computation, particularly for complicated systems such as a high order SC filter, is that an analytical analysis of the internal structure of the system is not required. What is required for the case of switched capacitor noise analysis is a reliable computer simulation scheme which will simulate an SC system (adopting a noise model such as that of figure 5.2) and generate a

string of output time-domain values. Before discussing two power spectrum estimation techniques of interest the concept of ergodicity and autocorrelation estimation should be discussed.

5.2.2 Principle of Ergodicity and Autocorrelation Estimation

In determining stochastic properties of a time-domain random process, x(t), such as its mean (η), its outocorrelation for a lag of τ, ($R_{xx}(\tau)$), and its power spectrum $S_{xx}(w)$, one ideally requires information of x(t) for $-\infty \leq t \leq \infty$. However, for computational purposes in power spectrum estimation it is not desireable nor possible to have an infinite record length of sampled time-domain values of x(n) for $-\infty \leq n \leq \infty$. Because spectrum estimation works with a finite record length of data x(n) for n=0,1,...,N-1 it is imperative to assume that x(n) is an ergodic process. For switch-capacitor spectrum estimation purposes it is important to insure that the noise model selected for a SC system and the computer modeling scheme adopted both produce an ergodic time-domain process in x(n). There are many definitions of the concept of ergodicity. Papoulis [30] offered one of the best definitions:

> "Ergodicity deals with the problem of determining the statistics of a process x(t) from a single observation: x(t) is ergodic in the most general

> form if (with a probability of 1) all its statistics can be determined from a single function $x(t,\zeta)$ of the process."

The ergodicity of the mean (η) of $x(t)$, available for $-Ts/2 \leq t \leq Ts/2$, is defined below:

$$\eta = E\{x(t)\}$$

$$\hat{\eta} = (1/Ts) \int_{-Ts/2}^{Ts/2} x(\tau)d\tau \qquad 5.2.6$$

$$E\{\hat{\eta}\} = \eta \quad (\text{as } Ts \Rightarrow \infty) \qquad 5.2.7$$

The ergodicity of the autocorrelation ($Rxx(\tau)$) of the process $x(t)$, available for $-Ts/2 \leq t \leq Ts/2$, is defined below:

$$Rxx(\tau) = E\{x(t+\tau)x(t)\} \qquad 5.2.8$$

$$\hat{Rxx}(\tau) = (1/Ts) \int_{-Ts/2}^{Ts/2} x(t+\tau)x^{*}(t)dt \qquad 5.2.9$$

$$E\{\hat{Rxx}(\tau)\} = Rxx(\tau) \quad (\text{as } Ts \Rightarrow \infty) \qquad 5.2.10$$

Equation 5.2.9 is in the form of what is usually referred to as an autocorrelation estimate. There are two types of autocorrelation estimates: unbiased and biased. The expected value of an unbiased autocorrelation estimate with the amount of information of $x(t)$ approaching infinity is the actual autocorraelation of the process. The expected value of a biased autocorrelation estimate under the same conditions is a converging approximation to the actual autocorrelation value. For a finite length sample of continuous data

of x(t) for -Ts/2≤t≤Ts/2 the unbiased and biased autocorrelation estimators are given as:

I. The unbiased autocorrelation estimator [37]:

$$x(t) \text{ for } -Ts/2 \le t \le Ts/2$$

$$\hat{R}'_{xx}(\tau) = 1/(Ts-|\tau|)\int_{-(Ts-|\tau|)/2}^{(Ts-|\tau|)/2} x(t+\tau)x^*(\tau)dt \qquad 5.2.11$$

$$\left.\begin{array}{l} E\{\hat{R}'_{xx}(\tau)\} = R_{xx}(\tau) \\ \text{or} \\ \hat{R}'_{xx}(\tau) \text{ --- } (Ts \Rightarrow \infty) \rightarrow R_{xx}(\tau) \end{array}\right\} \text{(unbiased)}$$

II. The biased autocorrelation estimator [37]:

$$x(t) \text{ for } -Ts/2 \le t \le Ts/2$$

$$\hat{R}_{xx}(\tau) = (1/Ts)\int_{-(Ts-|\tau|)/2}^{(Ts-|\tau|)/2} x(t+\tau)x^*(\tau)dt \qquad 5.2.12$$

$$\left.\begin{array}{l} E\{\hat{R}_{xx}(\tau)\} = (1-|\tau|/Ts)R_{xx}(\tau) \\ \text{or} \\ \hat{R}_{xx}(\tau) \text{ --- } (Ts \Rightarrow \infty) \rightarrow (1-|\tau|/Ts)R_{xx}(\tau) \end{array}\right\} \text{(biased)}$$

For a finite record length of x(n) for n=0,1,...,N-1 the unbiased and biased autocorrelation estimators are given as:

I. The unbiased autocorrelation estimator [28]:

$$x(n) \quad \text{for} \quad n=0,1,\ldots,N-1$$

$$\hat{R}'_{xx}(m) = 1/(N-|m|)\sum_{n=0}^{N-|m|-1} x(n+m)x^*(n) \qquad 5.2.13$$

$$\lim_{N\to\infty}\{\hat{R}'_{xx}(m)\} = R_{xx}(m) \qquad \text{(unbiased)}$$

II. The biased autocorrelation estimator [28]:

$$x(n) \quad \text{for} \quad n=0,1,\ldots,N-1$$

$$\hat{R}xx(m) = (1/N) \sum_{n=0}^{N-|m|-1} x(n+m)x^*(n) \qquad 5.2.14$$

$$\lim_{N\to\infty} \{\hat{R}xx(m)\} = [(N-|m|)/N]Rxx(m) \qquad \text{(biased)}$$

The accuracy, variance, and resolution of the spectrum estimation techniques to be discussed in sections 5.3 and 5.4 in approximating the actual power spectrum of a stochastic process depend to a large extend on the accuracy and the type of autocorrelation estimation technique adopted. Needless to say, the accuracy of any autocorrelation estimator improves for longer record lengths of time-domain data x(t). According to Kay and Marple [78], both Jenkins-Watts [17] and Parzen [32], recomend the use of the biased autocorrelation estimator since for many finite data sets it provides less mean-square error that the unbiased estimator.

There are two main spectrum estimation techniques: the windowed periodogram and the autoregressive spectrum modeling. Both of these techniques base their analysis on autocorrelation values for a finite set of sampled data. Either the biased or the unbiased autocorrelation estimators of equations 5.2.14 and 5.2.13 respectively can be used to obtain these autocorrelation values. Nonetheless, as explained

earlier, for most sets of sampled data the biased autocorrelation estimator provides least mean-square error. Both spectrum estimation techniques assume that the stochastic process under analysis is ergodic, and both techniques represent two distinct approaches in analyzing autocorrelation values.

5.2.3 Fundamental Principles of Windowed Periodogram Spectrum Estimation

The windowed periodogram technique, presented in more detail in section 5.3, essentially entails windowing a finite record length of sampled data and performing a fourier transform of the autocorrelation of this windowed data. The power spectrum of a stochastic process is defined as:

$$S(f) = \int_{-\infty}^{\infty} Rxx(\tau)e^{-j2\pi f\tau}d\tau \qquad 5.2.15$$

For an ergodic process where data, x(t), is available continuously over $-Ts/2 \leq t \leq Ts/2$ the autocorrelation of the process, Rxx(τ), can be defined in the following form [30], [78]:

$$Rxx(\tau) = \lim_{Ts\to\infty} (1/Ts) \int_{-Ts/2}^{Ts/2} X(t+\tau)X^*(t)dt \qquad 5.2.16$$

The power spectrum of this ergodic process is defined as [18]:

$$S(f)= \lim_{Ts\to\infty} E\{(1/Ts)\left|\int_{-Ts/2}^{Ts/2} x(t)e^{-j2\pi ft}dt\right|^2\} \qquad 5.2.17$$

For the case where a finite record length of sampled data of an ergodic process, x(n), is available for n=0,1,...,N-1 the discrete fourier transform of the autocorrelation estimate of such a process is defined as [18],[28]:

$$P_N(f) = Ts \sum_{m=-(N-1)}^{N-1} \hat{R}xx(m)e^{-j2\pi mfTs} \qquad 5.2.18$$

Where Ts is the sampling period between samples of x(n). Note that by definition [18]:

$$\hat{R}xx(-m)= \hat{R}^{*}xx(m) \qquad 5.2.19$$

Equation 5.2.18 can futher be modified into the following form [18], [28]:

$$P_N(f) = [1/(NTs)]\left|Ts \sum_{n=0}^{N-1} x(n)e^{-j2\pi fnTs}\right|^2 \qquad 5.2.20$$

$$\text{for } -1/2Ts \leq f \leq 1/2Ts$$

According to Kay and Marple [18] the factor Ts used in equation 5.2.20 ensures a conservation of integrated area between 5.2.17 and 5.2.20 as Ts approaches 0. Note that $P_N(f)$ is always an approximation or estimation of the actual power spectrum of the process, S(f), since an expectation

operation or ensemble averaging is not carried out in 5.2.20 as in 5.2.17. This rough approximation of $P_N(f)$ to S(f), plus the fact that an infinite number of x(n) points are not analyzed, raises the question of resolution and variance of $P_N(f)$ with respect to S(f). Resolution deals with the problem as to how well the estimation 'focuses' on sharp frequency responses in the ideal spectrum curve of S(f), such as sharp peaks. Needless to say, the larger the number of time-domain points of x(n) available the better the resolution. Variance on the other hand deals with the problem as to how much does the oscillatory behavior of a spectrum estimation curve deviates from the ideal power spectrum curve of S(f). For the windowed periodogram spectrum estimation technique there are two methods available for improving the variance of the estimation:

a) Partition of x(n) into smaller equal strings of data, performing a periodogram fourier operation (5.2.20) on each data set, and averaging the results.

b) Selection of a "weighting" window function w(n) to be multiplied to x(n) for n=0,1,...,N-1 so that the resulting spectrum estimation after a fourier analysis is a better reproduction of the ideal power spectrum.

Method (a) is an implied expectation operation on $P_N(f)$ as done in equation 5.2.17 for a finite string of continuous data. This method is a form of ensemble averaging of a set of spectrum estimation functions of the stochastic process, x(n). Method (a) is adopted in the Welch windowed periodogram spectrum estimation technique discussed in section 5.3. There are two points to consider in ensemble averaging windowed periodogram spectrum estimation:

1. The more partitions of x(n) taken the smaller the variance in the final estimation of the ideal spectrum.
2. The more partitions of x(n) the smaller the string of data available for windowed periodogram analysis which, even after ensamble averaging, can reduce the resolution of the final spectrum estimation.

Points (1) and (2) are essentially conflicting design criterias and there is no 'rule-of-thumb' solution which may help resolve this conflict. It is left to the engineer to decide the number of partitions for a particular string of data. However, in switched capacitor system analysis there are no restrictions involved, other than limits on computer processing time, for generating a large string of time-domain data from a computer noise modeling of the system. In such a

case there is more freedom in selecting larger number of partitions to improve the variance and not substantially affect the resolution of the final spectrum estimation.

Method (b) deals with the problem of improving the variance of the spectrum estimation and at the same time avoiding the potentially detrimental effects of "leakage" (to be explained shortly), produced by truncating x(n) to zero outside the data string of interest during a windowing operation. Unless x(n) is bandlimited in the region of n=0,1,...,N-1, which in most cases is not, setting the value of x(n) to zero outside the windowed region of interest may have detrimental effects on the spectrum estimation reproduction of the ideal power spectrum. The detrimental effect of most concern is the problem of leakage.

Consider an arbitrary stochastic process x(n) available for $-\infty \leq m \leq \infty$ as depicted in figure 5.4(a) which is then windowed for spectrum estimation purposes about the region of n=0,1,...,N-1 as shown in figure 5.4(b). When a spectrum estimation analysis is performed, it is the waveform depicted in figure 5.4(b) and not the more accurate one in figure 5.4(a) which will be analyzed. The effect of this inaccurate analysis is depicted by way of example in figure 5.5(c) in the reproduction by a $P_N(w)$, with a finite N value, of a

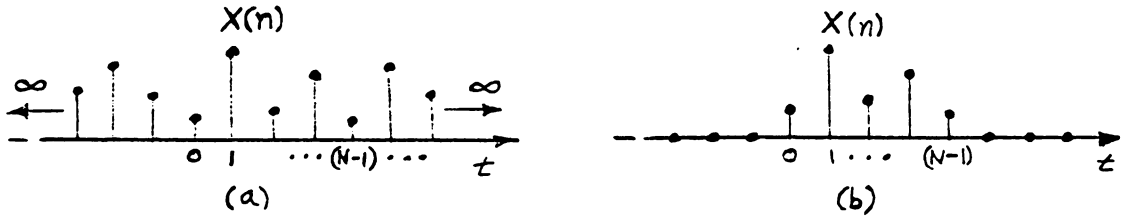

Figure 5.4. Infinite (a) and finite (b) string of system output samples.

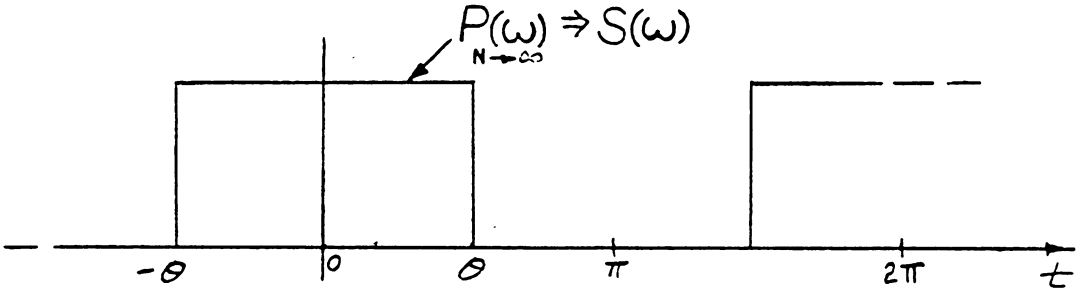

(a) Ideal spectrum estimation representation ($P_N(w)$).

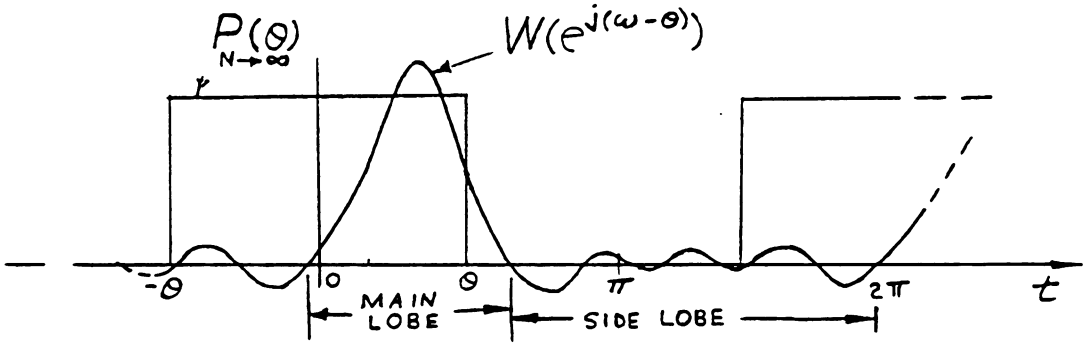

(b) Convolution of ideal spectrum estimation ($P_N(w)$) and window function ($W(e^{j\omega})$).

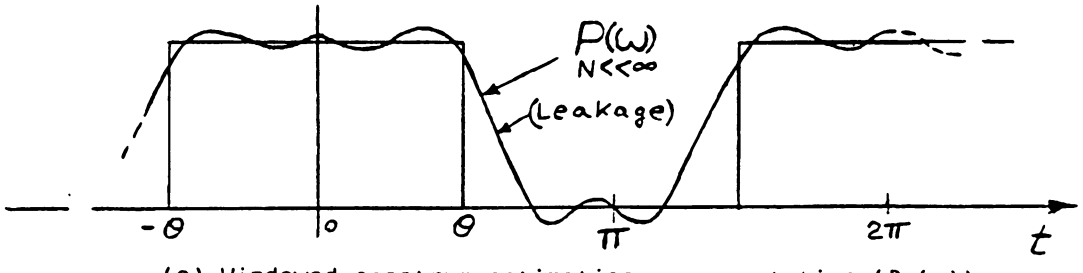

(c) Windowed spectrum estimation representation ($P_N(w)$).

Figure 5.5. Spectrum estimation representations ($P_N(w)$) of an ideal spectrum ($S(w)$) for infinite and finite (windowed) string of output samples.

rectangular repetitive power spectrum curve, as shown in figure 5.5(a), for a $P_N(w)$ with N set to infinity. Leakage, as depicted in figure 5.5(c), is the "seepage" of portions of spectral energy corresponding to one frequency lobe into another. In this case there is a leakage of spectral energy from the lobe of $-\theta \leq w \leq \theta$ to its two adjacent lobes. Leakage can have detrimental effects on the accuracy of the spectrum estimation specially when two spectral lobes of high energy concentration are very close to each other.

A windowed periodogram as depicted in figure 5.5(c) is defined as [78]:

$$P_{N<<\infty}(f) = [1/(2\pi)] \int_{-\pi}^{\pi} P_{N\to\infty}(\theta) W(e^{j(w-\theta)Ts}) d\theta \qquad 5.2.21$$

Where $W(e^{j\omega T_s})$ is the fourier transform of the window function w(n). Since the inverse fourier transform of $W(e^{j\omega T_s})$ is the window function itself:

$$w(n) = [1/(2\pi)] \int_{-\pi}^{\pi} W(e^{j2\pi fTs}) e^{j2\pi fn} \qquad 5.2.22$$

$P_N(f)$ can be redifined [78] into the following form:

$$P_{(f)} = Ts \sum_{n=-(N-1)}^{N-1} \hat{R}xx(n) w(n) e^{-j2\pi fnTs} \qquad 5.2.23$$

Note that w(n) is required to be an even function. It is with the use of the relationship of 5.2.23 that Welch gener-

alized equation 5.2.20 to the form of his formulation presented in section 5.3.

The windows of interests are given below [28] with the parameter N changed to M to comply with Welsh's windowed periodogram formulation of section 5.3:

I. Rectangular:

$$w(n) = 1 , \qquad 0 \le n \le (M-1) \tag{5.2.24}$$

II. Triangular:

$$w(n) = \begin{cases} 2n/(M-1) , & 0 \le n \le [(M-1)/2] \\ 2 - 2n/(M-1) , & [(m-1)/2] \le n \le (M-1) \end{cases} \tag{5.2.25}$$

III. Hanning:

$$w(n) = (1/2)\{1 - \cos[(2\pi n)/(M-1)]\} , \qquad 0 \le n \le (M-1) \tag{5.2.26}$$

IV. Hamming:

$$w(n) = 0.54 - 0.46\cos[(2\pi n)/(M-1)] , \qquad 0 \le n \le (M-1) \tag{5.2.27}$$

V. Blackman:

$$w(n) = 0.42 - 0.5\cos[(2\pi n)/(M-1)] + 0.08\cos[(4\pi n)/(M-1)] \tag{5.2.28}$$

Note that equations 5.2.18 and 5.2.20 use the standard rectangular window. The general form of these windows are giv-

en in figure 5.6 [28] and their fourier transform $W(e^{j\omega T_s})$ are in the form depicted in figure 5.5(b).

There is a useful borderline ratio which helps one make a decision as to when a spectrum estimation using a window other than the rectangular window provides less estimation variance. When this ratio, as provided below [28], is less than 1 the non-rectangular window should be used.

$$R = \frac{VAR[Sw(f)]}{VAR[Sw'(f)]} = \frac{1}{N} \sum_{n=-(M-1)}^{M-1} w^2(m) = \frac{1}{2\pi N} \int_{-\pi}^{\pi} W^2(e^{j\beta T_s}) d\beta \qquad 5.2.29$$

where: - Sw(f) defined by equation 5.3.1 uses a non-rectangular window.
- $Sw'(f)$ defined by equation 5.3.1 uses the rectangular window.

Table 5.1 [28] tabulates values of R for the windows of interest along with the approximate width of the main lobe of $W(e^{j\beta T_s})$ (see figure 5.5(c)), the importance of which will be explained shortly.

There are certain important points to be kept in mind when windowed periodogram spectrum estimation is used to analyze the noise spectrum of switched capacitor systems:

1. Spectral leakage can decrease the resolution of sharp peaks, valleys, and zeroes contained in the ideal power spectrum.

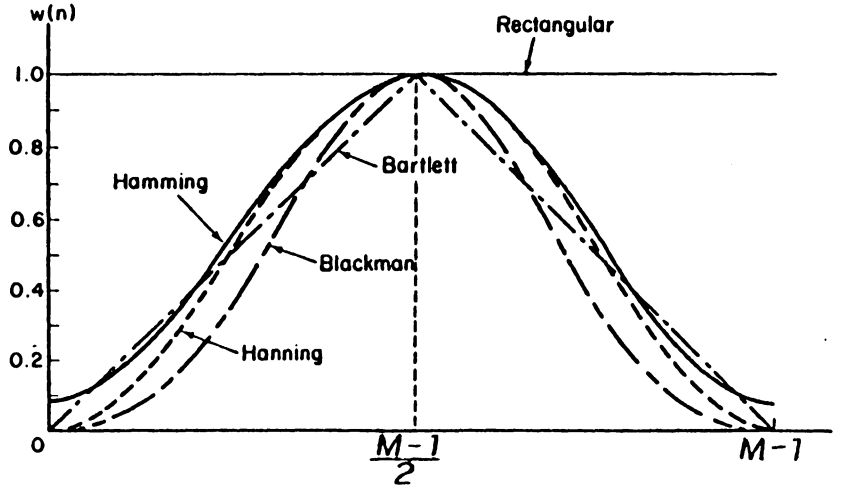

Figure 5.6. Window functions (w(n)) for an arbitrary record length (M) [28]

TABLE 5.1. Approximate Width of Main Lobe and Approximate Variance Ratio (R) of Windows of Interest [28].

Window	Approx. Width of Main Lobe	Approximate Variance Ratio (R)
Rectangular	$4\pi/M$	1
Triangular	$8\pi/M$	$M/(3N)$
Manning	$6\pi/M$	$(0.375M)/N$
Manning	$6\pi/M$	$(0.3974M)/N$

2. To avoid leakage:
   a) Increase the number of points.
   b) Select a window where the main lobe of its fourier transform (see figure 5.5(c)) is as short as possible. The approximate main lobe widths the windows of interests are listed in table 5.1.
3. Selecting a window with a short main lobe usually entails high energy side lobes which can increase leakage.

Note that points 2(b) and 3 are in conflict with each other. For this reason there is no preferred window function. The criteria for selecting a particular window is left to the engineer.

5.2.4 Fundamental Principles of Autocorrelation (AR) Spectrum Estimation Modeling

Many discrete-time deterministic and stochastic processes can be approximated by a linear rational autoregressive moving average (ARMA) transfer function model defined by the following linear difference equation [28],[18]:

$$x(n) = \sum_{\ell=0}^{q} b(1)n(n-1) - \sum_{k=1}^{P} a(k)x(n-k) \qquad 5.2.30$$

where n is the input driving sequence and x is the output sequence of the system. The Z-transform of equation 5.2.30 results in the Z-domain ARMA transfer function of the system:

$$H(Z) = \frac{X(Z)}{N(Z)} = \frac{\sum_{m=0}^{q} b(m)Z^{-m}}{\sum_{m=0}^{p} a(m)Z^{-m}} \qquad 5.2.31$$

where: (i) $z = \exp(j2\pi fTs)$ for $-1/2Ts \leq f \leq 1/2Ts$

(ii) Ts - sampling period of the process

The output noise power spectrum can then be written in the following form:

$$S_{ARMA}(Z) = H(Z)H(Z^{-1})S_n(Z) = \frac{X(Z)X(Z^{-1})S_n(Z)}{N(Z)N(Z^{-1})} \qquad 5.2.32$$

It is important to keep in mind that system modeling spectrum estimation $H(Z)$ and $S_n(Z)$ are not functions of $H_i(w)$ and $S_{Ni}(w)$ as depicted in figure 5.3. What system-modeling spectrum estimation will do is to assume that the system from which a set of time-domain values, x(n), is available has a transfer function of an arbitrary number of poles and/or zeroes and a single noise input spectral density function $S_n(Z)$. $S_n(Z)$ is assumed to be a white noise with zero mean and a variance of σ^2. According to Kay and Marple [*] $S_n(Z)$ should be defined as:

$$S(Z) = \sigma^2 Ts \qquad 5.2.33$$

where the Ts factor in the expression has been included so that "$S_{ARMA}(Z)$, when integrated over $-1/2Ts \leq f \leq 1/2Ts$, yields the true power of an analog signal". The AR spectrum modeling estimation techniques to be discussed will attempt to obtain proper values for a(m) and σ^2 for a selected order of the model.

Equation 5.2.32 can be expressed in the following form:

$$S_{ARMA}(f) = \frac{\sigma^2 Ts \left| 1 + \sum_{k=1}^{q} b(k) e^{-j2\pi fkTs} \right|^2}{\left| 1 + \sum_{k=1}^{p} a(k) e^{-j2\pi fkTs} \right|^2} \qquad 5.2.34$$

From this point on some technique(s) must be implemented for determining the values of a(k), σ^2, and b(k) based on information available in the finite record length of system output time-domain samples, x(n). To date, no perfected or fully reliable technique or algorithm has been developed for computing the ARMA coefficients (σ^2,a(k),b(k)). For this reason autoregressive (AR)-modeled spectrum estimation will be adopted.

According to the Wold decomposition theorem [43], discussed by Kay and Marple [78], a stationary ARMA system of finite variance can be approximated by an AR model of higher order. This theorem is important since an AR-modeled spect-

rum estimation approach can be adopted to approximate the spectrum of a system which can possibly be an ARMA system. If an AR-modeled system identification spectrum estimation technique is adopted the following all-pole spectrum formulation is obtained from the general ARMA-modeled formulation of equation 5.2.34 [18]:

$$S_{AR}(f) = \frac{\sigma^2 Ts}{\left|1 + \sum_{k=1}^{P} a(k)e^{-j2\pi fTs}\right|^2} \qquad 5.2.35$$

What is now required is a technique for determining the AR parameters $(a(k),\sigma^2)$ using the available knowledge in the finite record of output samples, $x(n)$. Toward this end the Yule-Walker equations [18] were developed.

The Yule-Walker equations are formulated in the following manner [18]:

$$Rxx(k) = E[x(n+k)x^*(n)] \qquad 5.2.36$$

$$= E[x^*(n)(-\sum_{\ell=1}^{P} a(1)x(n-1+k) + n(n+k))]$$

Preferably adopting the biased autocorrelation estimator (5.2.14), equation 5.2.36 reduces into what is known as the Yule-Walker equations. These equations which relate the autocorrelation estimate of the available time-domain samples $x(n)$ of the system with the AR parameters of 5.2.35 are given below [18]:

$$\hat{R}xx(k)= \begin{cases} -\sum_{\ell=1}^{P} a(1)\hat{R}xx(k-1) & , \text{ for } k > 0 \\ -\sum_{\ell=1}^{P} a(1)\hat{R}xx(-1) + \sigma^2 & , \text{ for } k = 0 \end{cases} \qquad 5.2.37$$

5.2.37 define a Toeplitz matrix of the following form [18]:

$$\begin{bmatrix} \hat{R}xx(0) & \hat{R}xx(1) & \dots & \hat{R}xx(-p) \\ \hat{R}xx(1) & \hat{R}xx(0) & \dots & \hat{R}xx(-(p-1)) \\ \vdots & \vdots & & \vdots \\ \hat{R}xx(p) & \hat{R}xx(p-1) & \dots & \hat{R}xx(0) \end{bmatrix} \cdot \begin{bmatrix} 1 \\ a_1 \\ \vdots \\ a_p \end{bmatrix} = \begin{bmatrix} \sigma \\ 0 \\ \vdots \\ 0 \end{bmatrix} \qquad 5.2.38$$

Note that $\hat{R}xx(-m) = \hat{R}^{*}xx(m)$.

A solution of 5.4.38 can efficiently be provided by the Levison-Durbin (LD) algorithm [18]. Before defining the LD algorithm equation 5.2.35 must be redefined into the following form [18]:

$$S_{AR}(f) = \frac{\sigma^2(p)Ts}{\left|1 + \sum_{k=1}^{P} a(p,k)e^{-j2\pi fTs}\right|^2} \qquad 5.2.39$$

where: $-1/2Ts \leq f \leq 1/2Ts$

The LD algorithm defines a recursion where parameter sets of $a(i,i)$ and $\sigma^2(i)$ are computed until reaching the selected AR model order, p, in the following manner:

$\{a_{11}, \sigma_1\}$

$\{a_{21}, a_{22}, \sigma_2\}$

$\{a_1, a_2, \dots, a_{pp}, \sigma_p^2\}$

where: $a_{i,0} = 0$ for $i=1,2,\ldots,p$

$$a_{i,j} = 0 \text{ for } j>i$$

The Levison-Durbin algorithm is presented below [18]:

(a) Initialization:

$$a(1,1) = -\hat{R}xx(1)/\hat{R}xx(0) \qquad 5.2.40(a)$$

$$\sigma^2(1) = (1- |a(1,1)|^2)\hat{R}xx(0) \qquad 5.2.40(b)$$

(b) Recursion: for $i=2,3,\ldots,p$ and $k=1,2,\ldots,i$

$$a(i,i)= -[\hat{R}xx(i) + \sum_{\ell=1}^{i-1} a(i-1,1)\hat{R}xx(i-1)]/\sigma^2(i-1) \qquad 5.2.40(c)$$

$$a(i,k)= a(i-1,k) + a(i,i)a^*(i-1,i-k) \qquad 5.2.40(d)$$

$$\sigma^2(i)= (1- |a(i,i)|^2)\sigma^2(i-1) \qquad 5.2.40(e)$$

The parameters $\{a_{11},a_{22},\ldots,a_{pp}\}$ often are refered to as reflection coefficients and are designated $\{K_1,K_2,\ldots,K_p\}$ respectively. They have the property that for the selected system model and system model order (as defined by 5.2.39) to be a valid representation of the power spectrum of the stochastic process x(n), it is a necessary and sufficient condition that [18]:

$$|K_i| \leq 1 \quad \text{for } i=1,2,\ldots,p$$

There is yet to be developed a fully reliable criteria for determining the optimum, or near optimum, AR-model order, p. Nevertheless, some criterias have been proposed and

tested with promising results and these are the Akaike-FPE, the Akaike-AIC, and the Parzen-CAT which are discussed in more detail by Kay and Marple [18] (see appendix B).

In most situations the AR-modeled spectrum estimation (AR) approach more powerful than conventional windowed periodogram (WP) approaches. The performance comparison between the two are listed below:

1. The AR approach usually offers better resolution of sharp frequency response characteristics, such as peaks, in the actual power spectrum.
2. The AR approach provides a smoother continuous spectrum estimation curve.
3. For both the AR and the WP approach the resolution and the variance of the spectrum estimation improves and decreases respectively for longer records of available x(n) data.
4. The WP approach may offer a better resolution of short, sharp valleys and zeroes in the actual power spectrum response. (Recall that the AR approach models an all-pole filter).

5.2.5 Discrete-Time and Analog Spectrum Relationships

The equivalent discrete-time output power spectrum ($S_D(j\Omega)$) of an analog system whose output is sampled with a

period Ts is an aliased version of the analog power spectrum ($S_A(jw)$). The relationship between discrete-time and analog power spectrums is similar to the relationship between discrete-time and analog transfer functions (equation 4.2.3). The discrete-time and analog power spectrum relationship is given below [5]:

$$S_D(j\Omega) = (1/Ts) \sum_{r=-\infty}^{\infty} S_A(j2\pi f + (2\pi r)/Ts) \qquad 5.2.41$$

where: f - analog frequency (Hz)

Ω - discrete-time frequency (r/s)

$$\Omega = 2\pi f Ts$$

If spectrum estimation analysis is restricted for $-1/2Ts \leq f \leq 1/Ts$, the following relationship is obtained:

$$S_D(j\Omega) = (1/Ts) S_A(j2\pi f) \qquad 5.2.42$$

Spectrum estimation analysis by windowed periodogram or AR-modeling is based on the assumption that the system output samples, x(n), correspond to a discrete-time system. The end result of such an assumption is the estimation of $S_D(j\Omega)$ in 5.2.42. If the system under consideration is analog, $S_A(j2\pi f)$ can be computed with the use of 5.2.42, as long as $-1/2Ts \leq f \leq 1/2Ts$. This is the reason why in order to compute $S_A(j2\pi f)$ the argument to the right of the equal sign in both 5.2.20 and 5.2.39 is multiplied by a factor of Ts. If the

system under consideration is discrete-time ,such as a switched capacitor filter, $S_D(j\Omega)$ can be computed by simply dividing 5.2.20 and 5.2.39 by Ts.

5.3 The Welch Windowed Periodogram

The following is a windowed periodogram algorithm developed by Welch [42], presented by Oppenheim and Shaeffer [28], and here modified following discussions on windowed periodograms by Kay and Marple [78] and the material presented in section 5.2.5:

A data segment x(n), for $0 \le n \le (N-1)$, is partitioned into K equal segments of M samples each so that N=KM, hence:

$$x_i(n) = x(n+iM-M), \quad 0 \le n \le (M-1), \quad 1 \le i \le K$$

Compute:

I. For the spectrum estimation of an analog system:

$$S_w(f) = [1/(NQTs)] \sum_{i=1}^{k} \left| Ts \sum_{n=0}^{M-1} x_i(n) w(n) e^{-jwn} \right|^2 \qquad 5.3.1$$

where: (i) $Q = [1/M] \sum_{n=0}^{M-1} w^2(n)$

(ii) w(n)= window function for $0 \le n \le (M-1)$ (see section 5.2.3)

(iii) Ts - sampling period between x(n) points.

(iv) $-1/2Ts \le f \le 1/2Ts$

II. For the spectrum estimation of a discrete-time system, the same algorithm presented above applies except that 5.3.1 divided by a factor of Ts.

$$S_W(f) <= S_W(f)/Ts \qquad 5.4.2$$

A more detailed discussion on windowed periodograms is provided in section 5.2.2.

5.4 The Yule-Walker and Burg AR-Modeling Spectrum Estimation Techniques

Two techniques are here provided for solving the AR parameters of in equation 5.2.39. Both techniques take different approaches in using the Levison-Durbin equations (5.2.40) for solving the matrix of 5.2.38.

5.4.1 The Yule-Walker Algorithm

The Yule-Walker algorithm for computing the ouput power spectrum estimation ($S_A(f)$) of an analog system is presented in the flow diagram of figure 5.7. To compute the output power spectrum estimation of a discrete-time system equation 5.39 ($S_D(f)$) in the above algorithm is divided by a factor of Ts.

$$S_D(f) <= S_A(f)/Ts \qquad 5.4.1$$

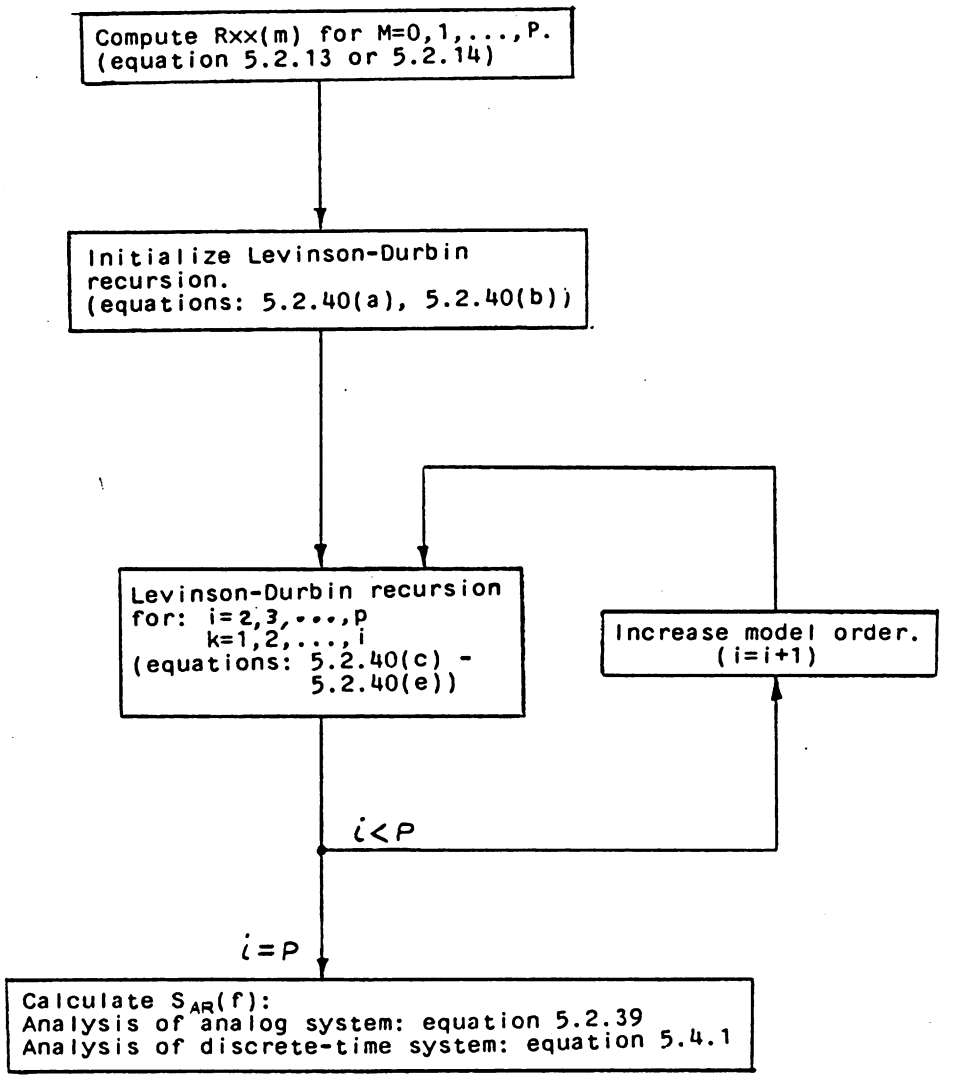

Figure 5.7. Yule-Walker AR-modeled power spectrum estimation algorithm.

5.4.2 The Burg Algorithm

The derivation of the Burg algorithm is beyond the scope of this chapter and will not be presented. The derivation of the algorithm is well presented by Kay and Marple [18]. Listed below is a set of equations used by the algorithm:

$$e(i,k)= e(i-1,k) + K_i b(i-1,k-1) \qquad 5.4.2$$

$$b(i,k)= b(i-1,k-1) + K_i^* e(i-1,k) \qquad 5.4.3$$

$$e(0,k)= b(0,k)= x(k) \text{ for } k=0,1,\ldots,N-1 \qquad 5.4.4$$

$$a(i,i)= \hat{K}_i = \frac{-2\sum_{k=i}^{N-1} b^*(i-1,k-1)e(i-1,k)}{\sum_{k=i}^{N-1} |b(i-1,k-1)|^2+|e(i-1,k)|^2} \qquad 5.4.5$$

The Burg algorithm for computing the power spectrum estimation of an analog system is presented in figure 5.8. To compute the power spectrum estimation of a discrete-time system replace 5.2.39 with 5.4.1.

5.5 Power Spectrum Estimation and Analytical Spectrum Analysis of an Example SC Noise-Modeled Circuit.

The noise-modeled LDI parasitic-sensitive circuit of figure 5.2, as analyzed by Gobet and Knob, results in the following analytical formulations for the output noise power spectrum [13]:

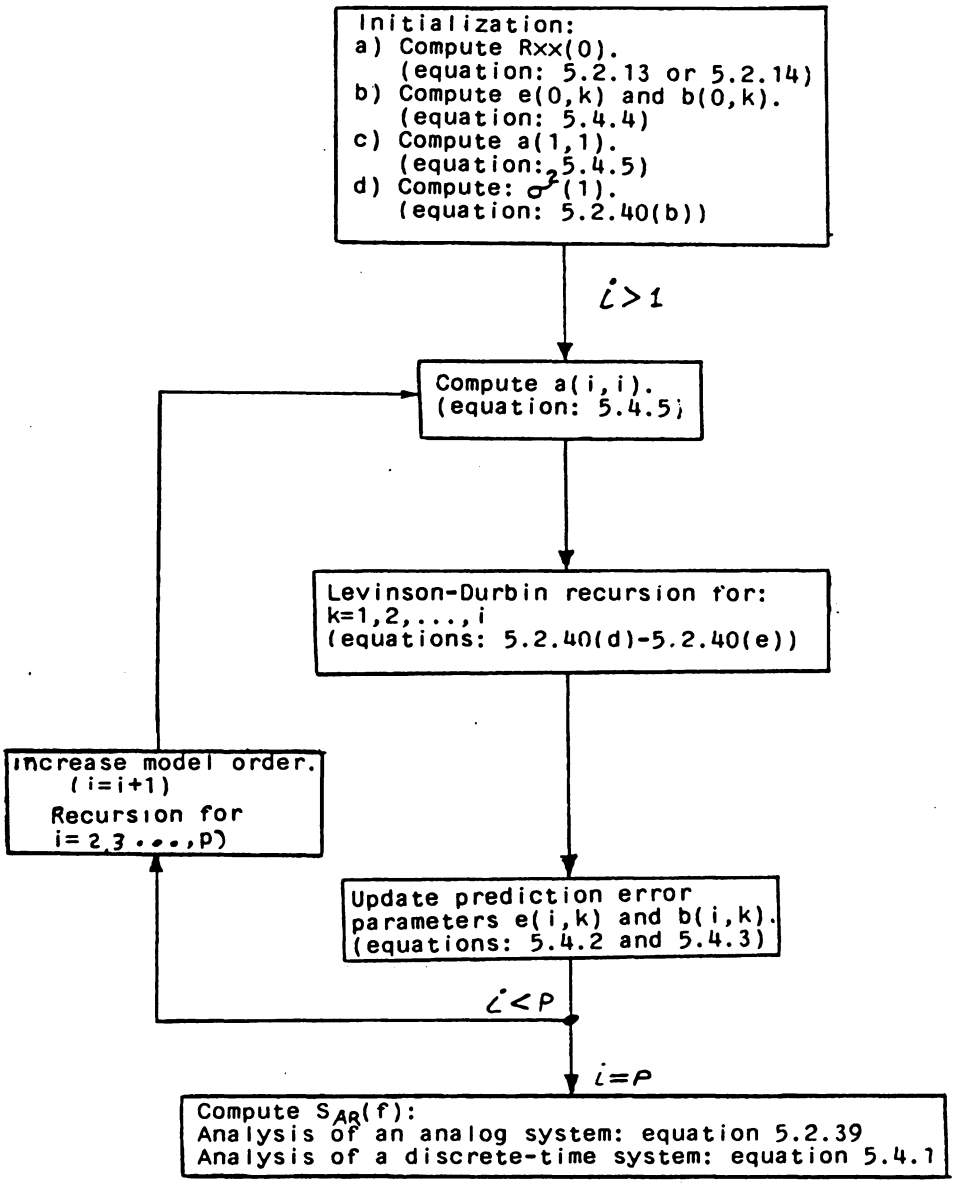

Figure 5.8. Burg AR-modeled power spectrum estimation algorithm.

$$S_{n_1}(f) = [(K\theta)/(Fs\alpha C)]\{\alpha/[2\pi F/Fs]\}^2 \qquad 5.5.1$$

$$S_{n_2}(f) = \frac{K\theta}{Fs\alpha C} \cdot \left[\alpha^2(\tau Fs) \cdot \frac{Fs}{Beq} + \left[\frac{\alpha}{2\pi F/Fs}\right]^2 \cdot \frac{\pi}{\alpha+1} \cdot \frac{Fb}{Beq} \right] \qquad 5.5.2$$

where: $Beq = (2R_2\alpha C)^{-1}$

$$S_{n_3}(f) = S_{ni} \cdot \frac{Fb}{Fs} \left[(1+\alpha\tau Fs(\alpha+2) \cdot \frac{Fs}{Fb} + \left[\frac{\alpha}{2\pi F/Fs}\right]^2 \cdot \frac{\pi}{\alpha+1} \right] \qquad 5.4.3$$

$$S_n(f) = S_{n1}(f) + S_{n2}(f) + S_{n3}(f) \qquad 5.5.4$$

Table 5.2 tabulates values used by Gobet and Knob for the parameters in the above equations. A computer simulation of 5.5.4 was carried out by Li [24] giving the analytical power spectrum frequency response result depicted in figure 5.9. The noise-modeled circuit of 5.2 was computer simulated by McCall [27] with the use of TCAPS [34], a computer program for SC simulation developed by Riad [34]. A record of 250 time-domain output points, at 10 μsec apart,was generated. Analyzing this record of data, the computer program SPECTRA (see Appendix C) performed windowed periodogram and AR-system modeling output power spectrum estimation analyses of

Table 5.2. Gobet and Knob Parameter Values for Equations 5.5.1 Through 5.5.4 [12].

Parameter	Value
K	1.38×10^{-23} J/°K
θ	300°K
Fs	10 kHz
α	1
C	10 pF
Fb	700 kHz
Beg	14.451 MHz
τ	25 sec
S_{NOA}	$2.512(10)^{-14} V^2/Hz$

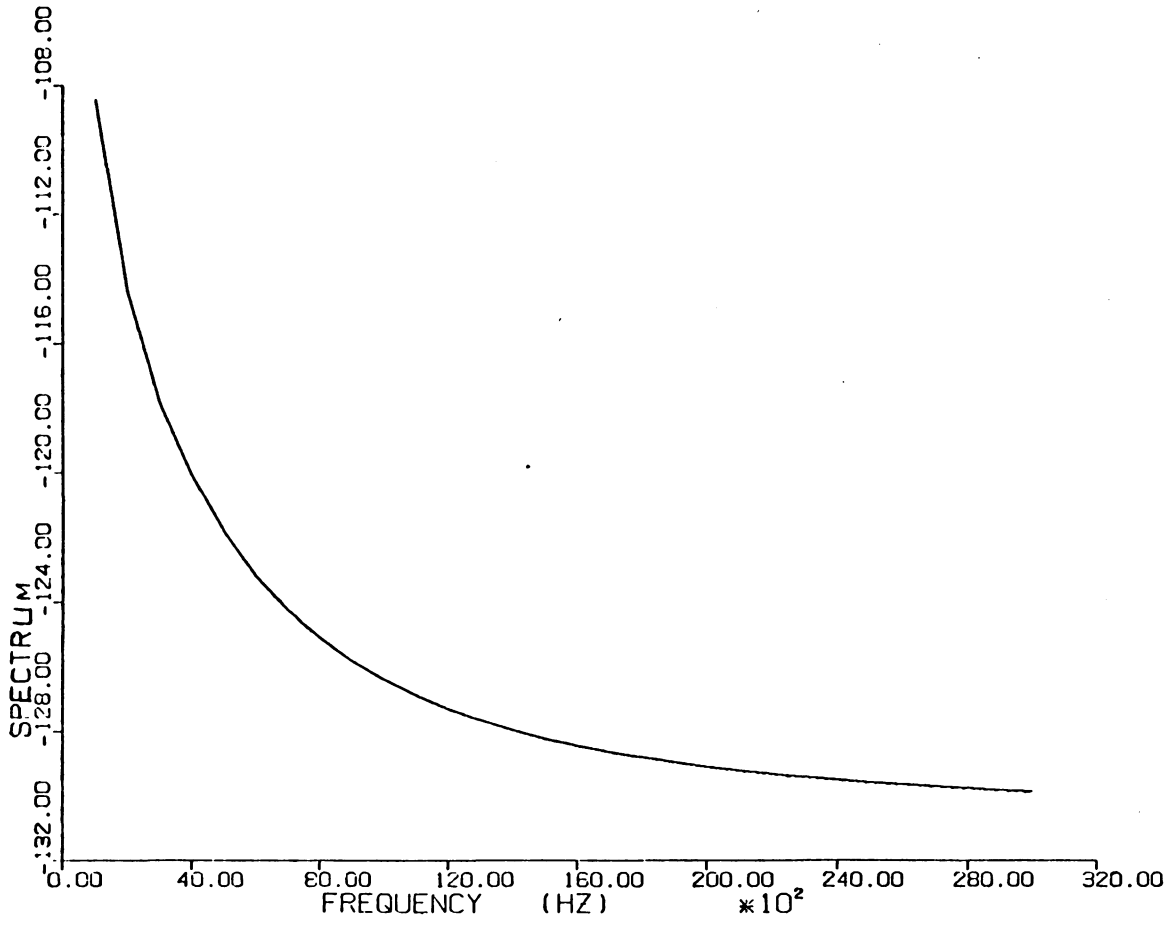

Figure 5.9. Analytical output noise power spectrum of circuit in Figure 5.2 (equation 5.5.4).

the circuit in figure 5.2. The results of these analyses are depicted in figures 5.10 through 5.12.

Implementing one periodogram and individually adopting the window functions discussed in section 5.2.3, the Welch periodogram technique produced seperate spectrum estimation results, depicted in figure 5.10, for the output noise power spectrum of figure 5.2. Note that when compared to the analytical spectrum in figure 5.9, the use of the rectangular window provided the windowed periodogram spectrum estimation with the least variance and the most resolution. With the number of periodograms increased to 10, the windowed periodogram spectrum estimation results depicted in figure 5.11 were obtained. Note that for all the windowed periodogram spectral estimations, the resolution and the variance decreases by increasing the number of periodograms. These results are expected since by increasing the number of periodograms to decrease the variance there is less number of time-domain points available for each periodogram, thereby decreasing the resolution. Note that with the use of 10 periodograms the Blackman window provided the best spectrum estimation performance, in terms of variance and resolution, while, in this case, the rectangular window provided the worst performance. This result is not surprising in light

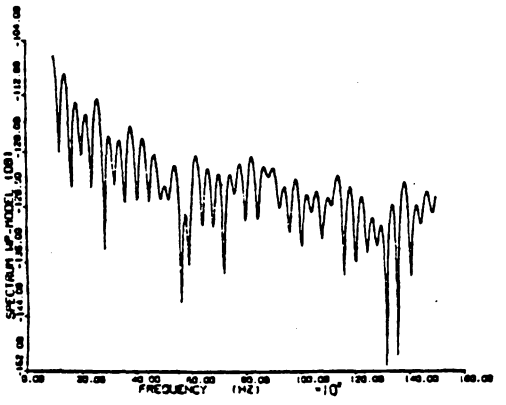

(a) Rectangular window

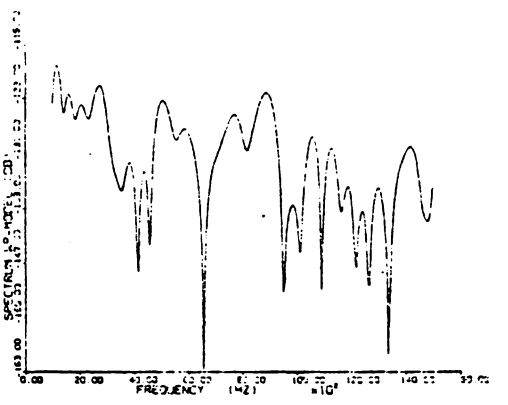

(b) Triangular window.

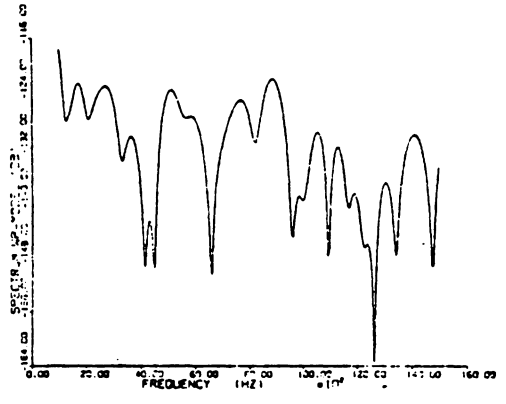

(c) Hanning window.

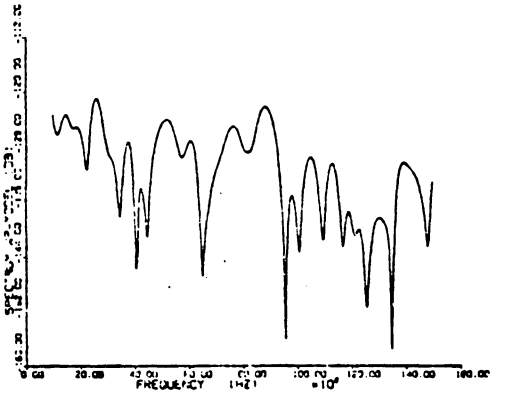

(d) Hamming window.

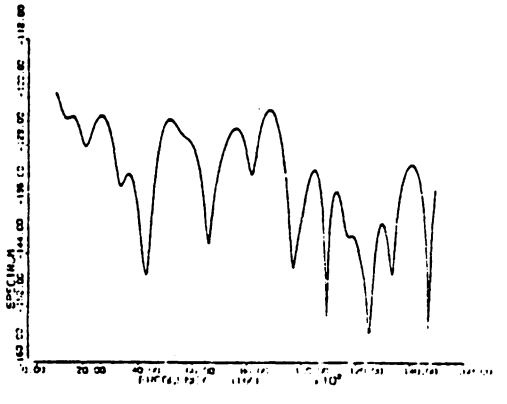

(e) Blackman window.

Figure 5.10. Welch windowed periodogram noise power spectrum estimation of circuit in Figure 5.2 (1 periodogram)

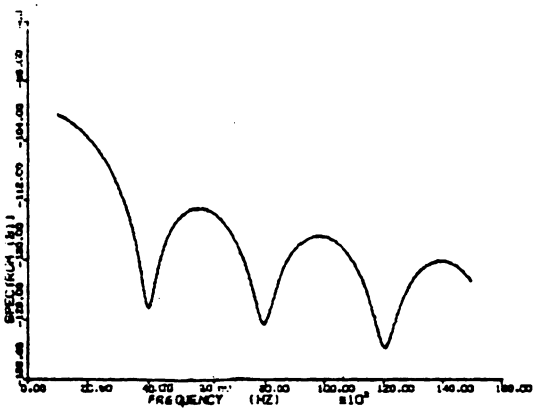

(a) Rectangular window.

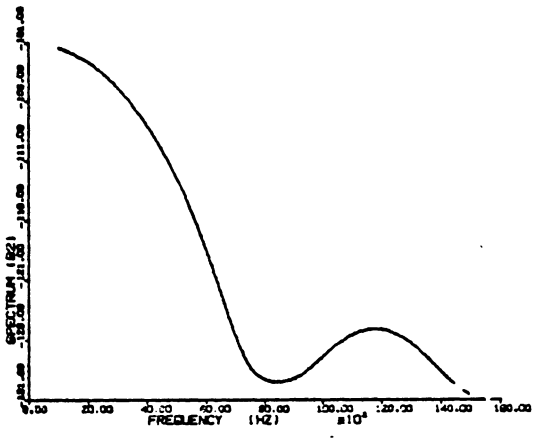

(b) Triangular window.

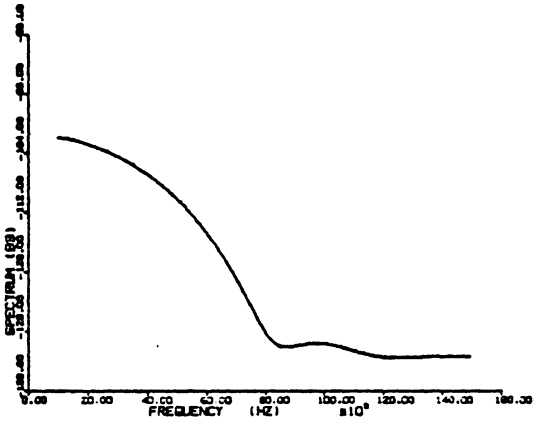

(c) Hanning window.

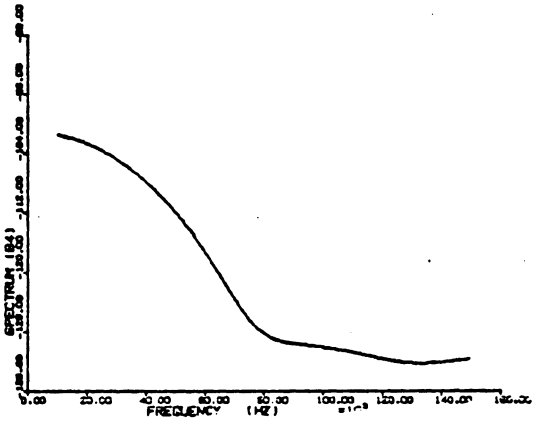

(d) Hamming window.

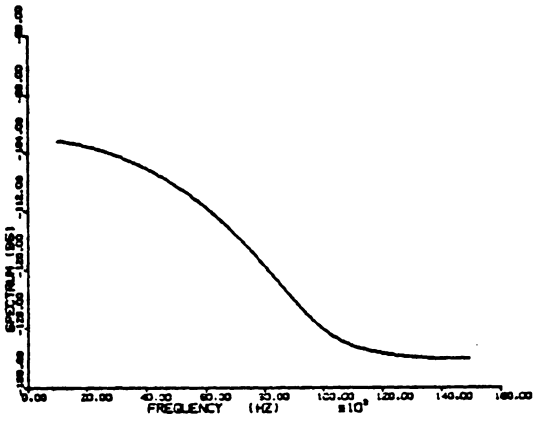

(e) Blackman window.

Figure 5.11. Welch windowed periodogram noise power spectrum estimation of circuit in Figure 5.2 (10 periodograms).

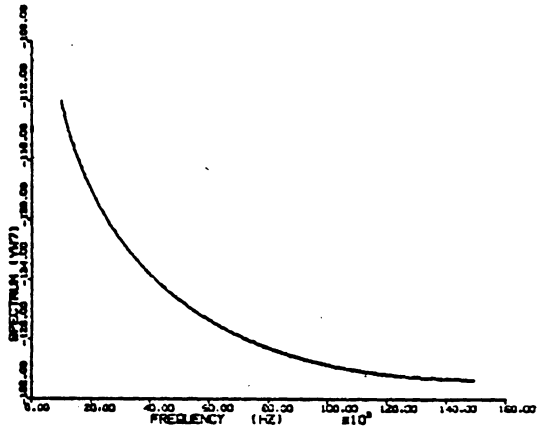

(a) Yule-Walker: model order = 7

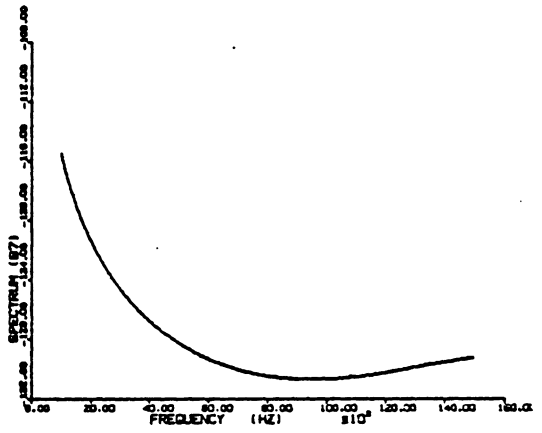

(b) Burg: model order = 7

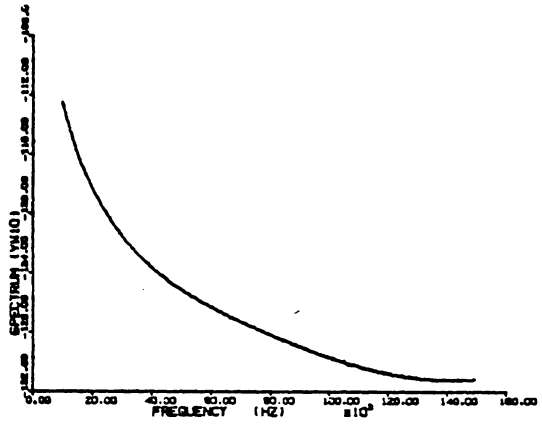

(c) Yule-Walker: model order = 10

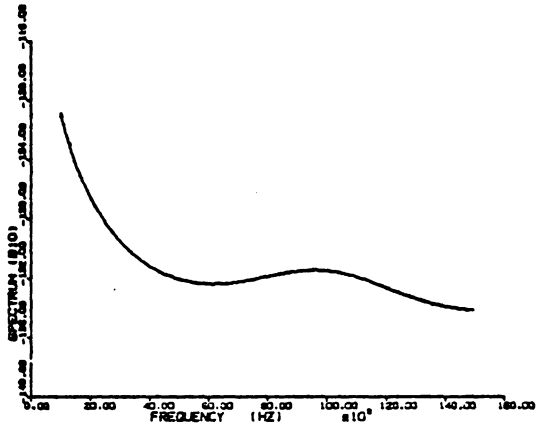

(d) Burg: model order = 10

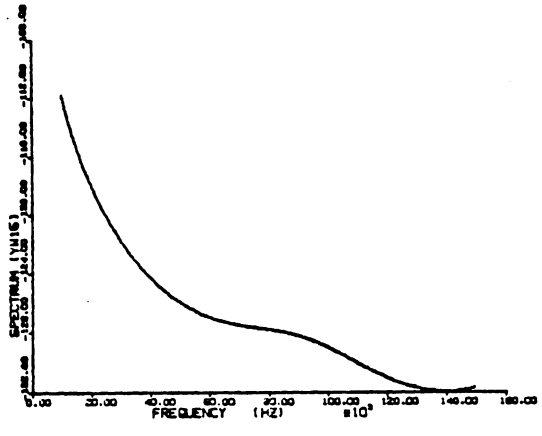

(e) Yule-Walker: model order = 15

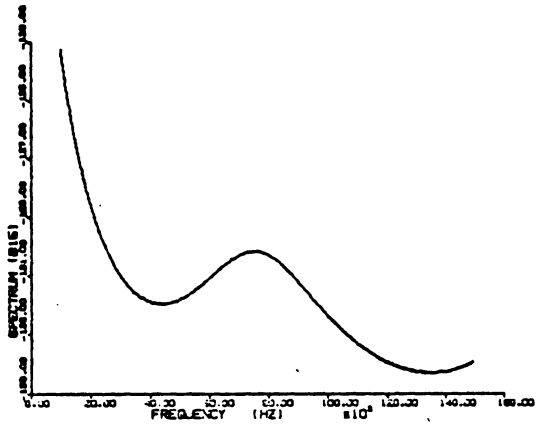

(f) Burg: model order = 15

Figure 5.12. Yule-Walker and Burg AR-modeled noise power spectrum estimation of circuit in Figure 5.2 for model orders 7, 10, and 15.

of the discussion made in section 5.2.3 on the varied performances of windows in tackling the conflicting tasks of improving the spectrum estimation and avoiding spectral leakage.

The Yule-Walker and Burg AR-system modeling spectrum estimations of of the output noise power spectrum of the circuit in figure 5.2 are depicted in figure 5.12. Note that for both techniques a consistent increase in specified model order does not necessarily guarantee an improved spectral estimation, in terms of variance and resolution, when compared to the analytical spectrum in figure 5.9. For both cases the variance and resolution of the spectrum estimation both improve by increasing the model order from 7 to 10, but degrades when the order is increased to 10. Nevertheless, when compared to the windowed periodogram spectrum estimations of figures 5.10 and 5.11 the AR-modeling spectrum estimations of figure 5.12 demonstrate substantial improvements in terms of variance and resolution. Note that the Yule-Walker spectrum estimation for an order of 7 (figure 5.12(c)) is a near perfect reproduction of the analytical spectrum in figure 5.9.

Chapter VI

CONCLUSIONS

Certain conclusions can be drawn from the computer simulations and test results of the bilinear double-sampled (BDS) and the LDI filters presented in chapter 4, and from the spectral estimation discussion and analysis presented in chapter 5. Listed below are some conclusions and recomendations concerning bilinear and LDI switched-capacitor (SC) filter and system designs:

1. For a fixed clock frequency, a BDS switched capacitor system operates at an effective sampling-to-characteristic frequency ratio which is twice that of the equivalent LDI system. The significance of this feature is:
   a) For a particular frequency window of operation, there is greater allowance for avoiding acute aliasing effects in BDS designs than in equivalent LDI designs, where the aliasing frequency is half that of the BDS system.
   b) With consideration paid to limitations imposed by dynamic characteristics such as slew rates and settling times of circuit components, BDS systems

can be implemented at higher frequency windows than LDI systems.

c) While limited by the demand of meeting fixed pass-band specifications, BDS filters require lower order specifications than equivalent LDI filters.

2. Due to their signal double-sampling nature, BDS switched capacitor filters require twice the number of switches and switched capacitors then their equivalent LDI SC systems. The consequences of this feature are:

a) No need for clock-phased signal-sampling schemes for BDS filter designs as in LDI filter designs.

b) Greater requirements for switches and capacitors in BDS systems can increase their manufacturing costs and impose tighter small scale manufacturing restrictions when compared to equivalent LDI systems.

c) With twice the number of switches, BDS filters contain twice the number of noise sources than in corresponding LDI filters of equal orders.

The following remarks and recommendations can be made concernin the use of spectrum estimation for switched capacitor noise analysis:

1. Even though spectrum estimation obviates the need for the cumbersome and tedious computations prevalent in analytical spectrum analysis, it does require accurate SC system noise modeling and precise time-domain computer simulations of noise-modeled SC systems.
2. Since there is no ideal spectrum estimation technique, one of the following two spectral analysis strategies should be pursued:
   a) First adopt a windowed periodogram spectrum estimation technique, preferably using the rectangular window and one-periodogram realization, to obtain the asymptotic behavior of the actual power spectrum. Subsequently, pursue either a Yule-Walker or a Burg AR-system modeling spectrum estimation analysis with a random selection of model orders in pursuit of an order which converges the estimation to the desired spectral response.
   b) Adopt the Yule-Walker or the Burg AR-system modeling spectrum estimation technique in conjunction with an obtimum model order criterion, such as the Akaike-FPE, the Akaike-AIC, and the Parzen-CAT criteria.

Appendix A

BUTTERWORTH, TSCHEBYSCHEFF, AND JACOBI-ELLIPTIC S-DOMAIN APPROXIMATIONS AND COMPUTER PROGRAM ANT

All the material in this appendix, with the exception of the computer program ANT, are well known Butterworth, Tschebyscheff, and Jacobi-Elliptic s-domain approximations thouroughly compiled by Antoniou [3]. The FORTRAN language computer program ANT implements the Jacobi-Elliptic approximation algorithm presented here. Parameters not defined in this appendix are defined in chapter 3.

A.1 Butterworth S-Domain Approximation (Normalized for a cutoff frequency (wco) of 1 rad/sec)

A typical s-domain Butterworth loss characteristic normalized for a 3dB cutoff frequency of 1 rad/s is depicted in figure A.1 for which the following formulation applies:

$$L(w^2) = 1 + w^{2n}$$

$$A(w) = 10\log(1+w^{2n}) \qquad n = \text{order of filter}$$

$$L(-s^2) = 1 + (-s^2)^n = \prod_{k=1}^{2n} (S-S_k)$$

where:
$$S_k = \begin{cases} e^{j(2k-1)\pi/2n} & \text{for n even} \\ e^{j(k-1)\pi/n} & \text{for n odd} \end{cases}$$

The normalized transfer function:

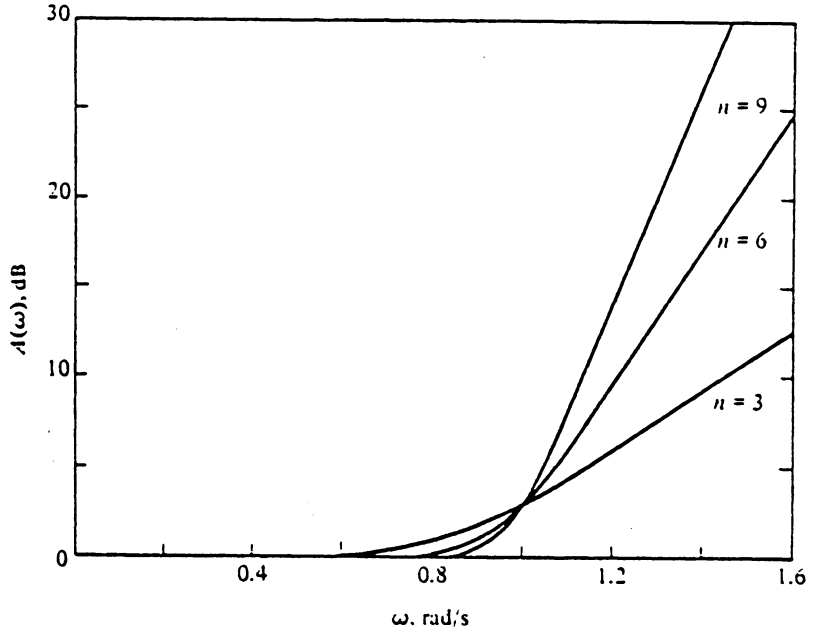

Figure A.1. Typical Butterworth lowpass attenuation-frequency response characteristic (orders n=3,6,9) [3].

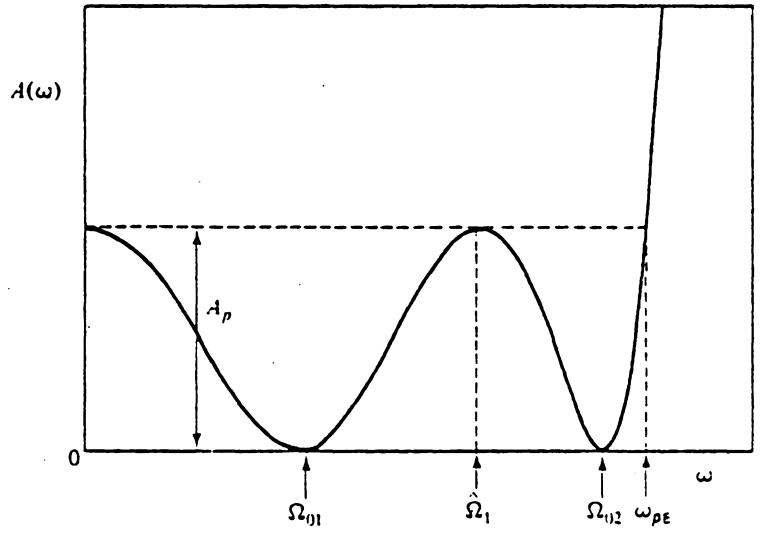

Figure A.2. Attenuation-frequency response characteristic of a 4th-order Tschebyscheff lowpass filter [3].

The normalized transfer function:

$$H_N(S) = \frac{1}{\prod_{i=1}^{n} (S-P_i)}$$

where: Pi (for i=1,2,...,n) are left-half s-plane poles of $L(-s^2)$

A.2 Tschebyscheff S-Domain Approximation (Normalized for a cutoff frequency of 1 rad/sec)

A typical 4th-order s-domain Tschebyscheff loss characteristic normalized for a passband edge frequency of 1 rad/s is depicted in figure A.2 for which the following generalized formulations apply:

$$L(-s^2) = 1 + \varepsilon^2[\cosh(n[\cosh^{-1}(s/j)])]^2$$

where n = order of filter

For $S_k = \sigma_k + jw_k$:

$$\sigma_k = \pm\sinh\{(1/n)\sinh^{-1}(1/\varepsilon)\}\sin[(2k-1)\pi/2n]$$

$$w_k = \cosh\{(1/n)\sinh^{-1}(1/\varepsilon)\}\cos[(2k-1)\pi/2n]$$

where: $\varepsilon^2 = 10^{0.1\ Ap} - 1$

The normalized transfer function:

$$H_N(S) = \frac{Ko}{\prod_{i=1}^{n} (S-P_i)}$$

where: (i) Pi for i= 1,2,...,n are the left-half s-plane zeros of $L(-S^2)$

$$\text{(ii)}\quad Ko = \begin{cases} 10^{-0.05\ Ap} \prod_{i-1}^{n} (-P_i) & \text{for n even} \\ \prod_{i=1}^{n} (-P_i) & \text{for n odd} \end{cases}$$

A.3 Jacobi-Elliptic S-Domain Approximation (Normalized for a cutoff frequency of 1 rad/sec)

The loss characteristic of a s-domain normalized lowpass elliptic approximation is depicted in figure A.3 where:

$$w_{pen} = \sqrt{K}$$

$$w_{sen} = 1/\sqrt{K}$$

$$w_{con} = \sqrt{w_{pen}\ w_{sen}}$$

The parameter K (further discussed in section 3.4) is a function of the characteristic frequencies of the filter specification. Once K is determined w_{pen} and w_{sen} of the corresponding normalized lowpass attenuation characteristic are related in the following manner:

$$K = \frac{w_{pen}}{w_{sen}}$$

The following algorithm has been developed by Antoniou [3] following the work by Grossman [15] for obtaining the normalized lowpass s-domain Jacobi-Elliptic transfer function ($H_N(s)$) in biquadratic sections. Starting with the required filter order (n), passband loss (Ap), and parameters (q) and (K) (see section 3.4), $H_N(s)$ is computed in the following biquadratic sections format:

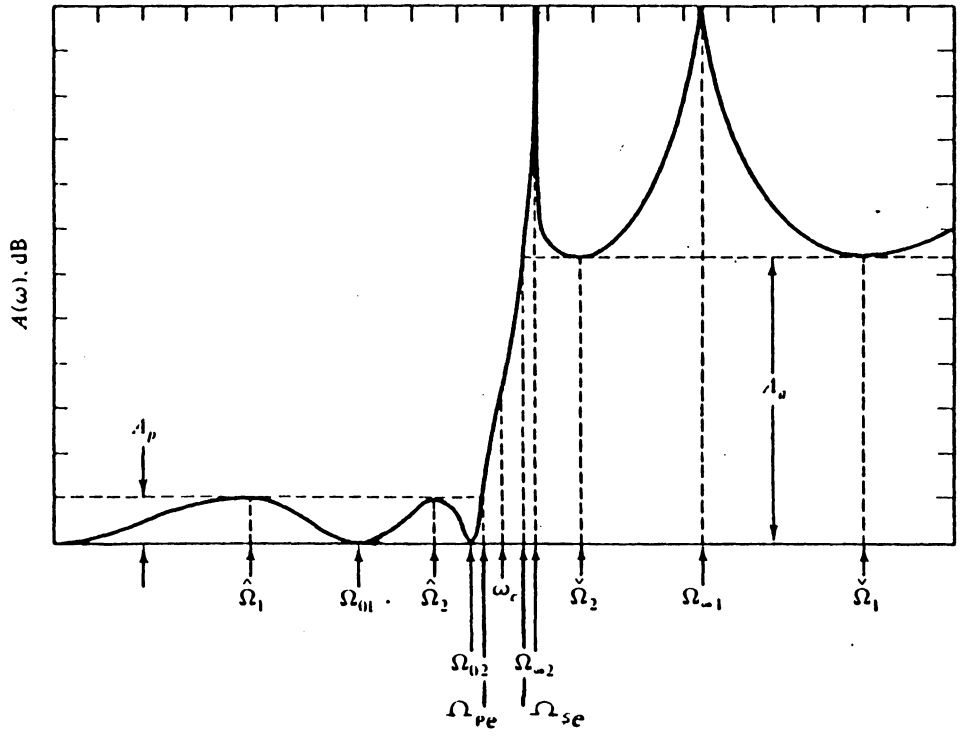

Figure A.3. Attenuation-frequency loss characteristic of a 5th-order elliptic lowpass filter [3].

$$H_N(s) = \frac{K_0}{D_0(s)} \prod_{i=1}^{r} \frac{s^2 + A_{0_i}}{s^2 + B_{1_i}s + B_{0_i}}$$

$$r = \begin{cases} (n-1)/2 & n \text{ odd} \\ n/2 & n \text{ even} \end{cases}$$

$$D_0(s) = \begin{cases} s + \sigma_0 & n \text{ odd} \\ 1 & n \text{ even} \end{cases}$$

(σ_0 to be derived)

Algorithm for A_{oi}, B_{oi}, B_{1i}, K_o, $D_o(s)$ derivation:

$$\Lambda = \frac{1}{2n} \ln \frac{10^{0.05\ Ap} + 1}{10^{0.05\ Ap} - 1}$$

$$\sigma_0 = \left| \frac{2q^{1/4} \sum_{m=0}^{\infty} (-1)^m q^{m(m+1)} \sinh[(2m+1)\Lambda]}{1 + 2 \sum_{m=1}^{\infty} (-1)^m q^{m^2} \cosh(2m\Lambda)} \right|$$

$$W = \sqrt{(1+K\sigma_0^2)(1 + \sigma_0^2/K)}$$

For i = 1,2,...,r compute:

$$\Omega_i = \frac{2q^{1/4} \sum_{m=0}^{\infty} (-1)^m q^{m(m+1)} \sin[(2m+1)\pi\mu/n]}{1 + 2 \sum_{m=1}^{\infty} (-1)^m q^{m^2} \cos[2m\pi\mu/n]}$$

where: $\mu = \begin{cases} i & n \text{ odd} \\ i - 1/2 & n \text{ even} \end{cases}$

$$V_i = \sqrt{(1-K\Omega_i^2)(1-\Omega_i^2/K)}$$

$$A_{0_i} = 1/\Omega_i^2$$

$$B_{0_i} = [(\sigma_0 V_i)^2 + (\Omega_i w)^2]/[1 + \sigma_0^2 \Omega_i^2]^2$$

$$B_{1_i} = [2\sigma_0 V_i]/[1 + \sigma_0^2 \Omega_i^2]$$

$$K_0 = \begin{cases} \sigma_0 \prod_{i=1}^{r} (B_{0_i}/A_{0_i}) & \text{for n odd} \\ 10^{-0.05\ Ap} \prod_{i=1}^{r} (B_{0_i}/A_{0_i}) & \text{for n even} \end{cases}$$

ANT, a fortran language computer program, which computes the parameters of equation A.1 by evaluating the above algorithm, is presented in the next page. Design specification parameters, whose values the user specifies, are defined in the main program and are specified in the subroutine PARAM. An example computer run is presented after the program listing for the 8th-order LDI elliptic low-pass switched-capacitor filter discussed in chapter 4.

```
C***            * * *     ANT     * * *
C***
C*** PROGRAMER: JOSE' VELAZQUEZ RAMOS
C***
C*** ELLIPTIC BILINEAR/LDI FILTER DESIGN BASED
C*** PREWARPING PASSBAND-STOPBAND EDGE FREQUENCIES
      IMPLICIT REAL*8(A-H,O-Z)
      DIMENSION A0(10),B0(10),B1(10)
      WRITE(6,93)
   93 FORMAT(///,' BIL. 3RD ORDER SC LP FCO=',
     X'1000HZ,FSE=2212.28HZ ',///)
      PASS=0.0
      PI=3.1415927
C*** PARAMETER DEFINITIONS:
C*** AS=STOPBAND LOSS
C*** AP=STOPBAND LOSS
C*** FC=CLOCK FREQUENCY(HZ)
C*** WZP=Z-DOMAIN PASSBAND EDGE FREQUENCY (R/S)
C*** WZS=Z-DAMAIN STOPBAND EDGE FREQUENCY (R/S)
C*** NBL=1(BILINEAR)/0(LDI)
C*** NDS=1(DOUBLE SAMPLED)/0(SINGLE SAMPLED)
C*** NN,RN=ORDER OF FREQUENCY
C*** INFNIT=(NO. TERMS IN SUMATIONS) ODD=1(ODD)/0(EVEN)
C*** MODE=1: LOWPASS SPECIFICATION
C***      2: HIGHPASS SPECIFICATION
      CALL PARAM(AS,AP,FC,WZP,WZS,NBL,NDS,NN,RN,
     1INFNIT,MODE,ODD)
C*** FIND SAMPLING PERIOD TS
      IF(NDS.EQ.1) TS=(1.0/FC)/2.0
      IF(NDS.EQ.0) TS=(1.0/FC)
      FS=1.0/TS
C*** WITH WZP=WZP, LET WZS=WZS IFF WZS<PI*FS
      VAL1=PI*FS
      IF(WZS.GT.VAL1) WZS=VAL1
C*** WP=PREWARPED S-DOMAIN STOPBAND EDGE FREQUENCY
      IF(NBL.EQ.0) GO TO 5
      RK0=(DTAN((WZP*TS)/2.0))/(DTAN((WZS*TS)/2.0))
      IF(MODE.EQ.1) RK0=RK0
      IF(MODE.EQ.2) RK0=1.0/RK0
      WP=DSQRT(RK0)
      IF(MODE.EQ.2) GO TO 61
      RLANDA=(TS*WP)/(2.0*DTAN((WZP*TS)/2.0))
      IF(PASS.EQ.0.0) GO TO 10
   61 RLANDA=(2.0*WP*DTAN((WZP*TS)/2.0))/TS
      IF(PASS.EQ.0.0) GO TO 10
    5 RK0=(DSIN((WZP*TS)/2.0))/(DSIN((WZS*TS)/2.0))
      IF(MODE.EQ.1) RK0=RK0
      IF(MODE.EQ.2) RK0=1.0/RK0
```

```
      WP=DSQRT(RKO)
      IF(MODE.EQ.2) GO TO 81
      RLANDA=(TS*WP)/(2.0*DSIN((WZP*TS)/2.0))
      IF(PASS.EQ.0.0) GO TO 10
   81 RLANDA=(2.0*WP*DSIN((WZP*TS)/2.0))/TS
   10 CONTINUE
C*** WRITE NBL,NDS,WZS,WZP,AP,AS,TS,RKO,WP,RLANDA
      WRITE(6,15) NBL,NDS,WZS,WZP,AP,AS,TS,RKO,WP,RLANDA
   15 FORMAT(///,'    NBL=',I2,/,'    NDS=',I2,
     A/,'    WZS=',E15.5,
     1/,'    WZP=',E15.5,/,'    AP=',E15.5,/,'    AS=',
     BE15.5,/,
     2'    TS=',E15.5,/,'    RKO=',E15.5,/,'    WP=',
     CE15.5,/,'    RLANDA,',
     3'=',E15.5,//)
C*** FIND REQUIRED ORDER(RNR)
      RKP=DSQRT(1.0-RKO**2)
      Q0=(0.5)*(1.0-DSQRT(RKP))/(1.0+DSQRT(RKP))
      Q=Q0+2.0*(Q0**5)+15.0*(Q0**9)+150.0*(Q0**13)
      EXPP=0.1*AS
      EXPS=0.1*AP
      D=((10.0)**EXPP-1.0)/((10.0)**EXPS-1.0)
      RNR=DLOG10(16.0*D)/DLOG10(1.0/Q)
C*** WRITE REQUIRED ORDER (RNR)
      WRITE(6,20) RNR
   20 FORMAT(///,'    REQUIRED ORDER OF FILTER=',E15.5,//)
C*** FIND NORMALIZED ELLIPTIC LOWPASS LAPLACE
C*** TRANSFER FUNCTION COEFFICIENTS
      EXPX=0.05*AP
      DELTA=(1.0/(2.0*RN))*DLOG((10.0**EXPX+1.0)/
     G(10.0**EXPX-1.0))
C*** FIND SUMMATION VALUES OF SUMMA
      I1=-1
      RI1=-1.0
      SUMA1=0.0
      SUMA2=0.0
      DO 25 I2=1,INFNIT
      I1=I1+1
      RI1=RI1+1.0
      RII1=RI1+1.0
      IF(I1.GT.0) GO TO 30
      FACTRA=1.0
      FACTRB=-1.0*Q
      IF(PASS.EQ.0.0) GO TO 35
   30 EXP1=I1*(I1+1)
      II1=I1+1
      EXP2=II1**2
      FACTRA=((-1.0)**I1)*(Q**EXP1)
```

```
      FACTRB=((-1.0)**II1)*(Q**EXP2)
   35 SUMA1=FACTRA*DSINH((2.0*RI1+1.0)*DELTA)+SUMA1
      SUMA2=FACTRB*DCOSH(2.0*RII1*DELTA)+SUMA2
   25 CONTINUE
      SUMMA=DABS((2.0*(Q**0.25)*SUMA1)/(1.0+2.0*SUMA2))
      W=DSQRT((1.0+RKO*(SUMMA**2))*(1.0+(SUMMA**2)/RKO))
      IF(ODD.EQ.1.0) NRR=(NN-1)/2
      IF(ODD.EQ.0.0) NRR=NN/2
      RI3=0.0
      DO 55 I4=1,NRR
      RI3=RI3+1.0
      IF(ODD.EQ.1.0) U=RI3
      IF(ODD.EQ.0.0) U=RI3-0.5
      I5=-1
      RI5=-1.0
      SUMB1=0.0
      SUMB2=0.0
      DO 50 I6=1,INFNIT
      I5=I5+1
      RI5=RI5+1.0
      RII5=RI5+1.0
      IF(I5.GT.0) GO TO 40
      FACTRA=1.0
      FACTRB=-1.0*Q
      IF(PASS.EQ.0.0) GO TO 45
   40 IXP1=I5*(I5+1)
      II5=I5+1
      IXP2=II5**2
      FACTRA=((-1.0)**I5)*(Q**IXP1)
      FACTRB=((-1.0)**II5)*(Q**IXP2)
   45 SUMB1=FACTRA*DSIN(((2.0*RI5+1.0)*PI*U)/RN)+SUMB1
      SUMB2=FACTRB*DCOS((2.0*RII5*PI*U)/RN)+SUMB2
   50 CONTINUE
      SUMMB=(2.0*(Q**0.25)*SUMB1)/(1.0+2.0*SUMB2)
      V=DSQRT((1.0-RKO*(SUMMB**2))*(1.0-(SUMMB**2)/RKO))
      AO(I4)=1.0/(SUMMB**2)
      BO(I4)=((SUMMA*V)**2+(SUMMB*W)**2)/
     G((1.0+(SUMMA**2)*(SUMMB**2))**2)
      B1(I4)=(2.0*SUMMA*V)/(1.0+(SUMMA**2)*(SUMMB**2))
   55 CONTINUE
      RHO=1.0
      DO 60 I8=1,NRR
      RHO=RHO*(BO(I8)/AO(I8))
   60 CONTINUE
      EXXX=-0.05*AP
      IF(ODD.EQ.1.0) RHO=SUMMA*RHO
      IF(ODD.EQ.0.0) RHO=((10.0)**EXXX)*RHO
C*** WRITE VALUES
```

```
      IF(ODD.EQ.0) GO TO 70
      WRITE(6,65) RHO,SUMMA
   65 FORMAT(///,'     RHO=',E20.8,/,'     DO(S)=S+',E20.8)
      IF(PASS.EQ.0.0) GO TO 75
   70 WRITE(6,80) RHO
   80 FORMAT(///,'      RHO=',E20.8,/,'      DO(S)=1.0')
   75 CONTINUE
      WRITE(6,85)
   85 FORMAT(///,'     VALUES NUMENATOR (AO) ',
     4'AND DENOMINATOR (BO) AND (B1',
     1') COEFFICIENTS:',//)
      DO 90 I9=1,NRR
      WRITE(6,100) I9,AO(I9),I9,BO(I9),I9,B1(I9)
  100 FORMAT('     AO(',I2,')=',E20.8,'     BO(',
     XI2,')=',E20.8,'     B1(',I2,')=',E20.8,/)
   90 CONTINUE
      STOP
      END
C
C
      SUBROUTINE PARAM(AS,AP,FC,WZP,WZS,NBL,NDS,
     5NN,RN,INFNIT,MODE,ODD)
      IMPLICIT REAL*8(A-H,O-Z)
      AS=82.11
      AP=0.03
      FC=10000.0
      WZP=6283.2
      WZS=11533.0
      NBL=0
      NDS=0
      NN=8
      RN=NN
      INFNIT=5
      MODE=1
      ODD=0.0
      RETURN
      END
```

EXAMPLE OUTPUT

Certain parameters presented in the output listing below are defined as follows:

RLANDA = λ

DO(S) = $D_0(s)$

RHO = K_0

AO(i) = A_0

BO(i) = B_0

B1(i) = B

```
 LDI 7th-ORDER SC LP FCO=1000HZ,FSE=2212.28HZ

 SPECIFIED PARAMETERS
    NBL= 0
    NDS= 0
    WZS=     0.11533D+05
    WZP=     0.62832D+04
    AP=     0.30000D-01
    AS=     0.82110D+02
    TS=     0.10000D-03
    RKO=     0.56678D+00
    WP=     0.75285D+00
```

COMPUTED NORMALIZED PARAMETER VALUES*REQUIRED FILTER ORDER*DENORMALIZING COEFFICIENT

RHO= 0.16474580D-04

D0(S)=1.0

REQUIRED ORDER OF FILTER= 0.71614D+01

RLANDA= 0.12181D-03

VALUES NUMENATOR (A0) AND DENOMINATOR (B0) AND (B1) COEFFICIENTS:

A0(1)= 0.38662439D+02 B0(1)= 0.14336501D+00
B1(1)= 0.66402350D+00

A0(2)= 0.50260339D+01 B0(2)= 0.30963578D+00
B1(2)= 0.50922384D+00

A0(3)= 0.24121785D+01 B0(3)= 0.50767878D+00
B1(3)= 0.29681586D+00

A0(4)= 0.18216260D+01 B0(4)= 0.62634605D+00
B1(4)= 0.94927475D-01

Appendix B

SPECTRA: A WINDOWED PERIODOGRAM AND AR-MODELING SPECTRUM ESTIMATION COMPUTER PROGRAM

SPECTRA, a FORTRAN language program, implements either a windowed periodogram or a AR-modeling spectrum estimation analysis of both analog and discrete-time systems for which records of time-domain output values are available. The program is capable of implementing either the Welch windowed periodogram or the AR-modeling power spectrum estimation techniques discussed in chapter 5. Either the Yule-Walker or the Burg algorithm can be used when pursuing an AR-modeling spectrum estimation analysis. For windowed periodogram spectrum estimation the following window functions are available:

a) Rectangular
b) Triangular
c) Hanning
d) Hamming
e) Blackman

For AR-modeling spectrum estimation the following model order criterias are available:

a) Akaike-FPE b) Akaike-AIC c) Parzen-CAT

Formulations for the Akaike-FPE, the Akaike-AIC, and the Parzen-CAT AR-model order criterias are presented below [18]:

$$E(i) = E(i-1)[1-|a(i,i)|^2]$$

where: (i) $i=1,2,\ldots,p$

(ii) $a(i,i)$ = reflection coefficients (see chapter 5)

(iii) p = optimum model order

(iv) $E(o) = \sum_{k=1}^{N} |x(k)|^2$

I. Akaike-FPE: $$AFPE(i) = E(i)\left[\frac{N+i+1}{N-i-1}\right] \qquad B.1$$

II. Akaike-AIC: $$AAIC(i) = Ln\{E(i)\} + 2(i+1)/N \qquad B.2$$

III. Parzen-CAT: $$PCAT(i) = \frac{1}{N}\sum_{j=1}^{i}\frac{1}{\hat{E}(j)} - \frac{1}{\hat{E}(i)} \qquad B.3$$

where: (i) $\hat{E}(j) = (N/(N-j))E(j)$

(ii) N = number of time-domain points per periodogram

During a recurrent increase of the AR-model order, i, the obtimum, or near-obtimum model order, p, is obtained when the value of the criteria parameter (AFPE, AAIC, or PCAT) is minimum.

SPECTRA is structured to read in first a data file containing a column of 19 'decision-making' values, which are defined in the first few lines of the program. With the use

of these values the operator can structure the program to operate in a desired mode of spectrum estimation analysis. The program then reads in a data file containing time-domain output samples from the system for which a spectrum estimation is desired. This data file should contain, from left to right, a column of time values versus a column of time-domain output values. Upon completion of a spectrum estimation analysis, the program will output relevant mode-of-operation information along with computed spectrum estimation versus frequency values. The program as presented here has yet to be expanded to implement, when desired, an FFT algorithm in windowed periodogram analyses. SPECTRA is listed in the next page and an example output for a Yule-Walker 5th-order AR-modeling spectrum estimation analysis of the circuit in figure 5.2 is presented after the program listing. The output values (S(w)) were scaled in the following manner:

$$S(w) <= 10.0*\log_{10}[S(w)]$$

```
C***            *  *  *   SPECTRA   *  *  *
C***
C***          PROGRAMER: JOSE' VELAZQUEZ RAMOS
C***
C*** WELCH AVERAGED WINDOWED PERIODOGRAM AND AR-MODELED
C*** SPECTRUM ESTIMATION PROGRAM. AR-MODELED SPECTRUM
C*** ESTIMATION USING EITHER THE YULE-WALKER OR BURG
C*** ALGORITHMS. MODEL ORDER FOR AR-MODEL SPECTRUM
C*** ESTIMATION EITHER ARBITRARILY SELECTED OR SELECTED
C*** BY ADOPTING EITHER THE AKAIKE-FPE, AKAIKE-AIC, OR
C*** PARZEN-CAT MODEL ORDER CRITERIAS.
      DIMENSION D(19),X(1000,2),SP(500),FP(500),SAR(500),
     XFAR(500),PRNT(500,3),A(40,40),RK(40),VAR(40)
C*** CONSTANTS DEFINITION
C*** DECIDE WHAT SPECTRUM ESTIMATION TECHNIQUE TO FOLLOW,
C     DETERMINE THE FREQUENCY WINDOW OF OPERATION, AND
C     SELECT OTHER PARAMETERS OF INTERESTS.
C     D(1)= 1: PERIODOGRAM/ 2: AUTOREGRATION (AR)
C     D(2)= PERIODOGRAM WINDOWS:
C           1: RECTANGULAR (BARLETT PROCEDURE)
C           2: BARLETT/ 3: HANNING/ 4: HAMMING
C           5: BLACKMAN
C     D(3)= AR FORMULATION TECHNIQUE: 1: YULE-WALKER 2: BURG
C     D(4)= PERIODOGRAM FREQUENCY WINDOW: 1: FFT
C                                         0: NO FFT
C     D(5)= (AVILABLE DECISION-MAKING PARAMETER)
C     D(6)= NO. OF TIME-DOMAIN SAMPLES
C     D(7)= NO. OF PERIODOGRAMS
C     D(8)= STARTING FREQUENCY (HZ)
C     D(9)= FINAL FREQUENCY (HZ)
C     D(10)= FREQUENCY INCREMENT (HZ)
C     D(11)= AR FORMULATION ORDER:
C            1: SPECIFIED/ 2: AKAIKE-FPE
C            3: AKAIKE-AIC/ 4: PARZEN-CAT
C     D(12)= SPECIFIED AR FORMULATION ORDER
C     D(13)= SAMPLING PERIOD (TS)
C     D(14)= 1: BIASED AUTOCORRELATION ESTIMATOR
C            2: UNBIASED AUTOCORRELATION ESTIMATOR
C     D(15)= 1: PRINT REFLECTION COEFFICIENTS
C            0: OTHERWISE
C     D(16)= 1: SPECTRA VALUES IN LINEAR SCALE
C            2: SPECTRA VALUES IN DB SCALE
C               (10.0*LOG(SPECTRA(W)))
C            3: SPECTRA VALUES IN DB SCALE
C               (20.0*LOG(SPECTRA(W)))
C     D(17)= 1: FREQUENCY IN RADIANS/SECOND (R/S)
C            2: FREQUENCY IN HERTZ (HZ)
```

```
C    D(18)= 1: FREQUENCY SCALE => LINEAR
C           2: FREQUENCY SCALE => 10.0*LOG(W) DB
C           3: FREQUENCY SCALE => 20.0*LOG(W) DB
C    D(19)= 1: SPECTRAL ESTIMATION OF ANALOG SYSTEM
C         = 2: SPECTRAL ESTIMATION OF DISCRETE-TIME SYSTEM
      PASS=0.0
      PI=3.1415927
      PK=0.0
      PASA=0.0
      SAME=0.0
C*** READ SPECTRUM ESTIMATION CRITERIA PARAMETERS
      DO 3 I=1,19
    3 READ(11,*) D(I)
      NX=D(6)
C*** READ SYSTEM TIME-DOMAIN OUTPUT SAMPLES
      DO 5 I=1,NX
      READ(12,*) (X(I,J),J=1,2)
    5 CONTINUE
      IF(D(1).NE.1.0) GO TO 10
      CALL PERIO(X,NX,D,PI,PASS,SP,FP,NFP)
      GO TO 15
   10 IF(D(1).NE.2.0) GO TO 30
      CALL AR(X,NX,D,PI,PASS,SAR,FAR,NFAR,RK,VAR,NORDER)
C*** PRINT RESULTS
   15 IF(D(1).NE.1.0) GO TO 35
      DO 40 I=1,NFP
      PRNT(I,1)=FP(I)
   40 PRNT(I,2)=SP(I)
      CALL PPRNT(RK,VAR,D,PRNT,NFP,NPLOTS,SAME,PASA,PA,NORDER)
      GO TO 30
   35 IF(D(1).NE.2.0) GO TO 30
      DO 55 I=1,NFAR
      PRNT(I,1)=FAR(I)
   55 PRNT(I,2)=SAR(I)
      CALL PPRNT(RK,VAR,D,PRNT,NFAR,NPLOTS,SAME,PASA,PA,NORDER)
   30 STOP
      END
C*******************************************************
C
C     SUBROUTINE PERIO: PERIODOGRAM SPECTRUM COMPUTATION
C
C*******************************************************
      SUBROUTINE PERIO(X,NX,D,PI,PASS,SP,FP,NFP)
      DIMENSION D(19),X(1000,2),SP(500),FP(500),WC(1000),
     1XW(40,400)
      COMPLEX*8 SPJ(400),WEX
      RM=D(6)/D(7)
      M=RM
```

```
      W=0.0
      DO 10 I=1,M
      IF(D(2).EQ.1.0) WC(I)=1.0
      IF(D(2).EQ.2.0) CALL BARLT(I,M,WC)
      IF(D(2).EQ.3.0) CALL HAN(I,M,WC)
      IF(D(2).EQ.4.0) CALL HAM(I,M,WC)
      IF(D(2).EQ.5.0) CALL BLC(I,M,WC)
      W=W+WC(I)**2
   10 CONTINUE
      W=W/RM
      RKONS=1./(D(6)*W*D(13))
      NP=D(7)
      RM=D(6)/D(7)
      M=RM
      DO 15 I=1,NP
      DO 20 J=1,M
      IX=J+(I-1)*M
      XW(I,J)=X(IX,2)*WC(J)
   20 CONTINUE
   15 CONTINUE
C     FFT OR FT ?
      NFP=(D(9)-D(8))/D(10)
      DO 25 I=1,NFP
      FP(I)=D(8)+(I-1)*D(10)
      W=-1.0*2.0*PI*FP(I)*D(13)
      RRP=W/(2.0*PI)
      JW=RRP
      PPR=JW
      W=2.0*PI*(RRP-PPR)
      FP(I)=2.0*PI*FP(I)
      SP(I)=0.0
      DO 30 J=1,NP
      SPJ(J)=CMPLX(0.0,0.0)
      DO 35 K=1,M
      WE=W*(K-1)
      WEX=CMPLX(0.0,WE)
      SPJ(J)=SPJ(J)+XW(J,K)*CEXP(WEX)
   35 CONTINUE
      SPJ(J)=D(13)*SPJ(J)
      SP(I)=SP(I)+(REAL(SPJ(J)))**2+(AIMAG(SPJ(J)))**2
   30 CONTINUE
      SP(I)=RKONS*SP(I)
      IF(D(19).EQ.2.0) SP(I)=SP(I)/D(13)
   25 CONTINUE
      RETURN
      END
```

```
C
C*************************************************************
C
C        AUTOREGRESSIVE FORMULATION: YULE-WALKER AND BURG
C
C*************************************************************
C
      SUBROUTINE AR(X,NX,D,PI,PASS,SAR,FAR,NFAR,RK,VAR,NORDER)
      DIMENSION X(1000,2),SAR(500),FAR(500),RXX(40),
     1A(40,40),VAR(40),B(40,1000),E(40,1000),RK(40),D(19)
      COMPLEX*8 DENO,WEXP
      YES=0.0
      NORDER=D(12)+1.0
      NEEE=1
      RMOM=D(14)
      D(14)=1.0
      CALL CRXX(NEEE,X,NX,D,RXX)
      EC=RXX(1)
      D(14)=RMOM
      IF(D(11).NE.1.0) GO TO 11
      IF(D(3).EQ.1.0) NRXX=D(12)+1.0
      IF(D(3).EQ.2.0) NRXX=1
      IF(PASS.EQ.0.0) GO TO 12
   11 IF(D(3).EQ.1.0) NRXX=2
      IF(D(3).EQ.2.0) NRXX=1
   12 CALL CRXX(NRXX,X,NX,D,RXX)
      IF(D(3).EQ.2.0) GO TO 10
      I=2
      A(2,2)=-1.0*RXX(2)/RXX(1)
      RK(2)=A(2,2)
      VAR(2)=(1.0-A(2,2)**2)*RXX(1)
      GO TO 30
   10 I=2
      A(1,1)=1.0
      RK(1)=1.0
   25 RNUME=0.0
      RDENO=0.0
      IEB=I-1
      DO 20 K=I,NX
      KB=K-1
      KE=K
      CALL EB(X,NX,IEB,KB,KE,RK,B,E)
      RNUME=RNUME+B(IEB,KB)*E(IEB,KE)
      RDENO=RDENO+(B(IEB,KB))**2+(E(IEB,KE))**2
   20 CONTINUE
      RK(I)=(-2.0*RNUME)/RDENO
      A(I,I)=RK(I)
      IF(I.NE.2) GO TO 35
```

```
      A(2,2)=RK(2)
      VAR(2)=(1.0-A(2,2)**2)*RXX(1)
      GO TO 30
   15 A(I,I)=-1.0*RXX(I)
      NULIM=I-1
      DO 40 L=2,NULIM
      KR=I-(L-1)
      A(I,I)=A(I,I)-1.0*A(NULIM,L)*RXX(KR)
   40 CONTINUE
      A(I,I)=A(I,I)/VAR(NULIM)
      RK(I)=A(I,I)
   35 NULIM=I-1
      VAR(I)=(1.0-A(I,I)**2)*VAR(NULIM)
      II=I-1
      DO 45 K=2,II
      I1=I-1
      I2=I-K+1
C     IF(I2.GT.I1) A(I1,I2)=0.0
C     IF(I2.LE.1) A(I1,I2)=1.0
C     IF(K.GT.I1) A(I1,K)=0.0
C     IF(K.LE.1) A(I1,K)=1.0
      A(I,K)=A(I1,K)+A(I,I)*A(I1,I2)
   45 CONTINUE
   30 EC=EC*(1.0-((RK(I))**2))
      IF(D(11).EQ.2.0) CALL AFPE(EC,D,I,YES)
      IF(D(11).EQ.3.0) CALL AAIC(EC,D,I,YES)
      IF(D(11).EQ.4.0) CALL PCAT(EC,D,I,YES)
      IF(YES.EQ.1.0) NORDER=I
      IF(YES.EQ.1.0) GO TO 50
      IF(D(11).NE.1.0) GO TO 33
      IF(I.GE.NORDER) GO TO 50
33    I=I+1
      IF(D(3).EQ.2.0) GO TO 25
      IPR=I+1
      CALL CRXX(IPR,X,NX,D,RXX)
      IF(D(3).EQ.1.0) GO TO 15
   50 NFAR=(D(9)-D(8))/D(10)
      DO 55 IAR=1,NFAR
      FAR(IAR)=D(8)+(IAR-1)*D(10)
      W=2.*PI*FAR(IAR)*D(13)
      RRW=W/(2.0*PI)
      JW=RRW
      RPW=JW
      W=-2.0*PI*(RRW-RPW)
      FAR(IAR)=2.*PI*FAR(IAR)
      DENO=CMPLX(0.0,0.0)
      A(NORDER,1)=1.0
      DO 60 I=1,NORDER
```

```
      WW=W*(I-1)
      WEXP=CMPLX(0.0,WW)
      DENO=DENO+A(NORDER,I)*CEXP(WEXP)
   60 CONTINUE
      DENOM=(AIMAG(DENO))**2+(REAL(DENO))**2
      SAR(IAR)=(VAR(NORDER)*D(13))/DENOM
      IF(D(19).EQ.2.0) SAR(IAR)=SAR(IAR)/D(13)
   55 CONTINUE
      NORDER=NORDER-1
      RETURN
      END
C
C*********************************************
C
C        PERIODOGRAM WINDOWS SUBROUTINES
C
C*********************************************
C
C*** SUBROUTINE BARLT
      SUBROUTINE BARLT(I,M,WC)
      DIMENSION WC(1000)
      N=I-1
      RN=N
      RM=M
      LLIM=(M-1)/2
      ULIM=M-1
      LLLIM=0.0
      IF(N.GE.LLLIM.AND.N.LE.LLIM) WC(I)=(2.0*RN)/(RM-1.0)
      IF(N.GT.LLIM.AND.N.LE.ULIM) WC(I)=2.0-(2.0*RN)/
     1(RM-1.0)
      RETURN
      END
C
C*** SUBROUTINE HAN (HANNING WINDOW)
      SUBROUTINE HAN(I,M,WC)
      DIMENSION WC(1000)
      N=I-1
      RN=N
      RM=M
      PI=3.1415927
      WW=(2.*PI*RN)/(RM-1.0)
      WC(I)=0.5*(1.0-COS(WW))
      RETURN
      END
C
C*** SUBROUTINE HAM (HAMMING WINDOW)
      SUBROUTINE HAM(I,M,WC)
      DIMENSION WC(1000)
```

```
      N=I-1
      RN=N
      RM=M
      PI=3.1415927
      WW=(2.*PI*RN)/(RM-1.0)
      WC(I)=0.54-0.46*COS(WW)
      RETURN
      END
C
C*** SUBROUTINE BLC (BLACKMAN WINDOW)
      SUBROUTINE BLC(I,M,WC)
      DIMENSION WC(1000)
      N=I-1
      RN=N
      RM=M
      PI=3.1415927
      WW=(2.*PI*RN)/(RM-1.0)
      WWW=2.0*WW
      WC(I)=0.42-0.5*COS(WW)+0.08*COS(WWW)
      RETURN
      END
C
C*************************************************
C
C              BIASED AND UNBIASED
C     AUTOCORRELATION ESTIMATORS SUBROUTINE
C
C*************************************************
C
      SUBROUTINE CRXX(NRXX,X,NX,D,RXX)
      DIMENSION X(1000,2),RXX(40),D(19)
      DO 10 I=1,NRXX
      RXX(I)=0.0
      NULIM=NX-(I-1)
      DO 20 J=1,NULIM
      JX=J+(I-1)
      RXX(I)=RXX(I)+X(JX,2)*X(J,2)
   20 CONTINUE
      RN=NX
      RM=I-1
      IF(D(14).EQ.1.0) RXX(I)=(1.0/RN)*RXX(I)
      IF(D(14).EQ.2.0) RXX(I)=(1.0/(RN-RM))*RXX(I)
   10 CONTINUE
      RETURN
      END
```

```
C
C*****************************************
C
C     FORWARD (E) AND BACKWARD (E)
C     LINEAR PREDICTOR SUBROUTINES
C
C*****************************************
C
      SUBROUTINE EB(X,NX,IEB,KB,KE,RK,B,E)
      DIMENSION X(1000,2),B(40,1000),E(40,1000),RK(40)
      IF(IEB.NE.1) GO TO 10
C     B(1,KB)=X(KB,2)
C     E(1,KE)=X(KE,2)
      DO 20 I=1,NX
      B(1,I)=X(I,2)
      E(1,I)=X(I,2)
   20 CONTINUE
      GO TO 15
   10 IEBM=IEB-1
      KBM=KB-1
      KEM=KE-1
      B(IEB,KB)=B(IEBM,KBM)+RK(IEB)*E(IEBM,KB)
      E(IEB,KE)=E(IEBM,KE)+RK(IEB)*B(IEBM,KEM)
   15 CONTINUE
      RETURN
      END
C
C*********************************************************
C
C        AKAIKE-FPE AR-MODEL ORDER CRITERIA SUBROUTINE
C
C*********************************************************
C
      SUBROUTINE AFPE(EC,D,I,YES)
      DIMENSION D(19)
      P=I-1
      RCNUM=D(6)+P+1.0
      RCDEN=D(6)-P-1.0
      IF(RCDEN.EQ.0.0) YES=1.0
      IF(RCDEN.EQ.0.0) GO TO 10
      VALU=EC*(RCNUM/RCDEN)
C     WRITE(6,23) VALU
C  23 FORMAT('   HI  MOM  ',E20.5)
      IF(I.EQ.2) VAFPE=VALU
      IF(I.EQ.2) GO TO 10
      IF(VALU.LE.VAFPE) VAFPE=VALU
      IF(VALU.LE.VAFPE) GO TO 10
      YES=1.0
```

```
   10 CONTINUE
      RETURN
      END
C
C*********************************************************
C
C        AKAIKE-AIC AR-MODEL ORDER CRITERIA SUBROUTINE
C
C*********************************************************
C
      SUBROUTINE AAIC(EC,D,I,YES)
      DIMENSION D(19)
      P=I-1
      VALU=ALOG(EC)+2.0*((P+1.0)/D(6))
      IF(I.EQ.2) VAAIC=VALU
      IF(I.EQ.2) GO TO 10
      IF(VALU.LE.VAAIC) VAAIC=VALU
      IF(VALU.LE.VAAIC) GO TO 10
      YES=1.0
   10 CONTINUE
      RETURN
      END
C
C*********************************************************
C
C        PARZEN-CAT AR-MODEL ORDER CRITERIA SUBROUTINE
C
C*********************************************************
C
      SUBROUTINE PCAT(EC,D,I,YES)
      DIMENSION D(19)
      II=I-1
      VALU=0.0
      DO 10 K=1,II
      RK=K
      EP=(D(6)/(D(6)-RK))*EC
      VALU=VALU+1.0/EP
   10 CONTINUE
      VALU=(1.0/D(6))*VALU-(1.0/EP)
      IF(I.EQ.2) VPCAT=VALU
      IF(I.EQ.2) GO TO 20
      IF(VALU.LE.VPCAT) VPCAT=VALU
      IF(VALU.LE.VPCAT) GO TO 20
      YES=1.0
   20 CONTINUE
      RETURN
      END
```

```
C
C*************************************************************
C
C        SUBROUTINE PPRNT: OUTPUT COMPUTATION RESULTS
C
C*************************************************************
C
      SUBROUTINE PPRNT(RK,VAR,D,PRNT,NPT,NPLOTS,SAME,PASA,
     1PA,NORDER)
      DIMENSION PRNT(500,3),RK(40),VAR(40),D(19)
      PI=3.1415927
      MORDER=NORDER+1
      IF(D(15).NE.1.0.OR.D(1).NE.2.0) GO TO 31
      WRITE(6,15)
   15 FORMAT(///,'    AR-MO',
     1'DEL SPECTRUM REFLECTION COEFFICIENTS ',/)
      DO 20 I=2,MORDER
      II=I-1
      WRITE(6,25) II,RK(I)
   25 FORMAT('      K(',I2,')=',E15.5)
   20 CONTINUE
   31 IF(D(1).NE.2.0) GO TO 41
      WRITE(6,30)
   30 FORMAT(///,'    AR-MODEL SPE',
     1'CTRUM VARIANCE (VAR) AND ',/,'    SAMPL',
     2'ING PERIOD (TS) COEFFICIENTS',/)
      WRITE(6,40) II,VAR(MORDER),D(13)
   40 FORMAT('      VAR(',I2,')=',E15.5,
     1/,'          TS=',E15.5,/)
   41 N1=D(1)
      N2=D(2)
      N3=D(7)
      N4=D(3)
      N5=D(11)
      IF(D(1).EQ.1.0) NORDER=D(12)
      N6=NORDER
      N7=D(14)
      RN8=D(6)
      RN9=D(13)
      N10=D(16)
      N11=D(17)
      N12=D(18)
      N13=D(19)
      WRITE(6,145)
  145 FORMAT(///,'     POWER SPECTRUM ESTIMATION VALUES ',
     5'VS. FREQUENCY ',
     X//,'     NOTE: A) IF I= 1: PERIODOGRAM (COLUMN A)    '
     P,/,'                       2: AR-MODEL (COLUMN A)      '
```

```
   G,/,'            B) IF II= 1: RECTANGULAR WINDOW          '
   L,/,'                       2: TRIANGULAR WINDOW          '
   N,/,'                       3: HANNING WINDOW             '
   M,/,'                       4: HAMMING WINDOW             '
   Q,/,'                       5: BLACKMAN WINDOW            '
   O,/,'            C) III= NUMBER OF PERIODOGRAMS           '
   R,/,'            D) IV= 1: YULE-WALKER AR-SPECTRA MODEL'
   S,/,'                   2: BURG AR-SPECTRA MODEL          '
   J,/,'            E) V= 1: SPECIFIED ORDER                 '
   K,/,'                  2: AKAIKE-FPE ORDER CRITERIA       '
   B,/,'                  3: AKAIKE-AIC ORDER CRITERIA       '
   C,/,'                  4: PARZEN-CAT ORDER CRITERIA       '
   T,/,'            F) VI= SELECTED AR-SPECTRA MODEL ORDER'
   W,/,'            G) VII= 1: BIASED AUTOCOR. ESTI.         '
   U,/,'                   2: UNBIASED AUTOCOR. ESTI.        '
   Y,/,'            H) VIII= NO. OF TIME-DOMAIN  PTS.     ')
    WRITE(6,155)
155 FORMAT('             J) IX= SAMPLING PERIOD (SECONDS)    '
   A,/,'            K) X= 1: SPECTRA IN LINEAR SCALE         '
   C,/,'                  2: SPECTRA IN DB (10.0*LOG)        '
   D,/,'                  3: SPECTRA IN DB (20.0*LOG)        '
   E,/,'            L) XI= 1: FREQUENCY IN RAD/SEC           '
   4,/,'                   2: FREQUENCY IN HERTZS (HZ)       '
   5,/,'            M) XII= 1: FREQUENCY IN LINEAR SCALE     '
   6,/,'                    2: FREQUENCY IN DB (10.0*LOG)    '
   7,/,'                    3: FREQUENCY IN DB (20.0*LOG)    '
   8,/,'            N) XIII= 1: ANALOG SYSTEM                '
   9,/,'                    2: DISCRETE-TIME SYSTEM ')
    WRITE(6,45) N1,N2,N3,N4,N5,N6,N7,RN8,RN9,N10,N11,
   3N12,N13
 45 FORMAT('       I=',I2,/,'      II=',I2,/,'     II',-
   6'I=',I5,/,'       IV=',
   DI2,/,'        V=',I2,/,'      VI=',I5,/,'     VI',
   7'I=',I2,/,'    VIII=',E2
   Z0.5,/,'      IX=',E20.5,/,'       X=',
   8I2,/,'      XI=',I2,/,'     XII=',
   3I2,/,'    XIII=',I2)
    WRITE(6,166)
166 FORMAT(/,'        FREQUENCY          SPECTRUM  ',/)
    N3=2
    DO 50 I=1,NPT
    IF(D(17).EQ.2.0) PRNT(I,1)=PRNT(I,1)/(2.0*PI)
    IF(D(18).EQ.1.0) GO TO 122
    IF(D(18).EQ.2.0) TLOG=10.0
    IF(D(18).EQ.3.0) TLOG=20.0
    IF(PRNT(I,1).EQ.0.0) GO TO 122
    PRNT(I,1)=TLOG*ALOG10(PRNT(I,1))
122 IF(D(16).EQ.1.0) GO TO 211
```

```
      IF(D(16).EQ.2.0) RLOG=10.0
      IF(D(16).EQ.3.0) RLOG=20.0
      PRNT(I,2)=RLOG*ALOG10(PRNT(I,2))
  211 WRITE(6,55) (PRNT(I,J),J=1,N3)
   55 FORMAT(3(3X,E15.5))
   50 CONTINUE
      RETURN
      END
```

* * * EXAMPLE OUTPUT * * *

```
AR-MODEL SPECTRUM REFLECTION COEFFICIENTS

  K( 1)=   -0.97081E+00
  K( 2)=   -0.40540E+00
  K( 3)=   -0.21468E+00
  K( 4)=   -0.40573E-01
  K( 5)=   -0.14135E+00


AR-MODEL SPECTRUM VARIANCE (VAR) AND
SAMPLING PERIOD (TS) COEFFICIENTS

  VAR( 5)=    0.99659E-13
      TS=    0.10000E-04


 POWER SPECTRUM ESTIMATION VALUES VS. FREQUENCY

 NOTE: A) IF I= 1: PERIODOGRAM (COLUMN A)
                2: AR-MODEL (COLUMN A)
       B) IF II= 1: RECTANGULAR WINDOW
                 2: TRIANGULAR WINDOW
                 3: HANNING WINDOW
                 4: HAMMING WINDOW
                 5: BLACKMAN WINDOW
       C) III= NUMBER OF PERIODOGRAMS
       D) IV= 1: YULE-WALKER AR-SPECTRA MODEL
              2: BURG AR-SPECTRA MODEL
       E) V= 1: SPECIFIED ORDER
             2: AKAIKE-FPE ORDER CRITERIA
             3: AKAIKE-AIC ORDER CRITERIA
             4: PARZEN-CAT ORDER CRITERIA
       F) VI= SELECTED AR-SPECTRA MODEL ORDER
       G) VII= 1: BIASED AUTOCOR. ESTI.
               2: UNBIASED AUTOCOR. ESTI.
       H) VIII= NO. OF TIME-DOMAIN  PTS.
       J) IX= SAMPLING PERIOD (SECONDS)
       K) X= 1: SPECTRA IN LINEAR SCALE
             2: SPECTRA IN DB (10.0*LOG)
             3: SPECTRA IN DB (20.0*LOG)
       L) XI= 1: FREQUENCY IN RAD/SEC
              2: FREQUENCY IN HERTZS (HZ)
       M) XII= 1: FREQUENCY IN LINEAR SCALE
                 2: FREQUENCY IN DB (10.0*LOG)
```

```
                3: FREQUENCY IN DB (20.0*LOG)
      N) XIII= 1: ANALOG SYSTEM
               2: DISCRETE-TIME SYSTEM
   I= 2
  II= 1
 III=   10
  IV= 1
   V= 1
  VI=    5
 VII= 1
VIII=          0.25000E+03
  IX=          0.10000E-04
   X= 2
  XI= 2
 XII= 1
XIII= 2

    FREQUENCY          SPECTRUM

    0.0               -0.88012E+02
    0.50000E+03       -0.10328E+03
    0.10000E+04       -0.10918E+03
    0.15000E+04       -0.11265E+03
    0.20000E+04       -0.11510E+03
    0.25000E+04       -0.11698E+03

         *                  *

         *                  *

         *                  *

    0.13000E+05       -0.12735E+03
    0.13500E+05       -0.12742E+03
    0.14000E+05       -0.12748E+03
    0.14500E+05       -0.12753E+03
```

Appendix C

DYNAMIC RANGING OF THE 8TH-ORDER LDI FILTER

The following steps were taken in the dynamic ranging of the 8th-order LDI filter:

1. Arbitrarily select a constant value of switched capacitor for all the switched capacitors of the LDI filter. For this case let:

   $$Cu = Cui = 1{,}000 \text{ pF}$$

2. Using relations for integrating capacitors, Cki, and coupling-summation capacitors, Cxi, presented in table 4.5, the capacitor values listed in table C.1 were obtained.
3. Using the capacitor values in table C.1, the LDI filter when computer-simulated yielded the filter stage maximum gain values listed in table C.2.
4. Normalizing gain constants, Ki, were then computed with the purpose of normalizing each filter stage to yield maximum output gains equal to the peak gain of the output stage. The derivation of these gain constants for each of the stages is shown in table C.2.

Table C.1. Integrating Capacitor, Cki, and Coupling Capacitors, Cxi, values.

i	Cki	Cxi
1	1.7583 nF	0.1287877 nF
2	2.3333 "	0.1287877 "
3	3.1701 "	0.3427922 "
4	2.333 "	0.4116903 "
5	3.0927 "	0.2080414 "
6	2.5992 "	0.3136197 "
7	2.523 "	--------
8	1.7523 "	--------

Table C.2. Peak Gains and Output/Input Gain Constants of Individual Integration/Summation Stages

Stages	Maximum Gain	Output/Input Gain Constants
1	a= 2.3504174	K1= a/h= 2.2977936
2	b= 2.7313037	K2= b/h= 2.6701521
3	c= 2.3276892	K3= c/h= 2.2755742
4	d= 2.7202574	K4= d/h= 2.6593532
5	e= 2.1240024	K5= e/h= 2.0764478
6	f= 2.2723226	K6= f/h= 2.2214472
7	g= 1.729916	K7= g/h= 1.6911847
8	h= 1.0229019	K8= 1

5. The output signal of stage i was multiplied by Ki and its input signals divided by Ki, resulting in the signal multiplication constants presented in figure C.1(a). The value of each switched capacitor representing a particular signal path in figure C.1(a) is multiplied by the path's corresponding multiplicative constant[1] the values of which are presented in figure C.1(b). With the use of these new dynamic-ranged switched capacitor values and the Cki and Cxi relationships in figure 4.5, the dynamic-ranged design capacitor values of the LDI filter, listed in table 4.7, were obtained.

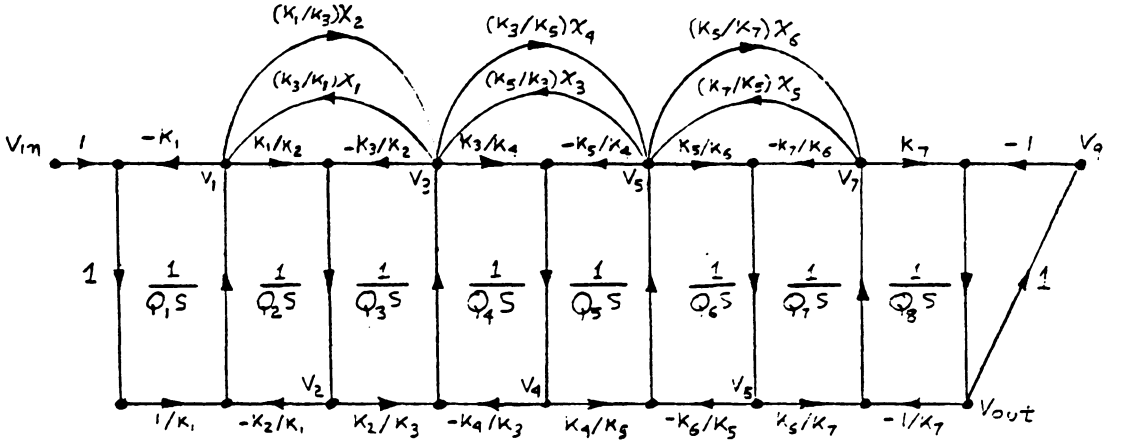

Figure C.1. Leapfrog signal flow diagram of the 8th-order LDI SC lowpass filter with multiplication constant relations.

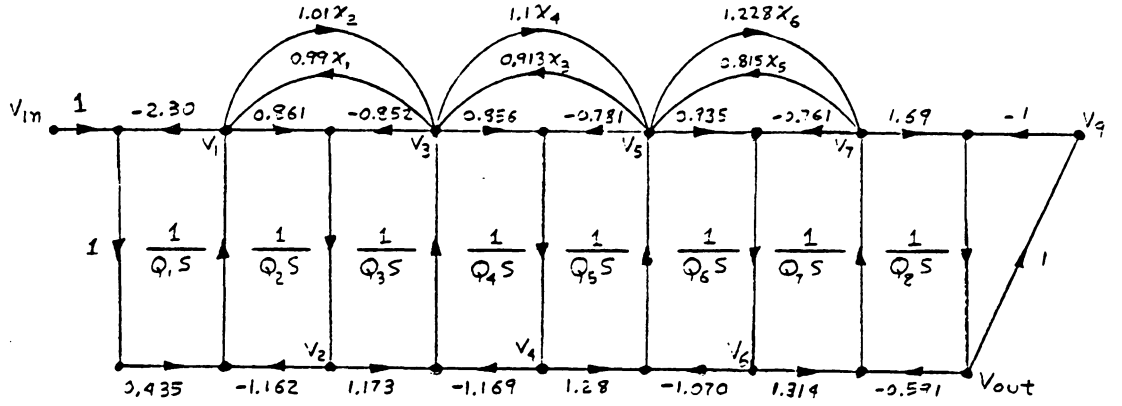

Figure C.2. Leapfrog signal flow diagram of the 8th-order LDI SC lowpass filter with values of multiplication constants.

REFERENCES

[1] P.E. Allen and L.P. Huelsman, 'Introduction to the Theory and Design of Active Filters', McGraw-Hill, New York, 1980.

[2] D.J. Allstot, R.W. Brodersen, and P.R. Gray, 'MOS switched capacitor ladder filters', IEEE Journal of Solid State Circuits, Vol. SC-13, pp. 806-814, December 1978.

[3] A. Antoniou, 'Digital Filters: Analysis and Design', McGraw-Hill, New York, 1979.

[4] D.J.M. Baez-Lopez, 'Synthesis and Sensitivity Analysis of Elliptic Networks', Ph.D. dissertation, Dept. of Electrical Engineering, University of Arizona, 1979.

[5] A.A. Beex, Ph.D., private communications, Dept. of Electrical Engineering, V.P.I.&S.U., Blacksburg, Virginia.

[6] R.E. Bogner and A.G. Constantinides, 'Introduction to Digital Filtering', John Wiley & Sons, New York, 1975.

[7] R.W. Brodersen, P.R. Gray, and D.A. Hodges, 'MOS switched capacitor filter', Proceedings of the IEEE, Vol. 67, pp. 61-67, January 1979.

[8] T.C. Choi and R.W. Brodersen, 'Considerations for high frequency switched-capacitor ladder filters', IEEE Transactions of Circuits and Systems, Vol. CAS-27, pp. 545-552, June 1980.

[9] R.D. Davis and T.N. Trick, 'Optimum design of low-pass switched-capacitor ladder filters', IEEE Transactions on Circuits and Systems, Vol. CAS-27, pp. 522-527, June 1980.

[10] B. Furrer and W. Guggenbuhl, 'Noise analysis of sampled-data circuits',International Symposium on Circuits and Systems, pp. 860-863, Chicago, 1981.

[11] B. Furrer and W. Guggenbuhl, 'Noise analysis of a switched-capacitor biquad', International Symposium on Circuits and Systems, pp. 460-463, Chicago, 1981.

[12] F.E. Girling and E.F. Good, 'The leapfrog or active ladder synthesis', Wireless World, pp. 341-345, July 1970.

[13] C.A. Gobet and A. Knob, 'Noise analysis of switched capacitor networks', International Symposium on Circuits and Systems, pp. 856-859, Chicago 1980.

[14] R. Gregorian, 'Switched-capacitor filter design using cascaded sections', IEEE Transactions on Circuits and Systems, pp. 515-521, Chicago 1980.

[15] A.J. Grossman, 'Synthesis of Tchebyscheff parameter symmetrical filters', Proceedings of the IRE, Vol. 45, pp.454-473, April 1957.

[16] G.M. Jacobs, D.J. Allstot, R.W.Brodersen, and P.R. Gray, 'Design techniques for MOS switched capacitor ladder filters', Vol. CAS-25, pp. 1014-1021, December 1978.

[17] G.M. Jenkins and D.G. Watts, 'Spectral analysis and its applications', San Francisco, CA: Holden-Day, 1968.

[18] S.M. Kay and S.L. Marple, 'Spectrum analysis : a modern perspective', Proceedings of the IEEE, Vol. 69, pp. 1380-1419, November 1981.

[19] A. Knob, 'Novel strays-insensitive switched-capacitor integrator realizing the bilinear z-transform', Electronics Letters, Vol. 16, pp. 173-174, February 28, 1980.

[20] K.R. Laker, 'Equivalent circuits for the analysis and synthesis of switched capacitor networks', The Bell System Technical Journal, pp. 729-769, March 1979.

[21] M.S. Lee and C. Chang, 'Switched-capacitor filters using the LDI and the bilinear Transformations', IEEE Transactions on Circuits and Systems, Vol. CAS-28, pp. 265-270, April 1981.

[22] M.S. Lee and C. Chang, 'Low-sensitivity switched-capacitor ladder filters', IEEE Transactions on Circuits and Systems, Vol. CAS-27, pp. 475-480, June 1980.

[23] M.S. Lee, G.C. Temes, C. Chang, and M.B. Ghaderi, 'Bilinear switched-capacitor ladder filters', IEEE transactions on Circuits and Systems, Vol. CAS-28, pp. 811-821, August 1981.

[24] E. Li, private communications, Dept. of Electrical Engineering, V.P.I.&S.U., Blacksburg, Virginia.

[25] F. Maloberti, F. Montecchi, and V. Svelto, 'Noise and gain in a SC integrator with real operational amplifier', Alta Frequenza, Vol. L, pp. 4-11, 1981.

[26] K. Martin and A.S. Sedra, 'Exact design of switched-capacitor bandpass filters using coupled-biquad structures', IEEE Transactions on Circuits and Systems, Vol. CAS-27, pp. 469-475, June 1980.

[27] W.L. McCall, private communications, Dept. of Electrical Engineering, V.P.I.&S.U., Blacksburg, Virginia.

[28] A.W. Oppenheim and R.W. Schafer, 'Digital Signal Processing', Prentice-Hall, Inc., New Jersey, 1975.

[29] H.J. Orchard and G.C. Temes, 'Spectral analysis of switched-capacitor filters designed using the bilinear z-transform', IEEE Transactions on Circuits and Systems, Vol. CAS-27, pp. 185-190, March 1980.

[30] A. Papoulis, 'Probability, Random Variables, and Stochastic Processes', McGraw-Hill, New York, 1965.

[31] A. Papoulis, 'Signal Analysis', McGraw-Hill, New York, 1977.

[32] E. Parzen, 'Mathematical considerations in the estimation of spectra', Technometrics, Vol. 3, pp. 167-190, May 1961.

[33] L.R. Rabiner and B. Gold, 'Theory and Application of Digital Signal Processing', Prentice-Hall, New Jersey, 1975.

[34] S.M. Riad, Ph.D., private communications, Dept. of Electrical Engineering, V.P.I.&S.U., Blacksburg, Virginia.

[35] R. Rohrer, L. Nagel, R. Meyer, and L. Weber, 'Computationally efficient electronic circuit noise calculations', IEEE Journal of Solid-State Circuits, Vol. SC-6, pp. 204-213, August 1971.

[36] Silvar-Lisco, private consulting and communication, Palo Alto, California.

[37] G. Szentirmai and G.C. Temes, 'Switched-capacitor building blocks', Vol. CAS-27, pp. 492-501, June 1980.

[38] G.C. Temes, 'The derivation of switched-capacitor filters from active-RC prototypes', Electronics Letters, Vol. 14, pp. 361-362, June 28 1978.

[39] G.C. Temes and I.A. Young, 'An improved switched-capacitor integrator', Electronics Letters, Vol. 14, pp. 287-288, April 27 1978.

[40] J. Vandewalle, H. De Man, and J. Rabaey, 'The adjoint switched capacitor network and its application to frequency, noise, and sensitivity analysis', International Journal on Circuit Theory and Applications, Vol. 9, pp. 77-88, 1981.

[41] H. Weinrichter, 'Equivalent noise sources of switched-capacitor network elements', International Symposium on Circuits and Systems, pp. 38-41, Chicago, 1981.

[42] P.D. Welch, 'The use of fast Fourier transform for the estimation of power spectra', IEEE trans. Audio Electroacoust., Vol. AU-15, pp. 70-73, June 1970.

[43] E.C. Whitman,'The spectral analysis of discrete-time series in terms of linear reqressive models', Naval Ordnance Labs Rep. NOLTR-70-109, White Oak, MD, June 23, 1974.

[44] A.I. Zverev, 'Handbook of Filter Synthesis', Wiley, New York, 1967.

The vita has been removed from the scanned document